5-2015

Two Types of Conformal Antennas for Small Spacecrafts

Salahuddin Tariq

TWO TYPES OF CONFORMAL ANTENNAS FOR SMALL SPACECRAFTS

by

Salahuddin Tariq

A thesis submitted in partial fulfillment
of the requirements for the degree

of

MASTER OF SCIENCE

in

Electrical Engineering

Approved:

Dr. Reyhan Baktur Major Professor	Dr.Charles M. Swenson Committee Member
Dr. Jacob Gunther Committee Member	Dr. Mark R. McLellan Vice President for Research and Dean of the School of Graduate Studies

UTAH STATE UNIVERSITY
Logan, Utah

2015

Abstract

Two Types of Conformal Antennas for Small Spacecrafts

by

Salahuddin Tariq, Master of Science

Utah State University, 2015

Major Professor: Dr. Reyhan Baktur
Department: Electrical and Computer Engineering

Conformal antennas have widespread applications in communication systems for vehicular bodies, aircrafts, and spacecrafts etc. They are non-protruding and can arbitrarily take any shape on the surface where they are etched. This thesis is a summary of two main projects. The first project employs a conformal array of four S-band and four GPS-band antennas for sub-payload of a sounding rocket. The sub-payload is a small cylinder and therefore the eight conformal antennas are based on curved patch geometry. The second project employs a conformal antenna for a CubeSat. The antenna is based on a cavity-backed slot and therefore can be conveniently integrated around the surface-mount solar cells of the CubeSat. Such an integration has enormous merits for CubeSat because there is no competition between the antennas and solar cells for the limited surface real estate. The antenna design operates UHF band with circular polarization, making it the first UHF non-deployed antenna for CubeSats. For both projects, problems such as isolation, impedance bandwidth, axial ratio bandwidth, and EMI shielding have been analyzed and resolved. This thesis work yields a prototype-ready design for the first project, and a final prototype and measurements for the second project.

(110 pages)

Public Abstract

Two Types of Conformal Antennas for Small Spacecrafts

by

Salahuddin Tariq, Master of Science

Utah State University, 2015

Major Professor: Dr. Reyhan Baktur
Department: Electrical and Computer Engineering

Spacecraft and vehicular bodies often require antennas that are conformal to their surface. The advantage of this choice is that they do not suffer from air drag or breakage and can be formed into any desirable shape. We can make them to operate at those frequencies at which simple wire antennas will require considerably longer length. Our thesis is about conformal antenna design for two space projects. The first project involves an array of patch antennas placed on multi-layer cylindrical substrate. Four of these antennas are S-band and four of them are GPS-band antennas. The second project deals with the design of a slot antenna for 3U CubeSats. 3U CubeSat is a type of miniaturized satellite having a volume of $10cm \times 10cm \times 30cm$. Our slot antenna operates in UHF band and saves a lot of space for integration of solar panels as well. We have presented solution strategies to achieve dual band operation, isolation between two slot antennas for uplink and downlink channels, circular polarization, and EMI shielding. At the end, the final model has been simulated and results have been discussed.

To my beloved Mother and Father

Contents

List of Tables

List of Figures

Acronyms

AR	Axial Ratio
ASSP	Auroral Spatial Structures Probe
CP	Circular Polarization
CPd	Circulary Polarized
CubeSat	Cube Satellite
VSWR	Voltage Wave Standing Ratio

Chapter 1

Wraparound Sounding Rocket Payload Antenna

1.1 Overview of the Project

This project is the first part of this thesis research, and it focuses on the design of conformal antenna wrapped around a cylindrical payload. A conformal antenna means it is designed to conform or follow some flat or curved surface. Conformal antennas are easy to integrate on different surfaces and are not protruding above or below the surface on which they are etched. These types of antennas are also one of the most desirable candidates for military applications, vehicular bodies and space aircrafts. Patch and slot antennas that are examined in this thesis also belong to the class of conformal antennas and are, basically, complementary to each with respect to radiation characteristics [1]. Research work to be covered in my thesis revolves around two projects and they employ patch and slot antennas for small spacecraft applications.

This project is a study and an alternative design of the payload antennas for USU's recent Auroral Spatial Structures Probe (ASSP) mission to measure small scale E-field variations during breakup aurora and geomagnetically active conditions of upper atmosphere. The sounding rocket for this mission has six identical sub-payloads deployed along as well perpendicular to the path of flight to record both temporal and spatial variations. Each sub-payload has diameter of six inches and height of four inches. Each sub-payload has four booms coming out of the surface and will be two meters long when fully deployed [2].

An array of four GPS antennas and four S-band antennas will be employed on outermost surface of each cylindrical sub-payload to cover the frequency/ies of 1575 MHz and 2210-2230 MHz respectively. Design requirements for these antennas are detailed in Table 1.1.

Table 1.1: Requirements for ASSP antennas' design.

Specification	Requirement	Comments
Diameter-Outside	<6.5 inch O.D.	
Diameter-Inside	4 inches tall	Surface mount on to a 6" diameter cylinder
Height	4 inches tall	Axial length
Thickness	<.25 inch	
VSWR S-band	<2.0:1 Max (2210MHz to 2230MHz)	Typical = 1.5:1
VSWR GPS-band	1.5:1 Max @ 1575.42MHz center frequency	1.5 VSWR across 10MHz bandwidth
S-band frequency	Center at 2220MHz	2210 to 2230MHz
GPS frequency	1575.42 MHz (L1)	RHPC polarization
RF connectors S-band	SMA male "Flying lead coax cable"	Cable length TBD
RF connectors GPS	SSMA male "Flying lead coax cable"	Cable length TBD
S-band polarization	Linear	
GPS polarization	RHS	GPS channel shall exhibit an omni-directional radiation pattern capable of maintaining GPS lock, while the antennas spinning at .1 to 2Hz
Materials	Non-magnetic	Nickel plating not allowed
Filter	Notch filter on GPS antenna	40 dB rejection in S-band

Table 1.1: Continued.

Power divider	Not allowed	Single feed only
Mounting	Flush mount using load bearing inserts (Ferrules). Must be low magnetic stainless steel	Austenitic grade 310 or 316
S-band gain	95 percent of radiation sphere > -8dBi	S-band antenna gain desired to be >-8dBi at all theta and phi angles excluding those within 3 degrees of axial nulls
GPS gain	95 percent of radiation sphere > -6dBi	GPS antenna gain desired to be >-6 dBi at all those theta and phi angles excluding those within 3 degrees of axial nulls
Temperature	Antenna will not be exposed to high temperature during mission environment	Antenna will be located under protective skin/fairing-prior to exo-atmospheric deployment

The initial feasibility study of this project was the thesis research of Muhammad Rafique [3] (a former student of Dr. Reyhan Baktur). As the previous study weights more on researching limiting factors and initial design, it is necessary to continue on the previous work and to present a more cost-effective, reliable, and mission-ready design.

1.2 Summary of Previous Work

Conformal array of S-band and GPS antennas was suggested for sub-payload design project [3]. First four S-band antennas were put on a cylindrical surface separated by angular distance of 90 degrees and were tuned to get an omni-directional response. Each antenna was fed with a separate port. Since the project required one port for excitation of S-band antenna array, hence feed network was changed to have one excitation port and it terminated to four 50 ohm branches using impedance transformation technique. After simulation on HFSS, it was found that feed line network and patch antenna array were interfering with each other and both of them needed to be isolated. A multilayer antenna structure was proposed to get rid of this problem. A sample layer by layer construction of such geometry has been shown in figure 1.1.

Finally the four GPS antennas and four S-band antennas were laid on the outermost surface of cylindrical multilayer design with the feed lines sandwiched between two G10 substrates. A simplified multilayer antenna structure was also modeled in HFSS that was using separate coaxial probes to feed each antenna. The purpose was to cross reference with actual multilayer structure and to compare the results from both simulations. Boom effect was also studied by including the booms of much shorter length than actual ones. After that isolation problem was addressed for the GPS and S-band antenna array but it did not improve and band pass filter or notch filter was suggested as a possible solution.

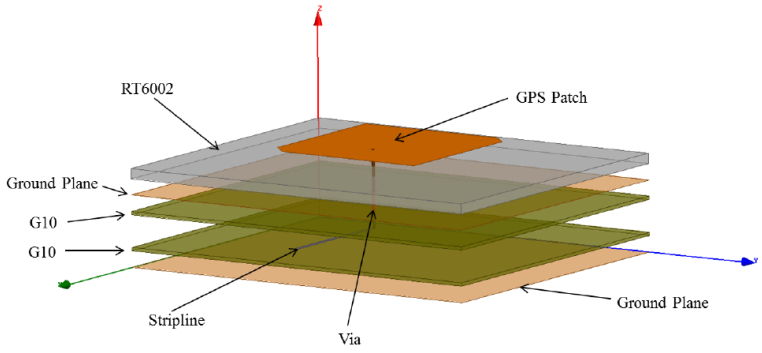

Fig. 1.1: Multi-layer structure as devised in Muhammad Rafique's thesis.

1.3 Development in ASSP Project

The previous study leaves room for improvements especially from the perspective of fabrication of this project. This section describes the research work that was done to fulfill the remaining design goals. The list of these tasks is stated below and each of it will be discussed in detail in this chapter.

1. Effect of temperature on the properties of conformal antennas for ASSP project;
2. Changes in the substrate material to optimize the overall cost of design;
3. Changes in the feed line design that are being used to excite GPS and S-band antenna arrays after incorporating the additional air holes in the substrate material;
4. Inclusion of suspended ground in the design to ease the fabrication process and to simulate this new model for making it consistent with the design goals;
5. To investigate the methods of conditioning radiation pattern by putting extra patch dipoles so that the gain is $>$ -8 dBi at all theta and phi angles and $>$ -6 dBi at all theta and phi angles for S-band and GPS-band antennas; respectively, except for excluding those within three degrees of axial nulls;
6. Improvement in axial ratio(AR) for GPS-band antenna array installed on the cylindrical sub-payload.

1.3.1 Effect of Temperature on the Substrate and Antenna Properties

The effect of temperature on the properties of substrate material should be studied to design conformal antennas for space-borne missions. Substrate materials may be exposed to high temperatures during flights and it may cause their thickness and dielectric constant to change [4]. The substrate material used for the feedline design of patch antennas was FR-4. Permittivity of this substrate was 5.2 [3]. It is important to check the effect of temperature variations on dielectric constant of substrate and hence on the properties of conformal antennas. We conducted a study on that by changing the dielectric constant of

FR-4 by ±10 percent and compared the results with the case when $\epsilon_r = 5.2$ (standard case). We changed the dielectric constant of substrate in HFSS and carried out simulations for $\epsilon_r = 4.68$, $\epsilon_r = 5.2$, and $\epsilon_r = 5.72$. Simulation model is shown in figure 1.2. This is a three-layered structure. The first two layers (starting from the innermost substrate) are made of FR-4 substrate and material for the outermost layer is Rogers 6002. There are four S-band antenna and four GPS antennas mounted alternately on the Rogers 6002 board surface and this study has been performed by exciting four GPS antennas. Plots from the simulations have been presented in section A.1 of Appendix A. Main observations from these results are as follows :

1. It can be seen from figure A.1 to figure A.3 that design is tolerant for the change in S_{11} parameters when dielectric constant changes by ±10 percent. Though the curves shift to the left (for $\epsilon_r = 5.72$) and right ($\epsilon_r = 4.68$) but the difference is not appreciable. From the formulas of strip lines , we calculated that change of ±10 percent in dielectric constant brought a change of 5 ohm (for $\epsilon_r = 4.68$) and 4.65 ohm (for $\epsilon_r = 5.72$) in the characteristic impedance of the strip line because there is an inverse square root relationship between characteristic impedance of the stripline and dielectric constant.

2. Minimum gain points (for 2-D gain plots at theta = 90 degree) are shifting inward for $\epsilon_r = 5.72$ due to greater loss. At GPS center frequency (1.575 GHz) the minimum gain point is -6.54 dB. For 3 percent higher frequency (1.622 GHz) and 3 percent lower frequency (1.527 GHz) minimum gain points are -9.93 dB and -7.56 dB, respectively. For $\epsilon_r = 4.68$ the gain curve is improved at the center frequency (1.575 GHz) which is due to the lesser losses. Value of minimum gain points for 1.575 GHz, 1.527 GHz, and 1.622 GHz are -6.38 dB , -9.42 dB and -9.16 dB, respectively. It means that minimum gain points for both cases ($\epsilon_r = 5.72$ and $\epsilon_r = 4.68$) tend to go below -8 dB, when 3 percent frequency shift occurs. All of these results have been shown from figure A.13 to A.21 in Appendix A.

3. From the vertical cuts of the 3-D gain pattern, the conclusions are same as described in point No. 2. The minimum gain point for $\epsilon_r = 5.72$ is -25.59 dB while it is -23.52

dB and -22.50 dB for $\epsilon_r = 5.2$ and $\epsilon_r = 4.68$, respectively. All of these results have been shown from figure A.22 to A.30 in Appendix A.

4. Axial ratio is critically dependent on the magnitude of corner truncations and location of feed point for the patch antennas which has not been changed, so axial ratio is not disturbed appreciably due to variation of dielectric constant at center frequency. However when the frequency shifts by ± 3 percent, values of axial ratio deteriorates badly even for the case when $\epsilon_r = 5.2$. So it is imperative that to maintain a good axial ratio there should be minimal change in the GPS center frequency. Plots have been shown from figure A.31 to A.33 in Appendix A.

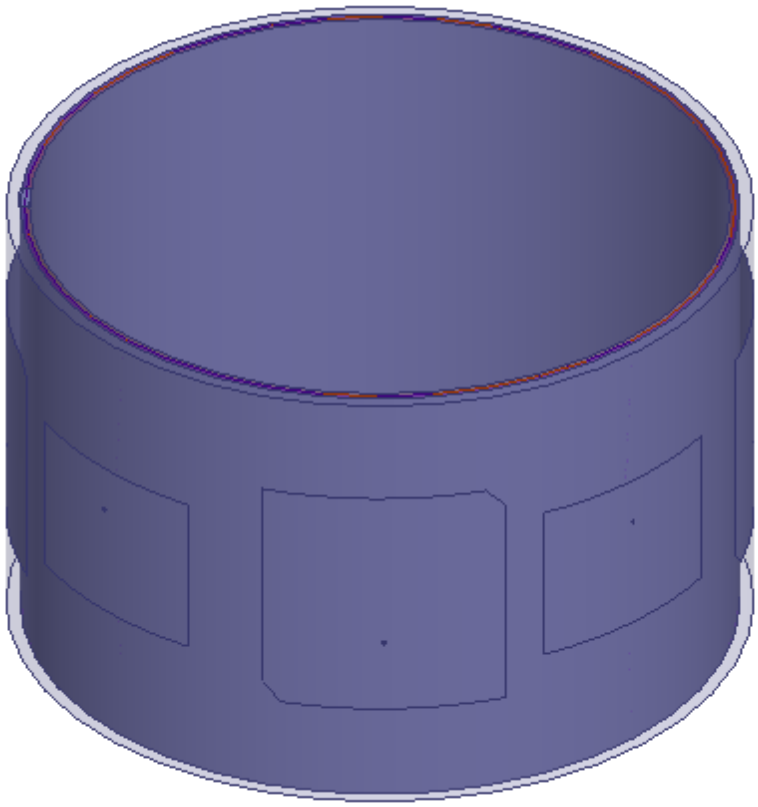

Fig. 1.2: Figure of the assembly that was simulated in HFSS.

1.3.2 Changes in the Substrate Material for First Two Layers of Multi-layer Design

Substrate used for designing feedlines in the previous ASSP antenna design [3] was FR-4 (G10) and it was changed to Rogers 6002 material, after having some meetings with SDL. It was suggested that Rogers material should be used for both the feedline and antenna designs. Rogers 6002 was proposed for this design since it is bendable material which is the essential requirement for designing antennas on cylindrical sub-payload.

Rogers 6002 material comes in the standard thicknesses of 5 mils, 10 mils, 20 mils, 30 mils, 60 mils and 120 mils [5]. Substrate for the patch antennas (outermost layer) was already Rogers 6002 and had a standard thickness of 120 mils so it was not changed. A market survey was carried out to optimize the thickness of feed lines and cost of respective substrate to make a right selection. We chose Rogers 6002 board with standard thickness of .762 mm to design feedlines. The minimum width of the 50 ohm trace using this board was calculated to be 1 mm. The analysis has been summarized in the Table 1.2.

1.3.3 Changes in the Feedline Design

Since the substrate for the feedlines was changed hence their widths were needed to be redesigned. Width of a stripline trace for any given impedance depends on the dielectric constant of the substrate [6]. Secondly feedlines as used in the previous designs did not have the terminations at the points where they practically had to be. After having a meeting with Space Dynamics Lab, we were given the aluminum core that was the base of cylindrical payload. We exported the .stp file to HFSS and fixed it inside our multi-layer structure so that feedlines could be laid out accordingly. Another purpose was to include air holes in the previous multi-layer structure in congruence with aluminum base so that their effect may be simulated in HFSS for rigorous analysis. Geometry of the aluminum core has been shown in the figure 1.3. There were 32 additional air holes that needed to be made in the multilayer structure. After finishing this task, the feedlines were redesigned and has been shown in figure 1.4.

Table 1.2: Comparison of Roger's board for feedline thickness and cost.

Material	Standard Thick-ness(in mm)	Standard Thick-ness(in mils)	Usage	Minimum Width of the Strip line Trace (in mm)	Price of 24×18Penal Board from Rogers
Rogers 6002	.127	5	Just for comparison	.1	675
Rogers 6002	.254	10	Just for comparison	.3	675.93
Rogers 6002	.381	15	Just for comparison	.5	675
Rogers 6002	.508	20	Just for comparison	.6	727.09
Rogers 6002	.762	30	Feed line Design	1	787.69
Rogers 6002	1.524	60	Just for comparison	2	787.69
Rogers 6002	3.048	120	Antennas design	2	787.69

1.3.4 Planar S-band Antenna with Suspended Middle Metal Layer and Grounded Middle Metal Layer

The concept of suspended middle metal layer and grounded middle metal layer is explained in figure 1.5 and figure 1.6. Firstly the single S-band antenna was designed at 2.22 GHz on a multi-layer planar substrate and was simulated to check, how the suspended ground affects the radiation properties and reflection coefficient. This antenna was excited by 50 ohm coaxial probe. Simulation model is shown in figure 1.7. Results from the sim-

ulations are presented below from figure 1.8 and 1.9. Reflection coefficient for suspended ground is -29 dB and reflection coefficient

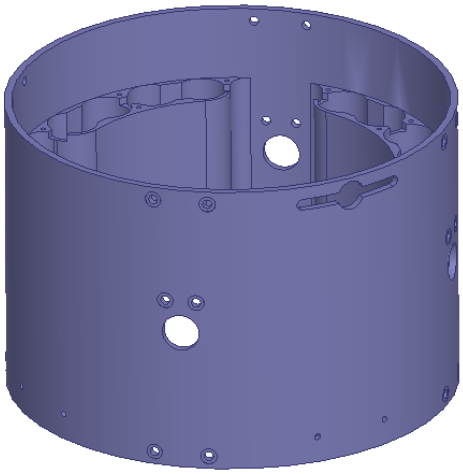

Fig. 1.3: Core of the sub-payload to be placed under the multi-layer substrate.

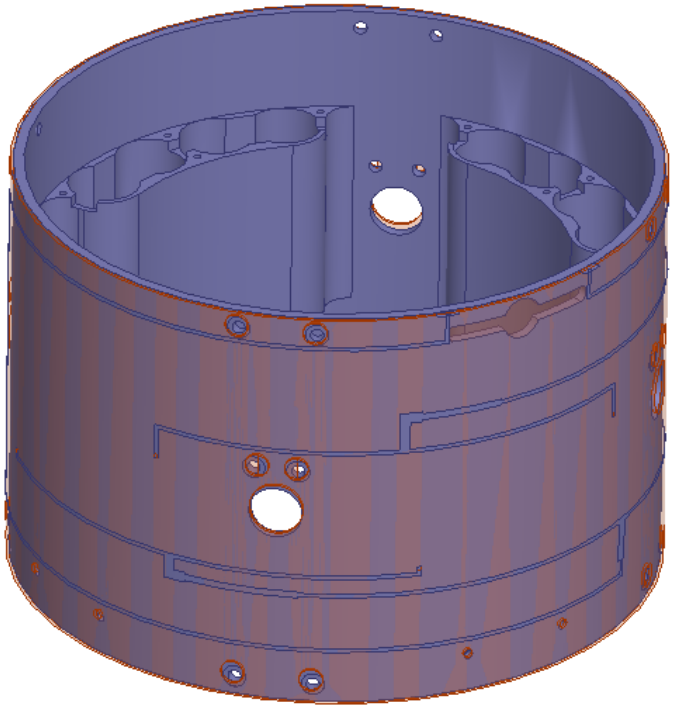

Fig. 1.4: Feedlines after the redesign.

for perfect ground is -34 dB at 2.22 GHz. There are more than one resonances (2.16 GHz and 2.22 GHz) for suspended ground case. This is due to the fact that modes other than TEM mode are also propagating in the feedline due to the inclusion of suspended metal sheet. The gain plot at both resonant frequencies were checked and it was found that resonance at 2.16 GHz was spurious. Comparing figure 1.10 and figure 1.11, it can be observed that there was loss of gain for the case when the second ground plane was suspended. The length of antenna with suspended ground was 37.3 mm. The length of antenna with perfect ground was 36.4 mm. Hence it can also be concluded that size of antenna and overall geometry did not change much with the inclusion of suspended ground for a single S-band antenna over multi-layer structure.

1.3.5 Planar S-band Array Antennas with Suspended Middle Metal Layer and Grounded Middle Metal Layer

As our goal was to incorporate suspended ground in real design, so we extended the same concept to compare the design of S-band array with suspended ground and perfect ground on a planar multi-layer structure. Geometry for this simulation model has been shown in figure 1.12.

All the parameters (dimensions of S-band antennas and feedline design etc.) have been kept the same as for the cylindrical structure. In other words, design of four S-band antennas have been translated to their equivalent planar geometry. For simplicity, the air holes due to screws and booms have not been included in this model. This simulation was run for both perfect and suspended ground on multi-layer structure.

Pattern of S_{11} plots is same as for the cylindrical structure. It is apparent from the reflection coefficient curves in figure 1.13 and figure 1.14 that antennas are not well-tuned at 2.22 GHz. It is due to the reason that tuning of various parameters was not done for planar model. Reflection coefficient for both the cases at 2.22 GHz is almost -6 dB. Inclusion of suspended ground is causing more losses (almost 1.2 dB in this case) as compared to the case when ground is perfect.

Gain plots are shown in figure 1.15 and figure 1.16. Due to planar structure, the shape

of 3-D gain plots is different from the cylindrical structure. It is more directive and is concentrated along z-axis, whereas in the cylindrical case we were taking benefit of circular symmetry and 3-D gain curve was omni-directional.

1.3.6 Cylindrical S-band Array of Antennas with Suspended Middle Metal Layer and Grounded Middle Metal Layer

After finishing the simulations on planar models, we put single S-band antenna on cylindrical structured without the inclusion of booms and air holes and checked simulation results for both perfect ground and suspended ground. Simulation model is shown in figure 1.17. Results from the simulation are shown from figure 1.18 to figure 1.19.

As a next move, four S-band antennas were put together on multi-layer cylindrical substrate and were fed separately with coaxial probes. The simulation model is shown in figure 1.20. There were no booms and air holes included in this design. The results have been shown from figure 1.21 to figure 1.22. After finishing the simulation for four S-band antennas on cylindrical substrates, four GPS antennas were added to the structure and the structure shown in the figure 1.23 was simulated. GPS antennas were not excited. The were no booms or air holes added in this structure. Reflection coefficient and gain plots for these simulations are shown from figure 1.24 to figure 1.29.

1.3.7 Summary of the S-band Antennas on Cylindrical Structure with Air Holes and Long Booms

When we tried to simulate the structure with suspended ground (with air holes included) and kept everything else the same as for perfect ground, it was taking too long to generate results and simulation was getting stuck at due to very large number of mesh elements in HFSS. Then we studied about different options as how the complexity of problem could be reduced. After solving the problem and getting the simulation results for suspended ground (with holes in structure) for S-band antennas, it was observed that S_{11} curve did not have sharp resonance at 2.22 GHz.

To eliminate the possibility that our simulation results might be wrong, we started

debugging the problem by simulating single S-band antenna with suspended ground and perfect ground on a plane and then kept on adding different levels of complexities. We ran the simulations of four S- band antennas for planar structure for both the suspended ground and perfect ground. It was confirmed that, suspended ground case was giving more than one resonances for planar case, which was spurious and could be neglected due to very low gain values.

So the task was to get good resonance (at least lower than -10 dB at 2.22 GHz) after inclusion of holes while keeping the ground as suspended. Since there were no other variables in the structure other than to change the dimensions of S-band antennas and feedline, so we tried to modify them and tune them to get optimum response. Changing the widths of feedline was not giving good results and that was also changing different parameters in the simulation model that were supposed to be kept constant. So the better option was to change the feed point of antennas to have a good match of impedances between the feed line terminations and antennas. So we ran series of simulations to get a good reflection coefficient at 2.22 GHz without inclusion of long booms. After getting good results then we moved on to include the long booms and results of that final design are being presented in the next section.

1.3.8 Approaches in Gain Pattern Conditioning of S-band Antennas

Requirement of gain for S-band antennas as described in the document provided by SDL was that "S-band antenna gain desired to be $>$ -8 dBi at all theta and phi angles, excluding those within 3 degrees of axial nulls." In the results presented until now, we were not able to achieve this goal. Since we had a limited space left on the cylindrical substrate after inclusion of S-band and GPS-band patch antenna array so we thought to add microstrip dipoles to fill in the areas of low gain.

Rectangular microstrip antennas can be classified into two main categories depending on their length-to-width ratio. An antenna with a narrow rectangular strip (typically strip width less than $.05\lambda$) is called microstrip dipole, whereas a broad rectangular antenna is called mircostrip patch. In addition to the microstrip dipole, another popular configuration

is the center-fed dipole. This geometry is a printed version of the free-space cylindrical dipole. The geometries of microstrip dipole and the rectangular patch being similar, their radiation characteristics are also expected to be similar. The longitudinal current distribution for the fundamental mode are similar on both structures. Therefore, their radiation patterns and gains are also similar [7]. The microstrip dipole has been rigorously compared with the microsrtip patch in terms of resonant length, resonant resistance, bandwidth, surface wave loss and mutual coupling. Microstrip dipoles have been designed and discussed in several papers; see in particular [8–10]. Radiation properties of microstrip dipoles have been discussed by Uzunoglu et al. [11] using surface current model.

1.3.9 Experiments before Addition of Microstrip Dipoles

Before adding the microstrip dipoles on the array of S-band and GPS-band antennas, we did two types of simulations as listed below.

1. In first simulation, we simulated all the four S-band antennas removing the four GPS-band antennas. Hence there were total of eight S-band antennas and all of them were excited.

2. In the second simulation, we removed four GPS-band antennas and replaced them with four S-band antennas and we kept these four S-band antennas as parasitic elements. In other words, we simulated eight S-band antenna with four of them as active elements while the rest of them were parasitic elements.

The impetus of doing these simulations was to check if replacing the GPS antennas with S-band antennas could give the gain pattern as required, though it was not correct practically, since we had to install the GPS antennas on the cylindrical model too. The first simulation in which four GPS-band antennas were replaced with four S-band antennas and all of the eight S-band antennas were excited, was giving omni-directional radiation pattern and did not have any nulls worse than -8 dB except for in the axial direction as shown in figure 1.30. For the results in second simulation, nulls were going down to -33 dB and -31 dB

and hence it was proved that four S-band antennas were not enough to generate a radiation pattern such that there is no null worse than -8 dBi, except for the axial nulls. The results for this simulation are shown in figure 1.31.

1.3.10 Adding Microstrip Dipole Antennas on the Cylindrical Model

As discussed in section 1.3.9 that radiation pattern due to microstrip dipole has same characteristics as a microstrip patch antenna so these printed dipoles can be utilized to condition the low gain regions of S-band antenna array by placing them in the gaps between S-band and GPS-band antennas.

We started off by experimenting with single T-shaped microstrip dipole by putting it on planar substrate as shown in figure 1.32 and simulating it to see if it could resonate at 2.22 GHz or not. The antenna was fed with 50 ohm coaxial probe. The results of the simulation for model shown in figure 1.32 are presented from figure 1.33 to figure 1.35.

To observe the combined radiation pattern of four T-shaped microstrip dipoles, we moved on and put four dipoles on the cylindrical model. Air holes were also included in the simulation and dipoles were excited using coaxial probes. Simulation model is shown in figure 1.36. Results from the simulation are shown from figure 1.37 to figure 1.39. 3-D gain plot is omni-directional. The minimum gain for this case came out to be of the order -15 dB (figure 1.39).

Now we put these four dipoles along with GPS and S-band antennas on cylindrical substrate and simulated the full scale model. We wanted to check that how they can bring the axial nulls along the z-axis (i.e. that were around -25 dB without the dipoles) back to some minimum value. Four microstrip dipole antennas were simulated along with the S band and GPS antennas. The holes in the structure were included in the simulation. Simulation model and the results have been shown in section A.3 of Appendix A. These results were not favorable. The reasons that we understood after carrying a lot of simulations are described in following paragraph.

When we simulated the microstrip dipole antennas by placing them at symmetrically on cylindrical substrate without including the GPS and S-band antennas (case-I and shown

in figure 1.40), checked for the gain plots for their phi cuts, the nulls were of the order of -15 dB (figure 1.41). Since we already had an array of four GPS and four S-band antennas placed on the cylindrical substrate so we had to shift them up by 15 mm (case-II and shown in figure 1.42) due to which the dipoles array got closer to the upper edge of cylinder and the symmetry of gain plots got disturbed and nulls became deeper. When the dipole were shifted up the 15 mm, the value of minimum gain points plummeted down to -27 dB, as shown below in figure 1.43.

To keep the microstrip dipoles symmetrical around the center of cylindrical model, we experimented with microstrip dipoles with different shape since the T-shaped dipoles were not yielding the desired benefits. Twelve such microstrip dipoles were placed on the cylindrical model and were fed from their centers using coaxial probes. We were only able to get the gain plot for this model as the simulation in HFSS could not be completed due to intensive processing. Results for this simulation model are shown in section A.4 of Appendix A.

1.3.11 Observations and Discussions about the Results

From results shown in section 1.3.10, it can be seen that minimum gain points are -22 dB and -18 dB, respectively, after inclusion of 12 strip dipoles. The reason that we understood by exciting the dipoles one by one and by observing the gain pattern was that each dipole had its own nulls and maximas. We had limited space to put these dipoles on the cylindrical model and the maximas due to each dipole were not exactly adding up to the nulls of four S-band antennas that is why we were not noticing any significant improvement.

It can be seen in figure 1.44 that maximum gain points were occurring at an angles of phi = 5, 95, 187, and 275 degrees (theta = 90 degree plane) when we excited only four S-band antennas with all strip dipoles turned off. It can be observed (figure 1.45) that 12 strip dipole antennas were introducing nulls in theta = 90 degree plane at an angles of phi = 43, 133, 226, and 316 degree and these nulls were adding up in the gain plot of four S-band antennas and were causing to decrease the overall gain. Vertical gain cuts for both of these cases are shown in figure 1.46 and figure 1.47, respectively. Another point that we

noted was that when we excited the four S-band antennas with the eight dipoles that are indicated below in figure 1.48, there is best improvement in the deep nulls as compared to any other combination of excitations for the given set of antennas. The results are shown from figure 1.49 to figure 1.51. It can be seen that the deep nulls have values of -10 dB and -16 dB. When all the 12 strip dipoles were excited along with four S-band antennas, values of these nulls were -21 dB and -15 dB. From the vertical cuts it is also clear that 12 dipole antennas are not offering an incentive in the gain at those points where the S-band antennas are experiencing deep nulls.

1.3.12 Tuning of Axial Ratio for GPS-band Antennas

We tuned the truncated corners of GPS antennas to reach optimum AR at maximum gain points. The two truncated corners result in two diagonal orthogonal modes with a 90 degree of phase shift [12]. The angle of the corner truncation was kept 45 degree. Also, both corners were symmetrically truncated. Different truncations were tried using hit and trial in HFSS and the resulting AR plots for those truncations are shown in figure 1.52. Best AR was found out to be at truncation length = 6.95 mm.

1.3.13 Final Design Results of GPS Antenna Array after Inclusion of Suspended Metal Layer and Complex Feed Line

These results were obtained by exciting the GPS antenna array while turning off the excitation port for S-band antenna array. This simulation model includes all the air holes in the structure. Long booms were also included in the structure and were 332 mm long. Simulation results for parameters of interest are shown from figure 1.53 to figure 1.58. Reflection coefficient at 1.575 GHz is -9.19 dB. There was a trade off between getting good reflection coefficient and axial ratio.

1.3.14 Final Design Results of S-band Antenna Array after Inclusion of Suspended Metal Layer and Complex Feed Line

These results were obtained by exciting the S-band antenna array while turning off the

excitation port for GPS-band antenna array. This simulation model includes all the air holes in the structure. Long booms were also included in the structure and were 332 mm long. Simulation results for parameters of interest are shown from figure 1.59 to figure 1.64.

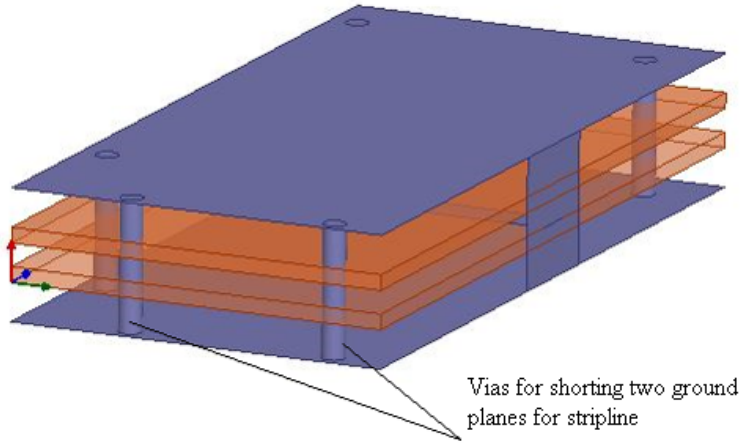

Fig. 1.5: Both the metal layers are connected (previous design).

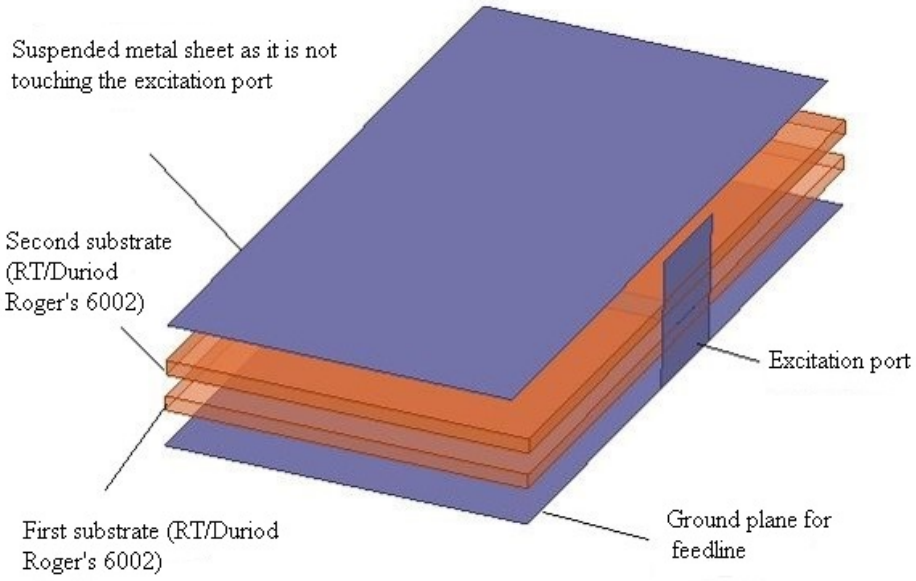

Fig. 1.6: Second metal layer is suspended (current design).

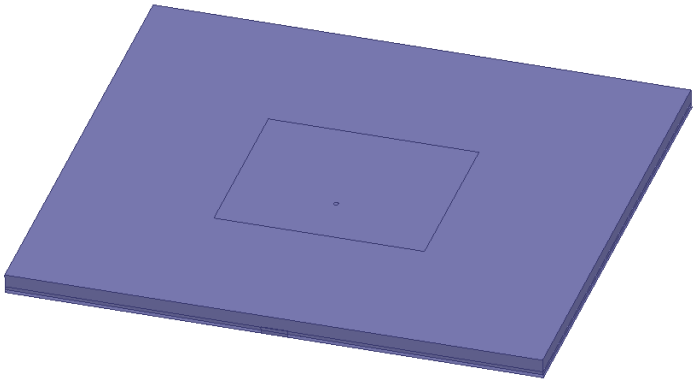

Fig. 1.7: Planar S-band antenna.

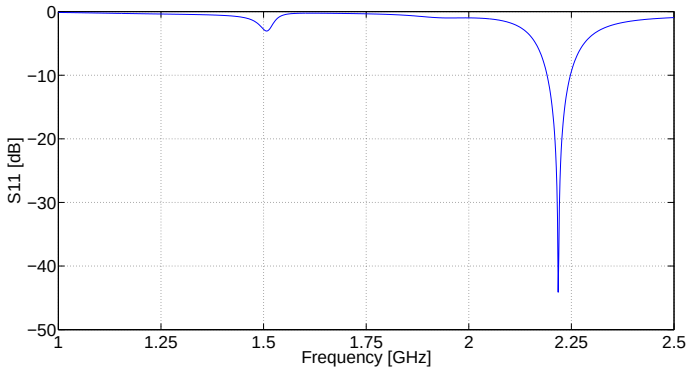

Fig. 1.8: Reflection coefficient for the case when second metal layer is grounded.

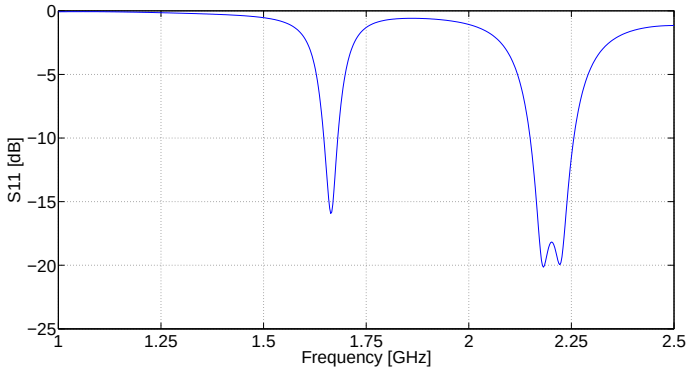

Fig. 1.9: Reflection coefficient for the case when second metal layer is suspended.

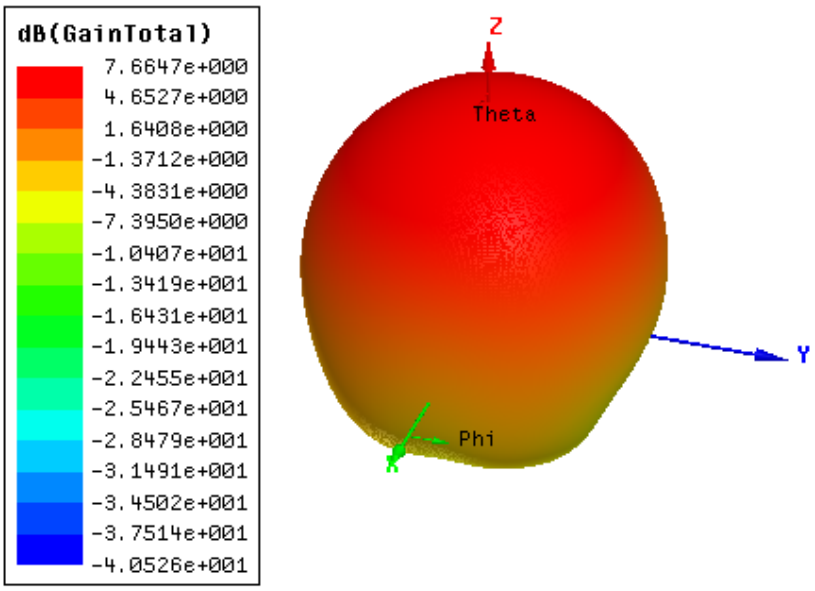

Fig. 1.10: 3-D gain plot when second metal layer is grounded.

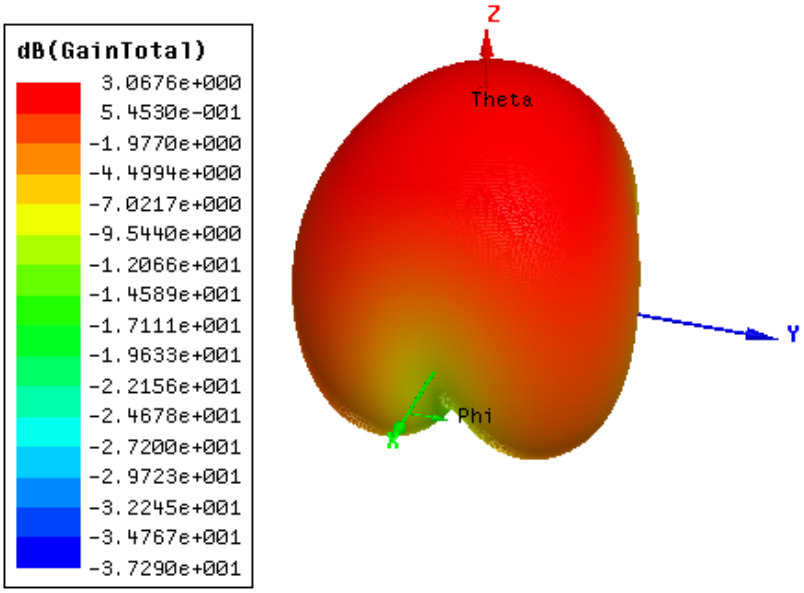

Fig. 1.11: 3-D gain plot when second metal layer is suspended.

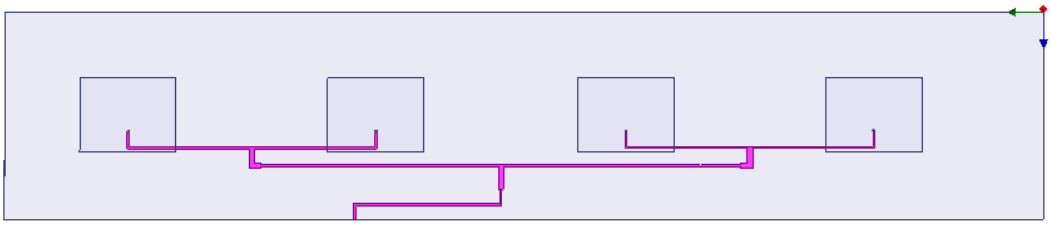

Fig. 1.12: Planar array of four S-band antennas.

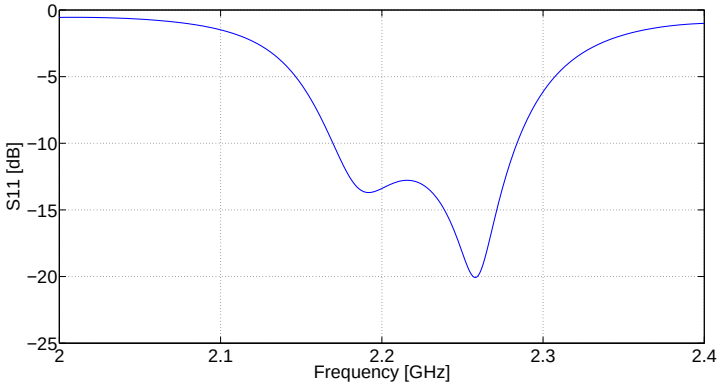

Fig. 1.13: Reflection coefficient for the case when two grounds are connected.

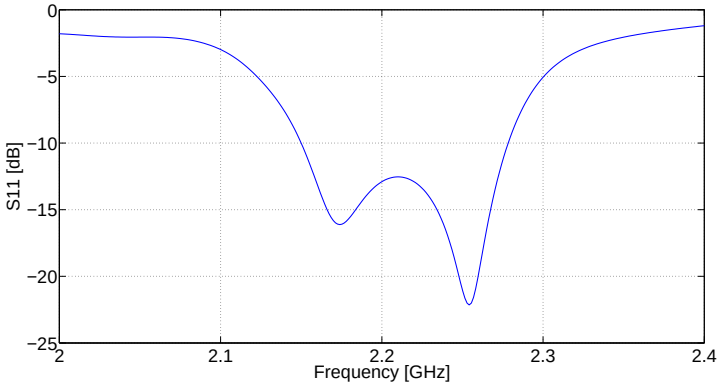

Fig. 1.14: Reflection coefficient for the case when second metal layer is suspended.

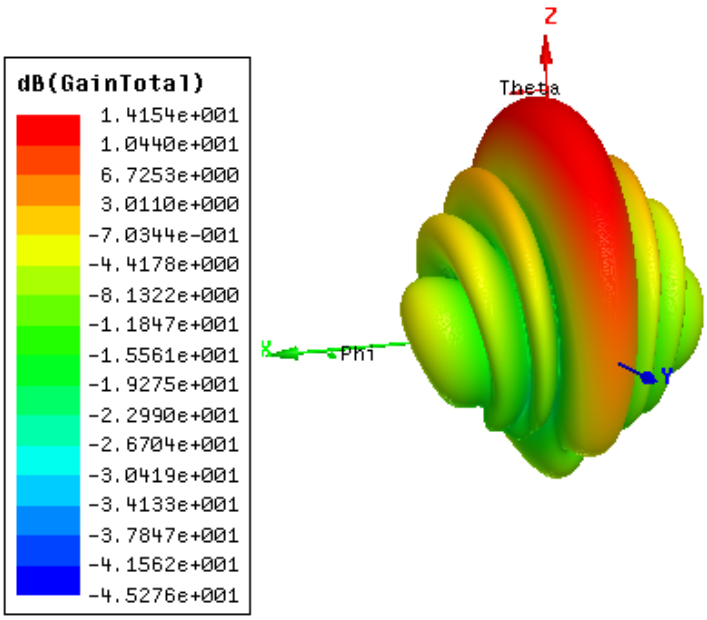

Fig. 1.15: 3-D gain plot for the case when both grounds are connected.

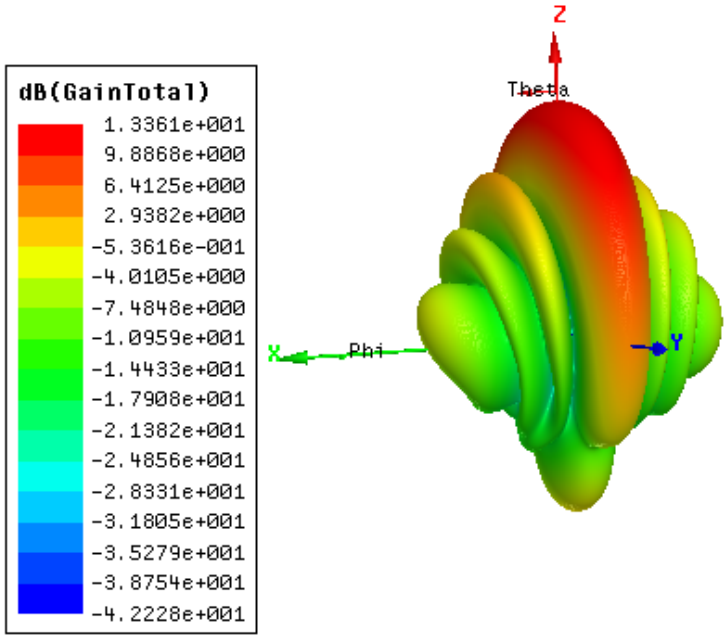

Fig. 1.16: 3-D gain plot for the case when second metal layer is suspended.

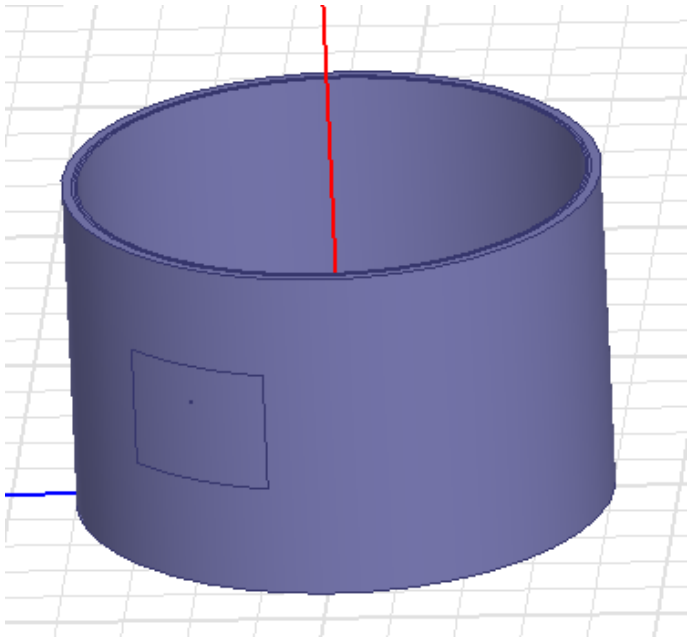

Fig. 1.17: Single S-band antenna on cylindrical structure with probe feed.

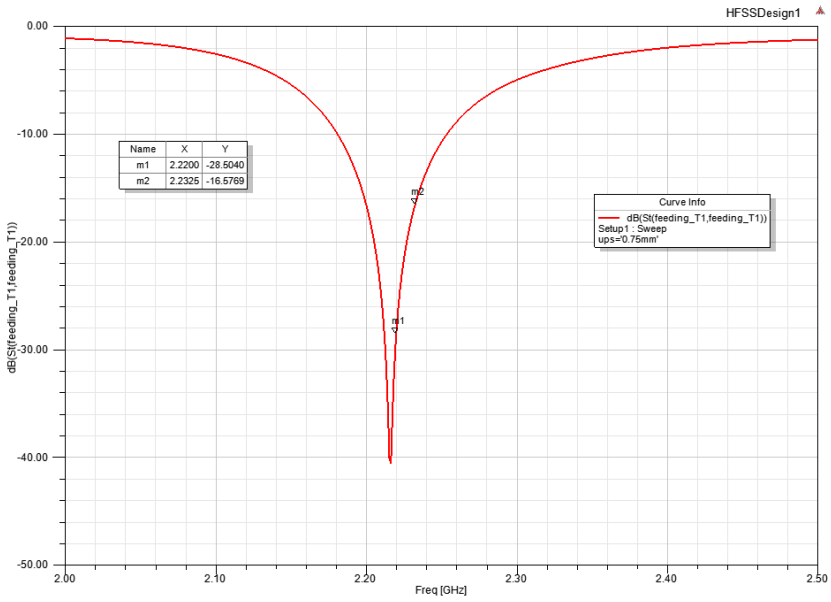

Fig. 1.18: Reflection coefficient for the case when two grounds are connected.

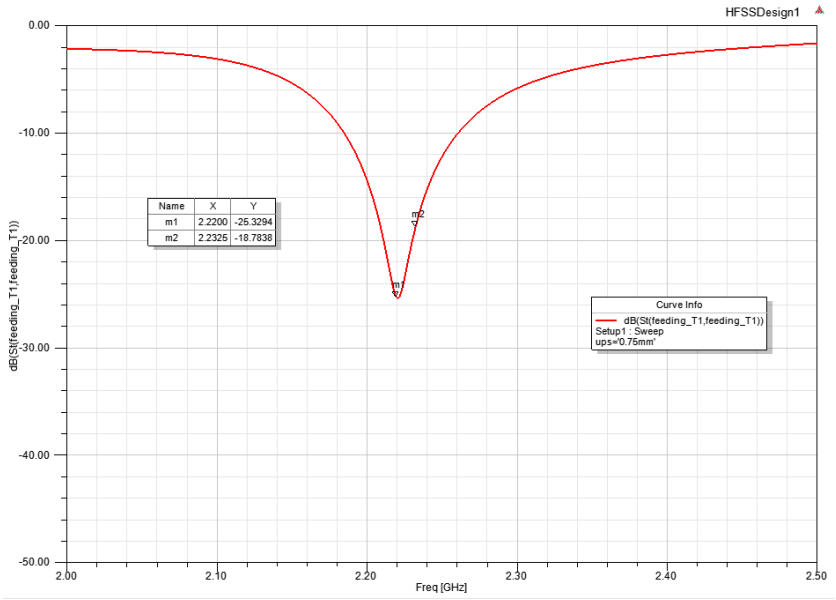

Fig. 1.19: Reflection coefficient for the case when second metal layer is suspended.

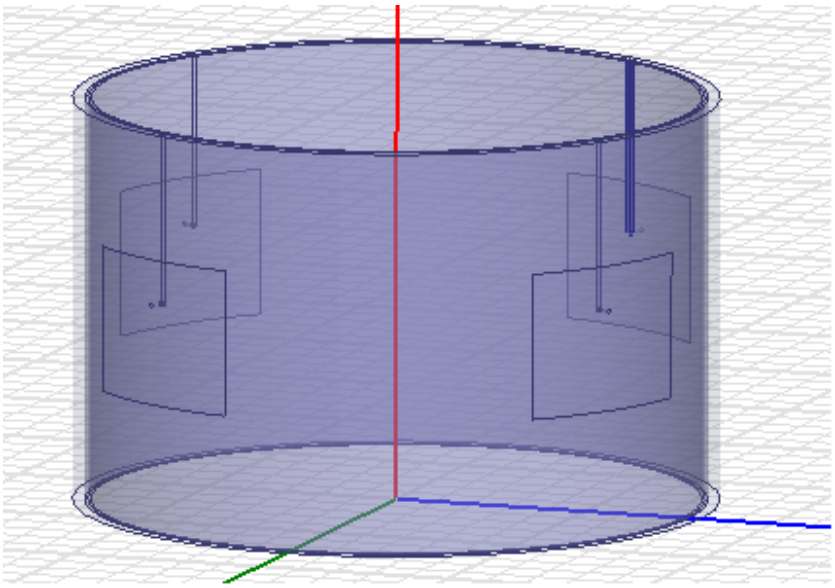

Fig. 1.20: Four S-band antennas on cylindrical structure with separate feeds.

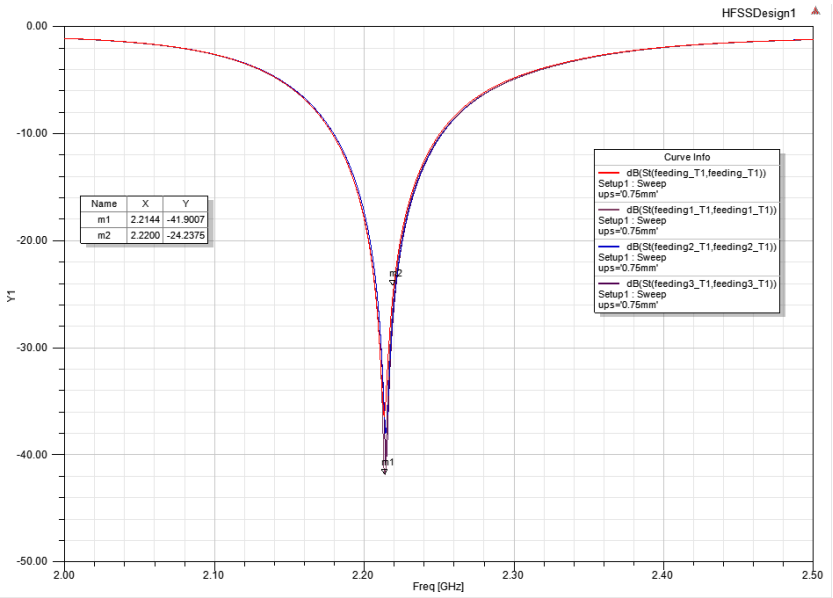

Fig. 1.21: Reflection coefficient for the case when two grounds are connected.

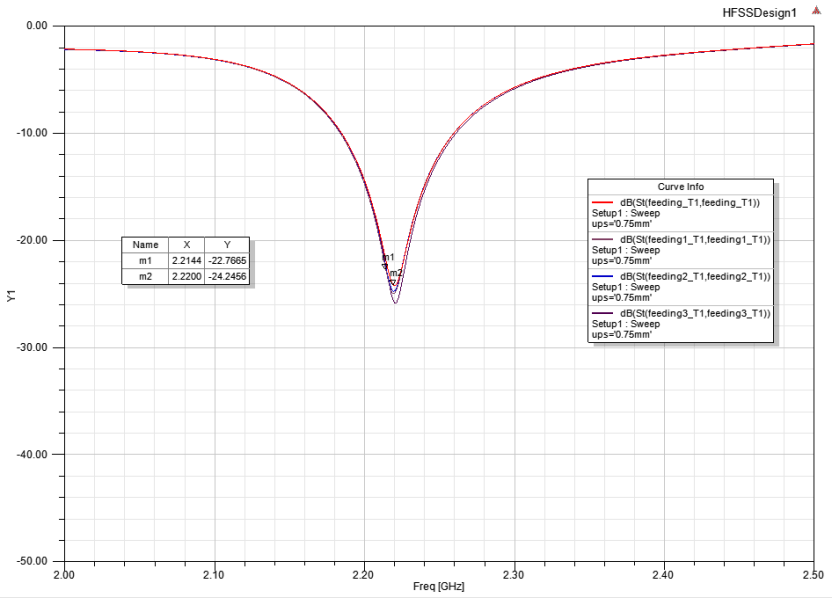

Fig. 1.22: Reflection coefficient for the case when second metal layer is suspended.

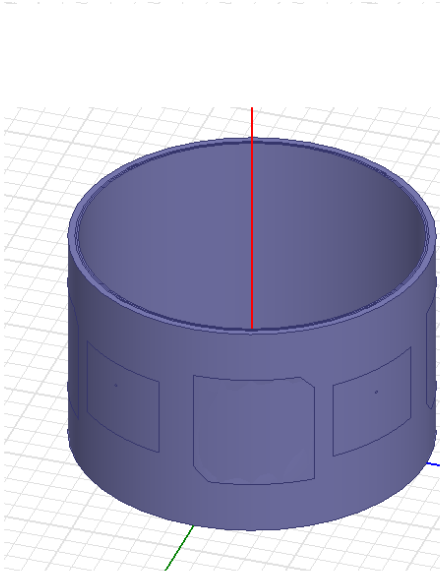

Fig. 1.23: Four S-band antennas with four GPS antennas added on cylindrical structure with separate feed (probe feed).

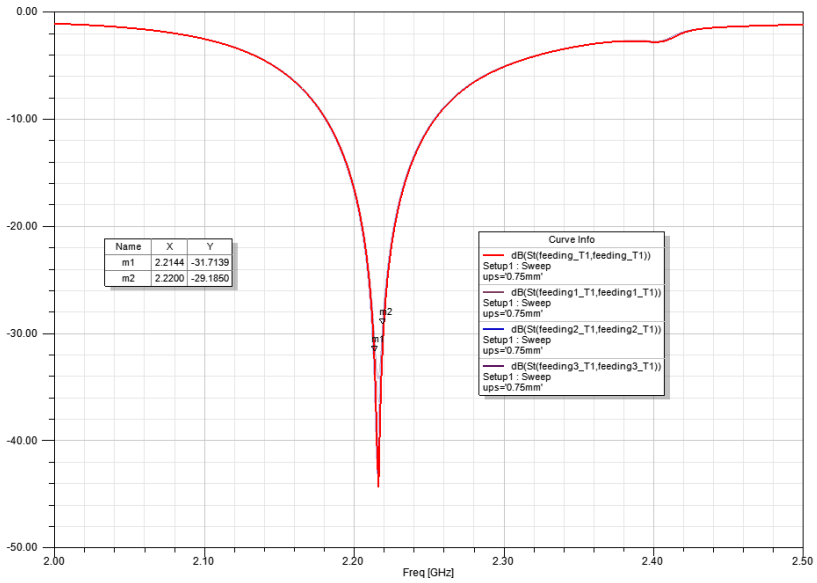

Fig. 1.24: Reflection coefficient for the case when two grounds are connected.

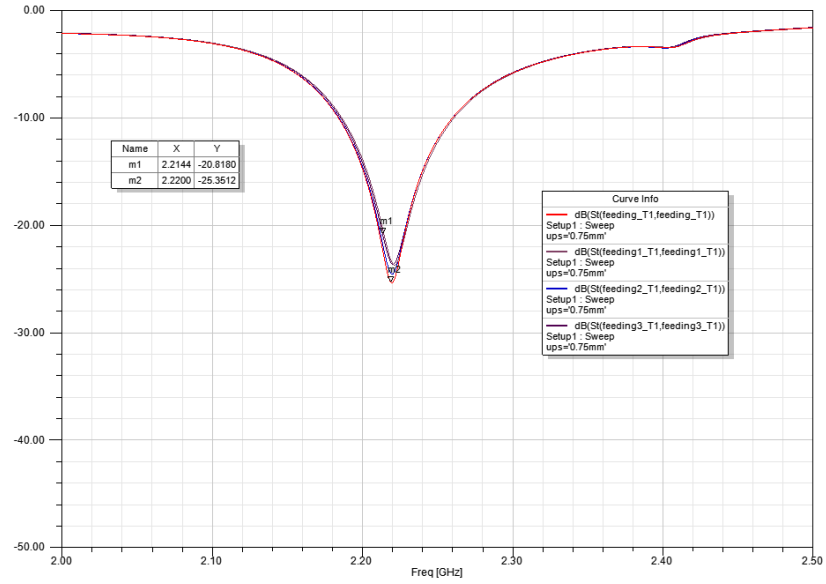

Fig. 1.25: Reflection coefficient for the case when second metal layer is suspended.

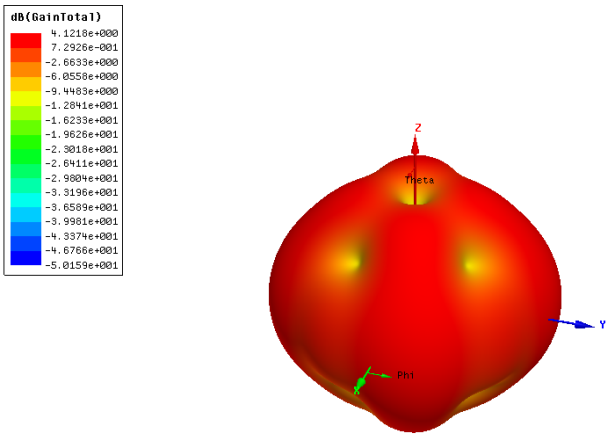

Fig. 1.26: 3-D gain plot when two grounds are connected.

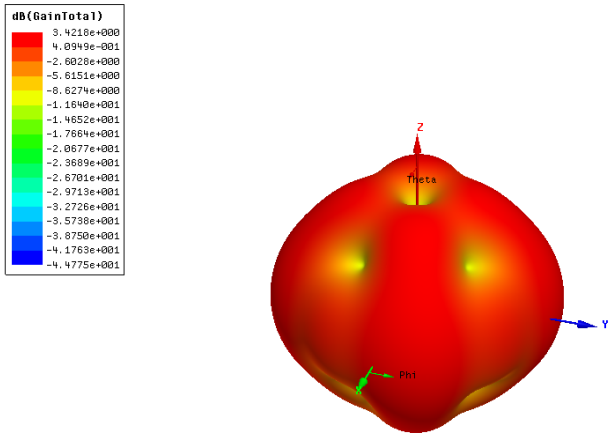

Fig. 1.27: 3-D gain plot when second metal layer is suspended.

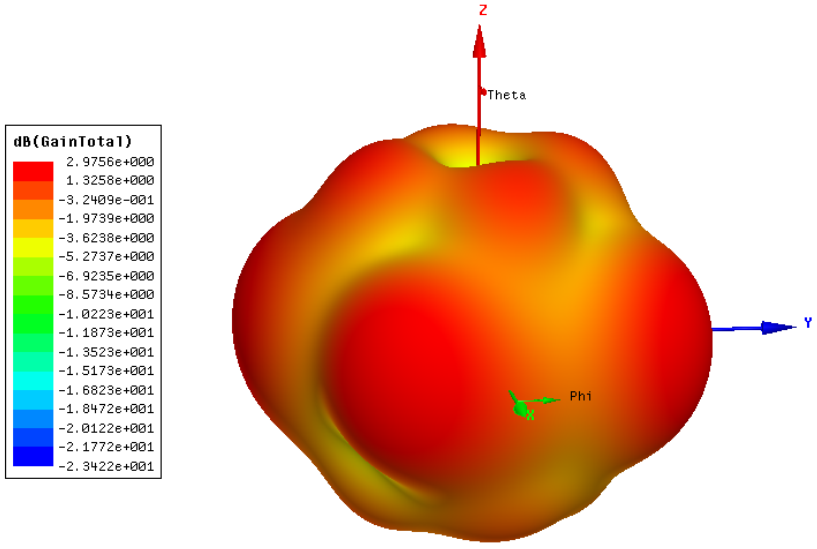

Fig. 1.28: 3-D gain plot (eight S-band antennas have been excited).

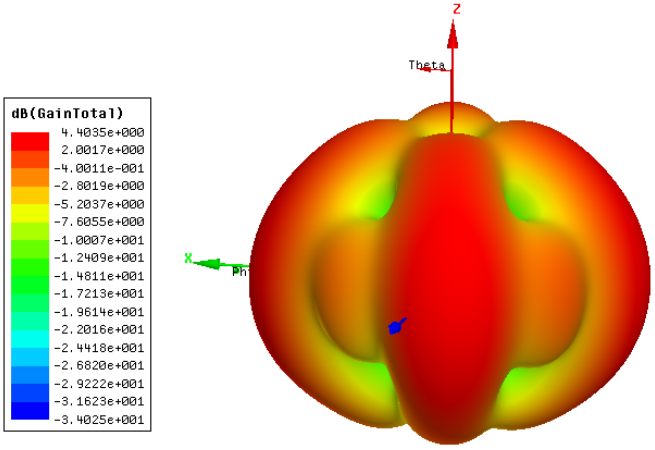

Fig. 1.29: 3-D gain plot of four S-band antennas excited and while four S-band antennas have been kept as parasitic elements.

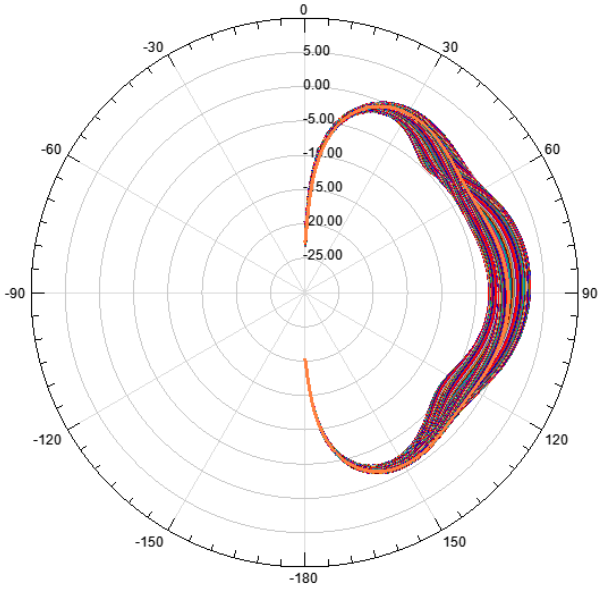

Fig. 1.30: 2-D gain pattern cuts for all phi (all eight S-band antennas were excited).

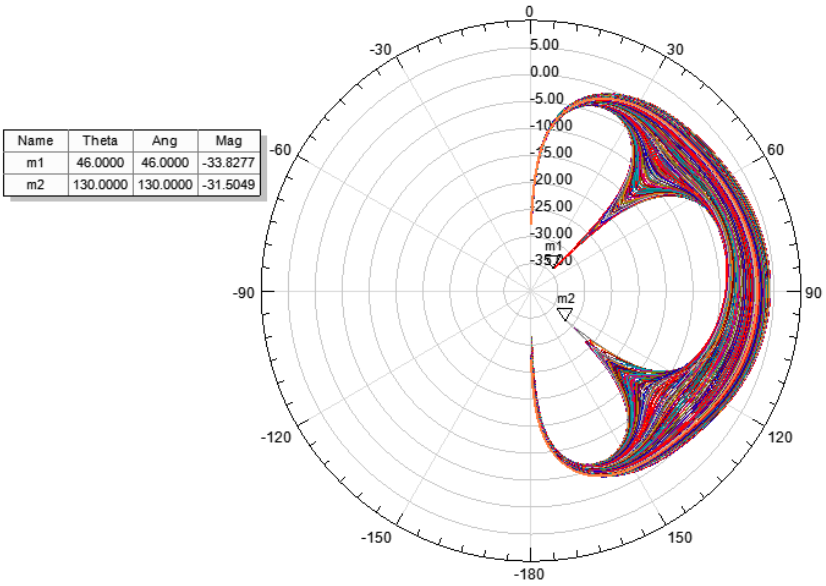

Fig. 1.31: 2-D gain pattern cuts for all phi (four S-band antennas excited and four were kept as parasitic elements).

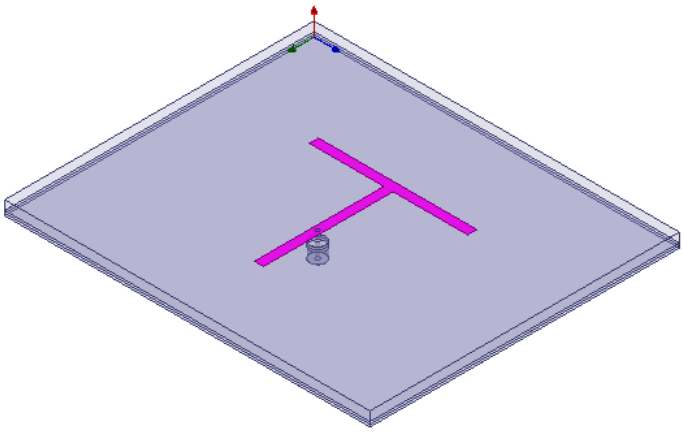

Fig. 1.32: T-shaped strip dipole fed by coaxial probe for 2.22 GHz.

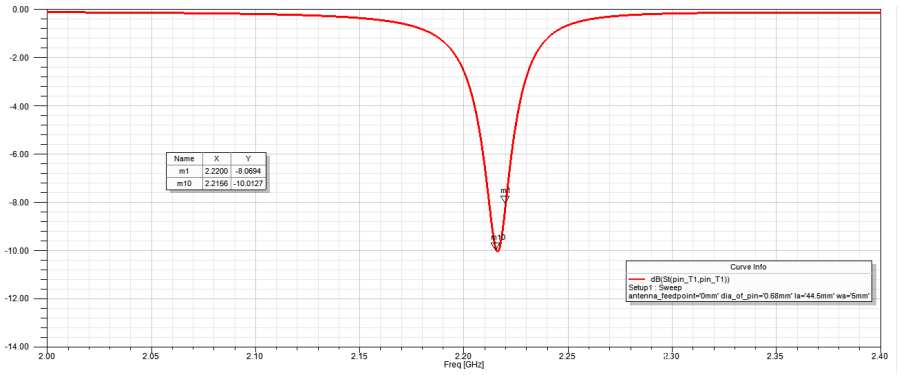

Fig. 1.33: Reflection coefficient of T-shaped microstrip dipole.

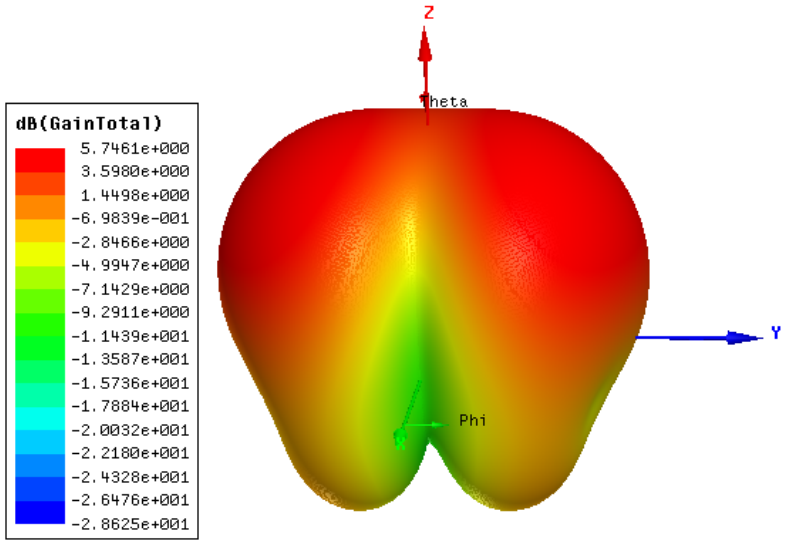

Fig. 1.34: 3-D gain plot of T-shaped microstrip dipole at 2.22 GHz.

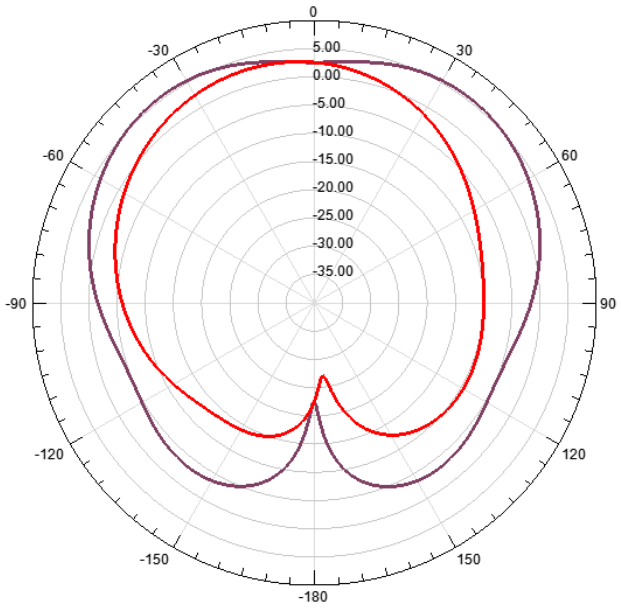

Fig. 1.35: 2-D gain plot at (phi = 0 degree and phi = 90 degree) of T-shaped microstrip dipole at 2.22 GHz.

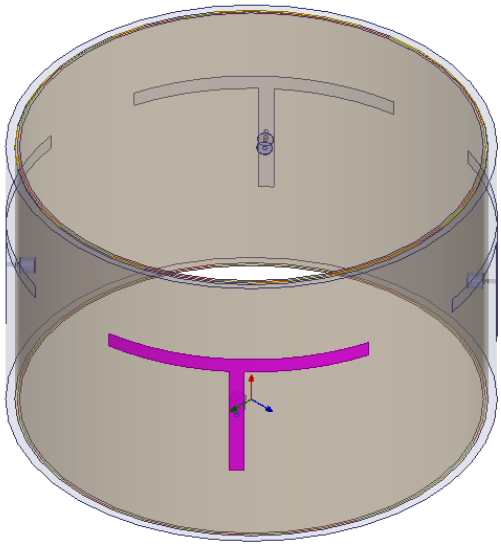

Fig. 1.36: Four dipoles on the cylindrical model (without GPS and S-band antennas).

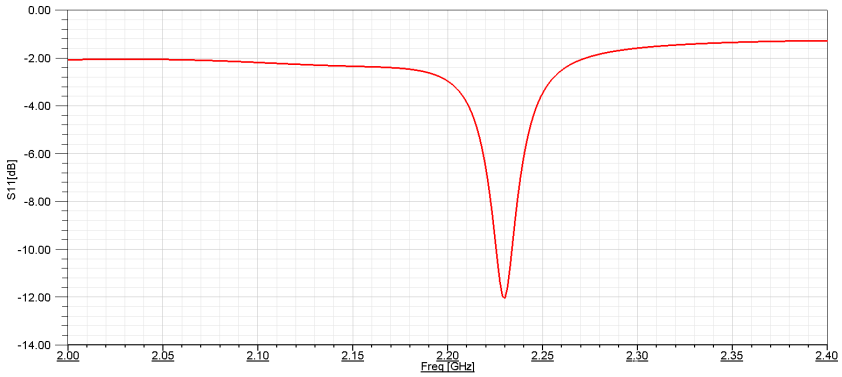

Fig. 1.37: Reflection coefficient of four T-shaped dipoles on cylindrical model.

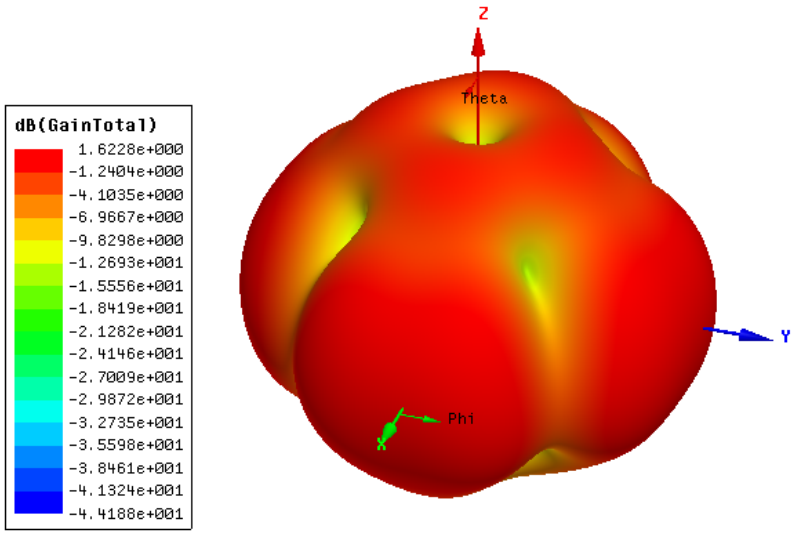

Fig. 1.38: 3-D gain plots of four dipoles on cylindrical model.

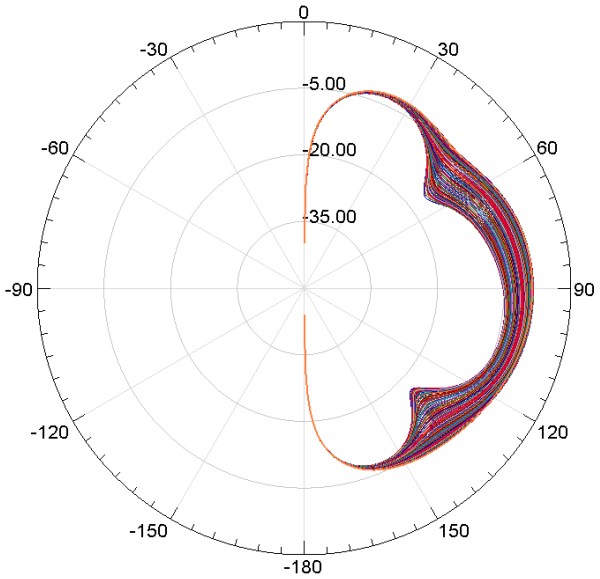

Fig. 1.39: 2-D gain plots of four dipoles on cylindrical model.

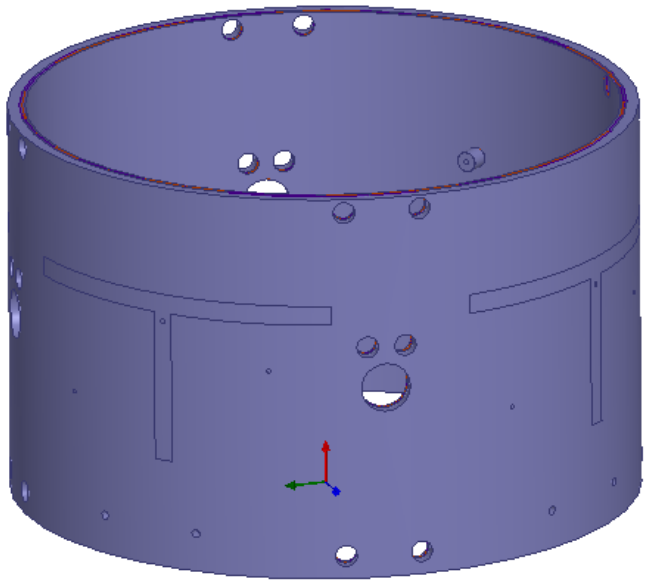

Fig. 1.40: Four microstrip dipoles placed symmetrically on the substrate (case-I).

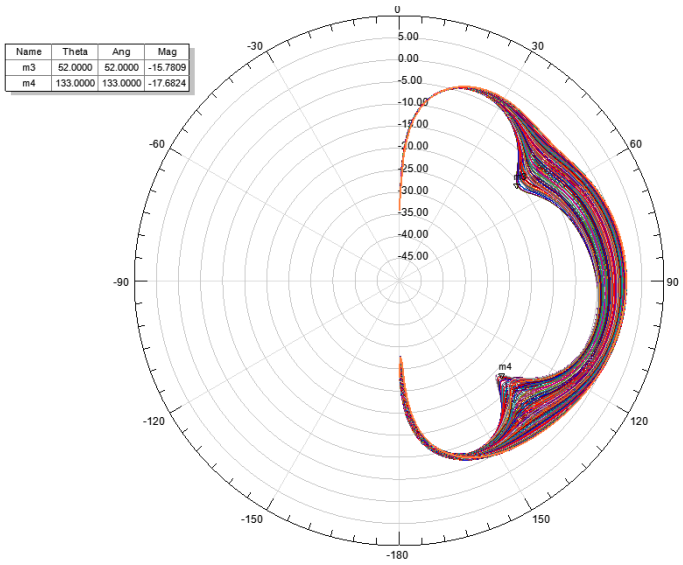

Fig. 1.41: 2-D gain cuts of four microstrip dipoles placed symmetrically on the substrate (case-I).

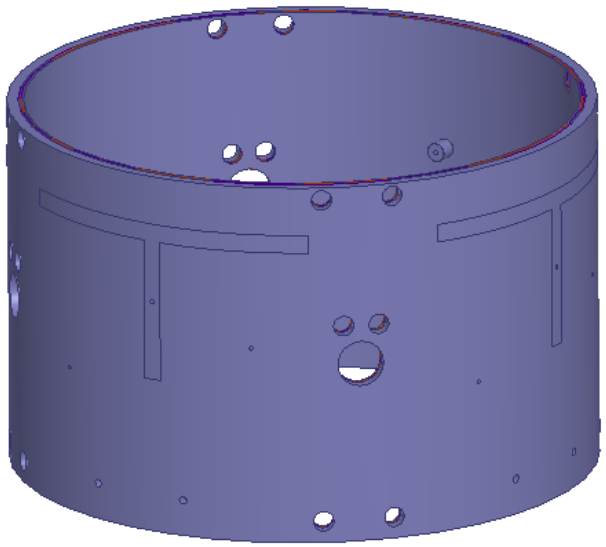

Fig. 1.42: Four microstrip dipoles placed symmetrically on the substrate and shifted up by 15 mm (case-II).

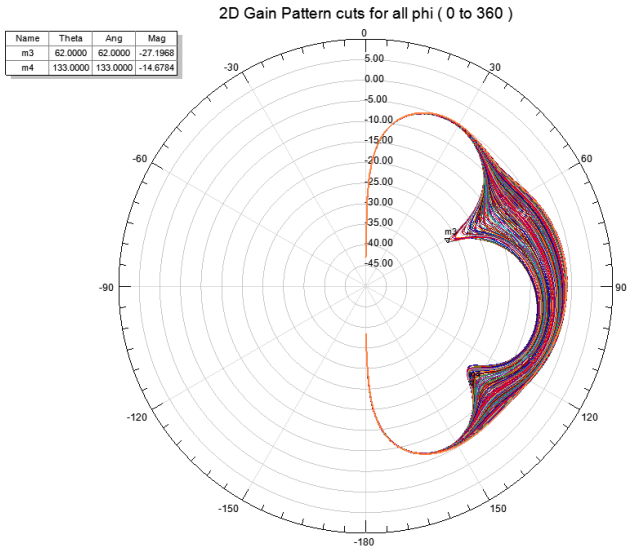

Fig. 1.43: 2-D gain cuts of four microstrip dipoles placed symmetrically on the substrate shifted up by 15 mm (case-II).

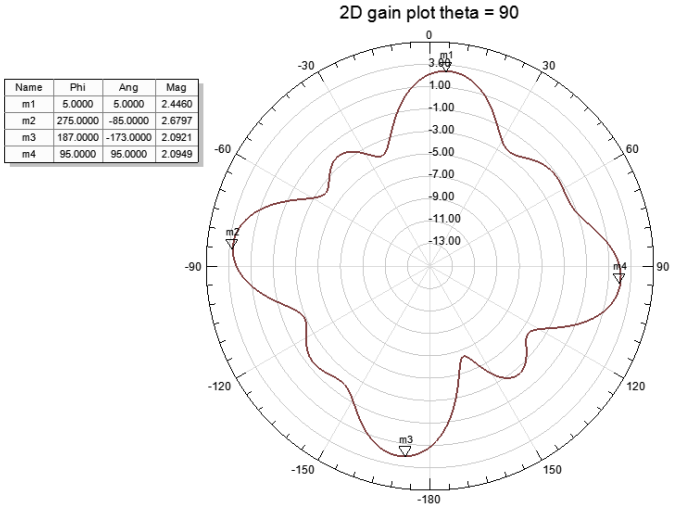

Fig. 1.44: Gain plot for four S band antennas excited (with 12 dipoles switched off i.e. source voltages = 0).

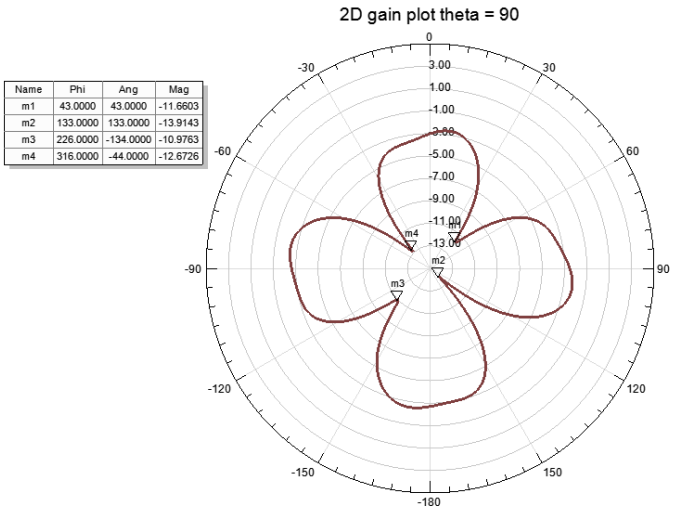

Fig. 1.45: Gain plot for 12 strip dipole antennas excited (with four S-band antennas switched off).

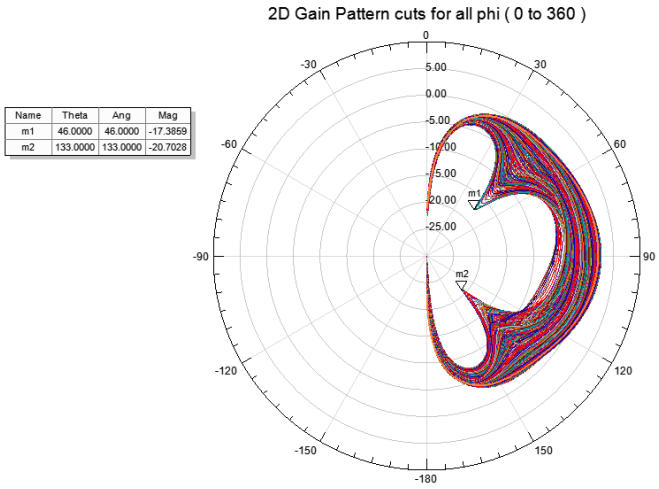

Fig. 1.46: Gain plot for four S-band antennas excited (with 12 dipoles switched off i.e. source voltages = 0).

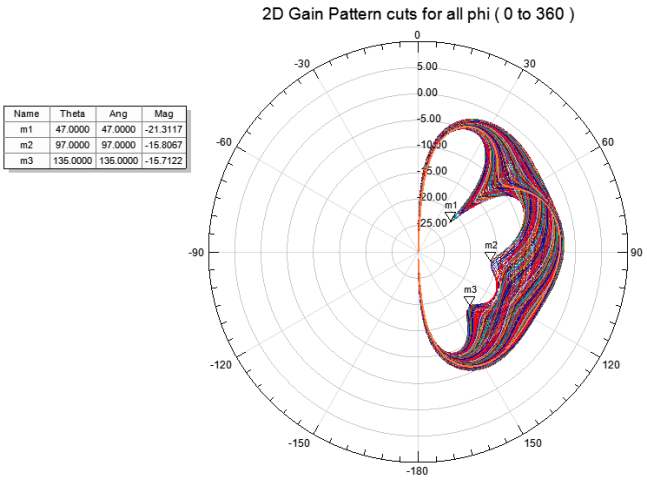

Fig. 1.47: Gain plot for 12 strip dipole antennas excited (with four S-band antennas switched off).

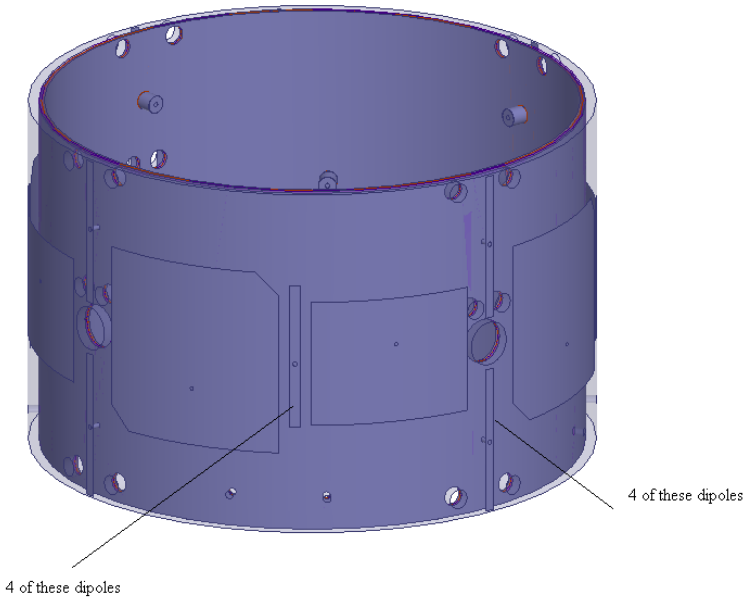

Fig. 1.48: Cylindrical model with 12 strip dipole antennas.

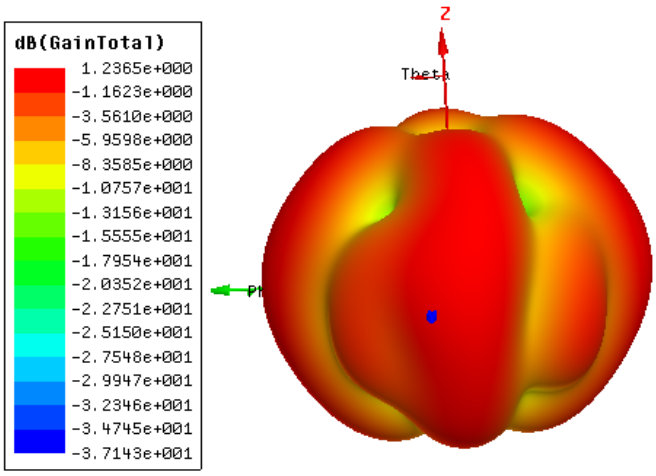

Fig. 1.49: 3-D gain plot.

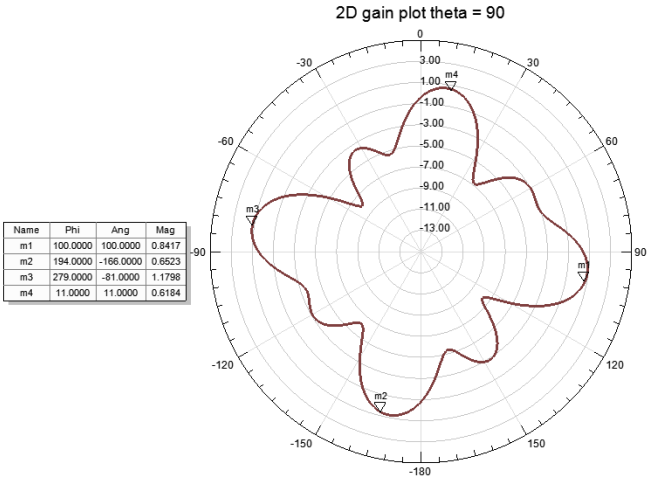

Fig. 1.50: 2-D gain plot for theta = 90 degree.

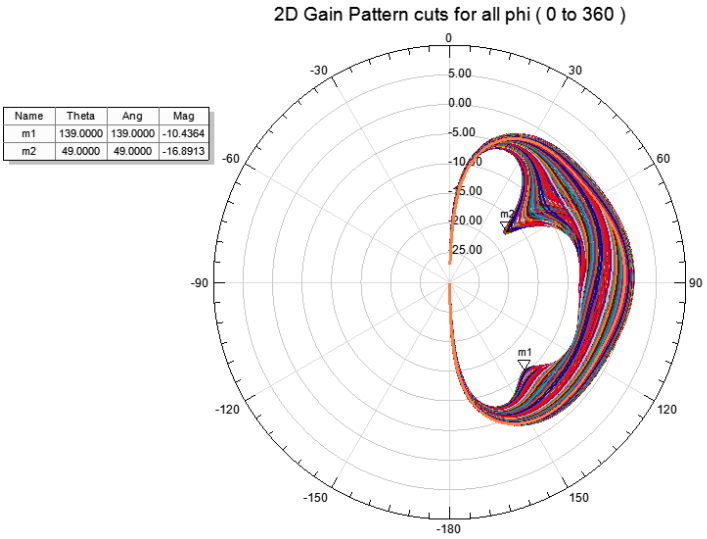

Fig. 1.51: Vertical gain cuts for all phi (0 degree to 360 degree).

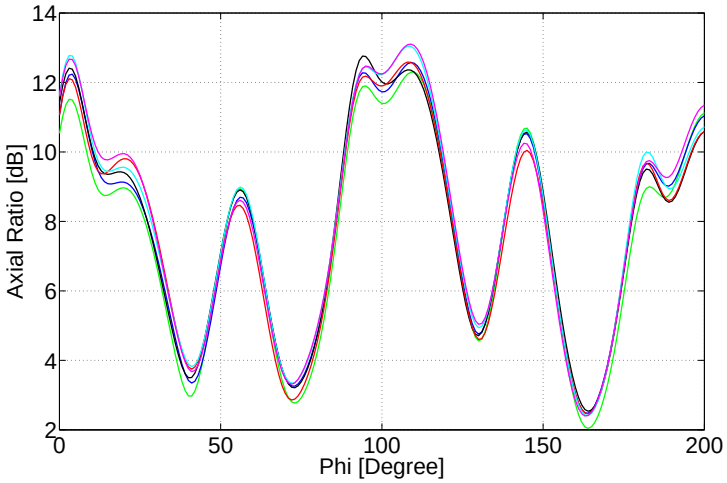

Fig. 1.52: Tuning of AR for GPS antenna array.

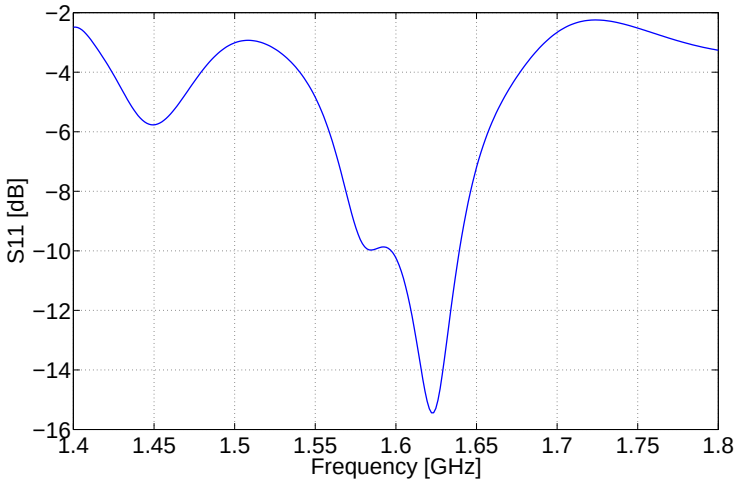

Fig. 1.53: Reflection coefficient of GPS antenna array.

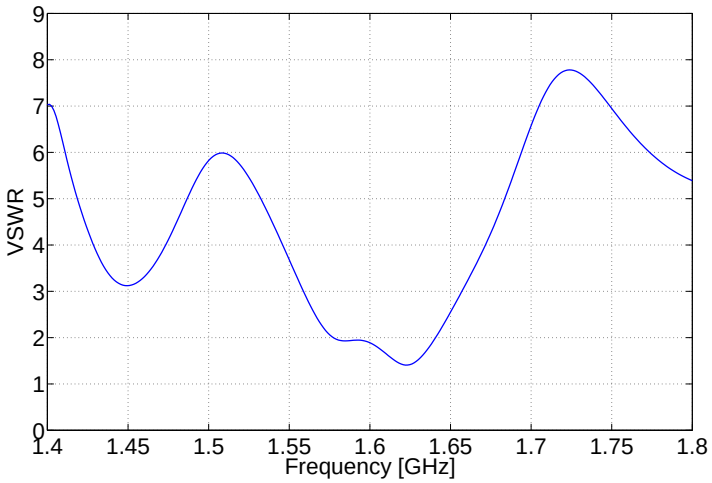

Fig. 1.54: VSWR of GPS antenna array.

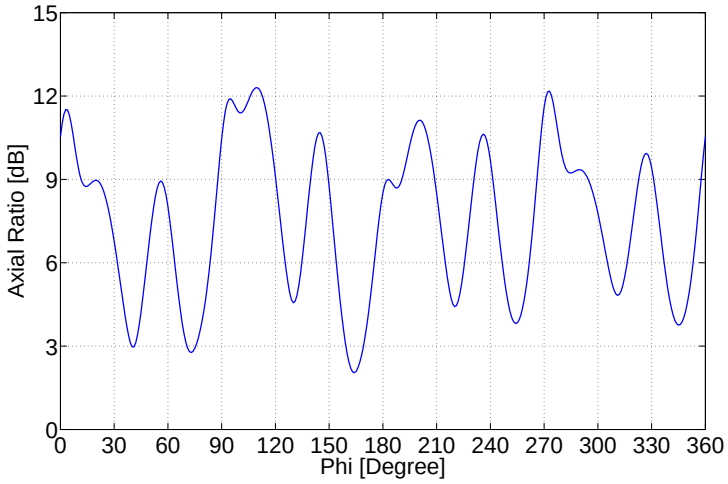

Fig. 1.55: AR of GPS antenna array at 1.575 GHz.

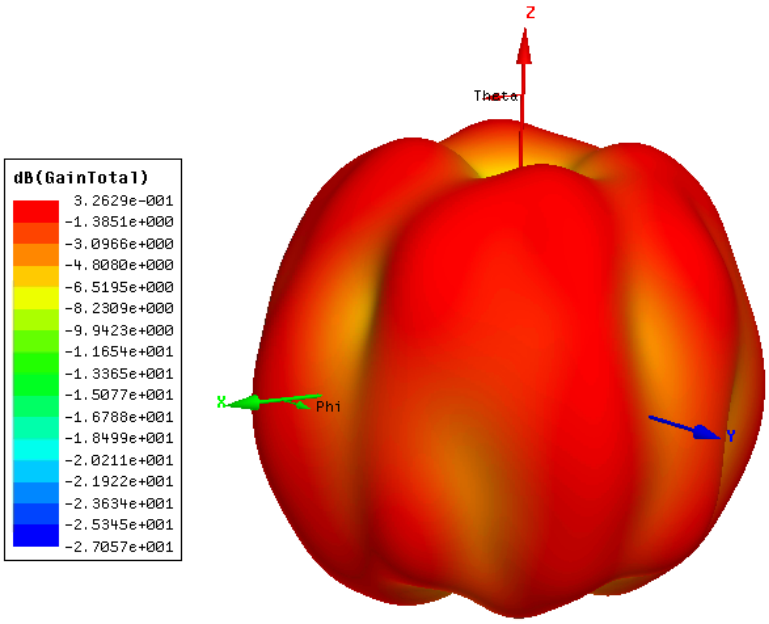

Fig. 1.56: 3-D gain plot at 1.575 GHz.

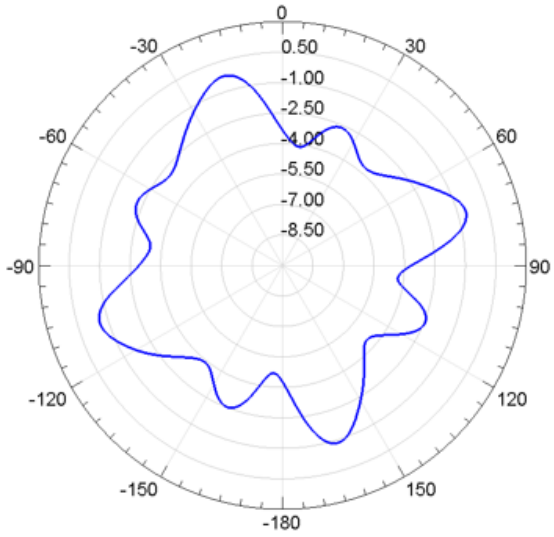

Fig. 1.57: 2-D gain plot for theta = 90 degree at 1.575 GHz.

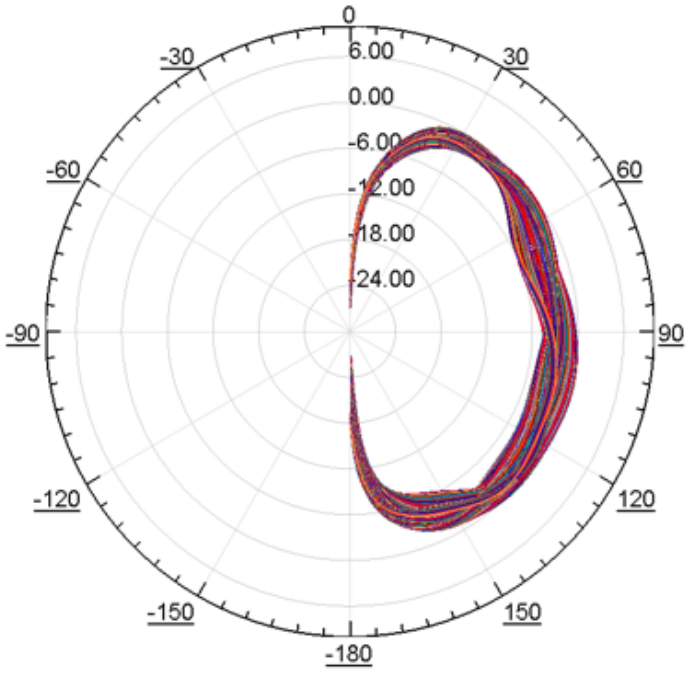

Fig. 1.58: 2-D gain plot for all phi angles at 1.575 GHz.

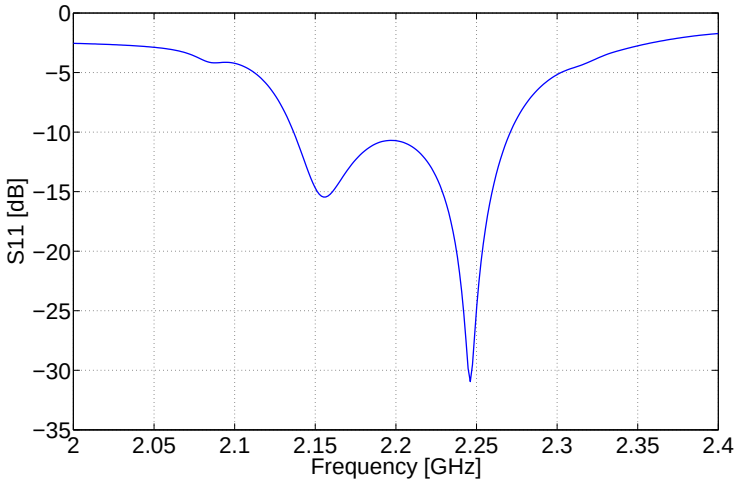

Fig. 1.59: Reflection coefficient of S-band antenna array.

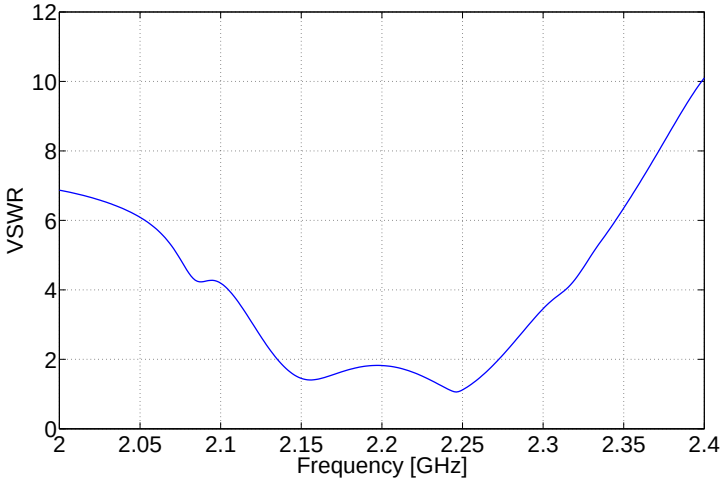

Fig. 1.60: VSWR of S-band antenna array.

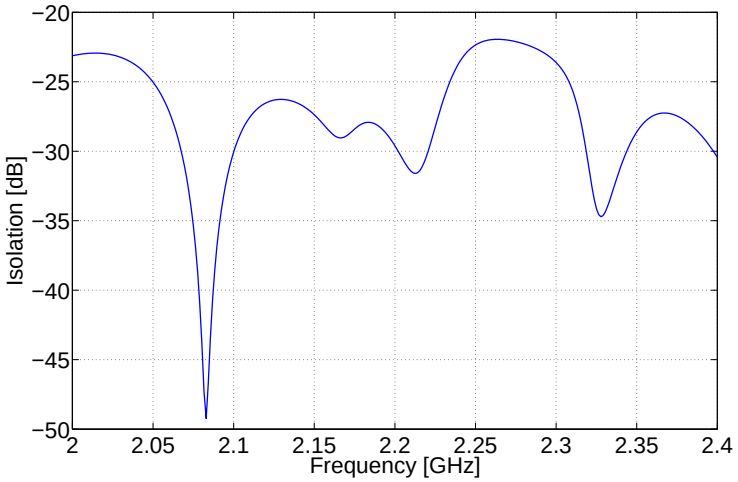

Fig. 1.61: Isolation between S-band and GPS-band antennas.

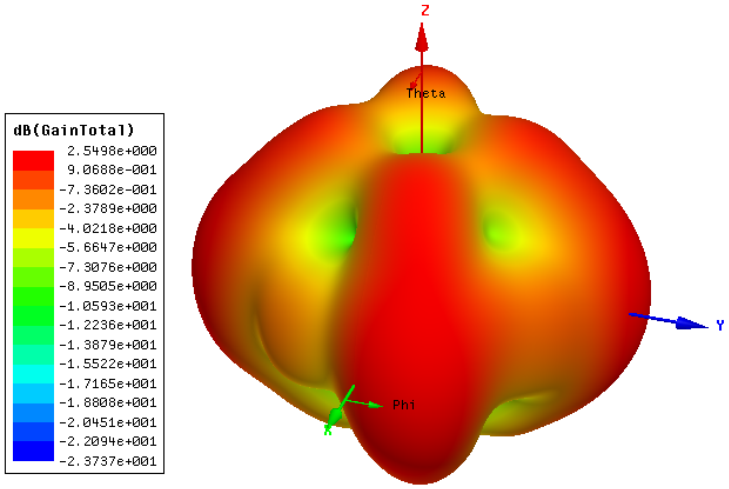

Fig. 1.62: 3-D gain plot at 2.22 GHz.

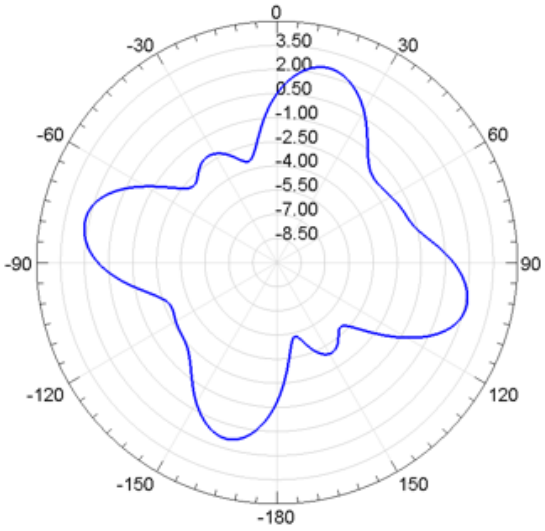

Fig. 1.63: 2-D gain plot for theta = 90 degree at 2.22 GHz.

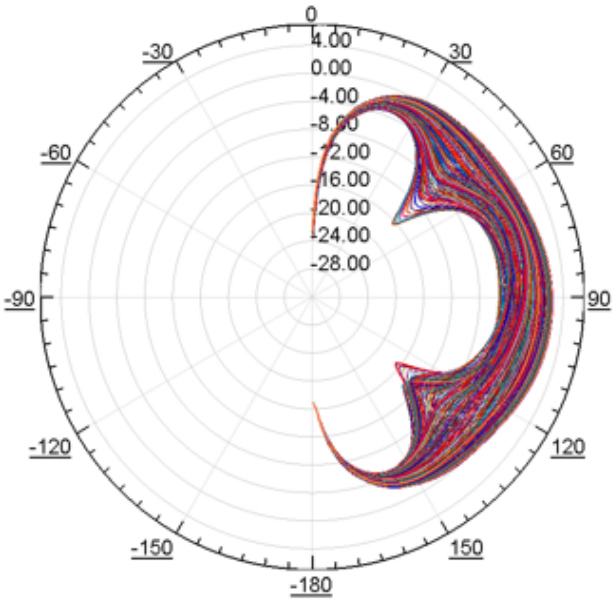

Fig. 1.64: 2-D gain plot for all phi angles at 2.22 GHz.

Chapter 2

Circularly Polarized Conformal Antenna Design for Up and Downlinks of 3U CubeSats

2.1 Cavity-backed Slot Antennas Integrated with Solar Panels

Previous studies have shown that it is feasible and efficient to integrate cavity backed slot antennas with solar panels [13–15]. While it is relatively easy to integrate a GHz band slot antenna with a small solar panel of CubeSats but UHF range is a challenge. This is because the size of the antenna can be too large to fit on a solar panel. In a previous study, a feasibility study of integrating a circularly polarized UHF antenna on CubeSat has been presented without final prototyping [14]. The present thesis project builds on the previous study and with major extensions and complete prototyping. For the continuity purpose, a brief overview of the previous studies on cavity backed slot antennas is summarized as follows.

Previous research work was limited to single band operation for slot antennas as well as impedance bandwidth was lesser than 1 MHz. Practical design for slot antenna over surface of 3U CubeSat was also not presented. We started working on this project taking care of these challenges. Before starting on the project, we did some literature review and to the best of our knowledge we did not come across any slot antenna that was circularly polarized at 450 MHz - 500 MHz range. However some circularly polarized slot antennas at higher frequencies have been reported by several. [16–19].

2.2 Objectives of the Project

Research tasks for this project are as follows:

1. To design the slot antennas for uplink and downlink frequencies of 450 MHz and 465 MHz respectively on 3U CubeSat surface;

2. To obtain a method of circularly polarized radiation over 10 MHz range for both uplink and downlink frequencies;

3. To obtain impedance bandwidth of 10 MHz for both uplink and downlink frequencies;

4. To make the final design practically implementable for fabrication after finishing the simulations on HFSS.

2.3 Microstrip Fed Wideband Slot Antenna

We decided to wrap a slot antenna around the 3U CubeSat surface and to determine its resonant frequency. Geometry of the slot should be such that it should not hinder the integration of solar panels on the remaining surface of 3U CubeSat. Another problem was to devise some method of achieving CP for this slot antenna and for that we decided to use T-junction feedline. The choice of substrate was left arbitrary, so we used Rogers 4003C with standard thickness of 1.524 mm and $\epsilon_r = 3.55$ as substrate. Before reflecting on some other ideas to enhance the impedance bandwidth, we thought to simulate slot antenna on a single substrate without any inner shield or metal. It will also act as reference for those models that are cavity backed or shielded from inside.

In this design, two slots were fed by T-junction microstrip line , separated by a certain distance (which was determined by hit and trial in HFSS) to give a wideband response. To resonate at a given frequency the wrapped-around slot should have an electrical length of λ in a given substrate. As shown in figure 2.1, the lower slot had a length of 331 mm (for 465 MHz) and upper slot had a length of 344 mm (for 450 MHz). Width of both slots was 3 mm. Both slots were excited using a microstrip T-junction. The concept to generate CP in our particular design was that one side of the wrapped-around slot should be excited with a phase difference of 90 degree as compared to adjacent side.

As shown in figure 2.2, -10 dB impedance bandwidth is 52 MHz, covering frequency range of 438 MHz to 490 MHz. It is more than twice the bandwidth that is required. 3-D

gain plots are shown below from figure 2.3 to figure 2.8 at six different frequencies ranging from 445 MHz to 470 MHz. It can be clearly seen that two slots are in fact providing wide impedance bandwidth without compromising on the quality of gain. Although this design offered benefit in terms of impedance bandwidth but it did not have shield for the electronic equipment that is needed to be placed inside the 3U CubeSat. But these simulations and their results gave us a base case for making a comparison with slot antennas having a metallic shield as innermost layer in CubeSat design.

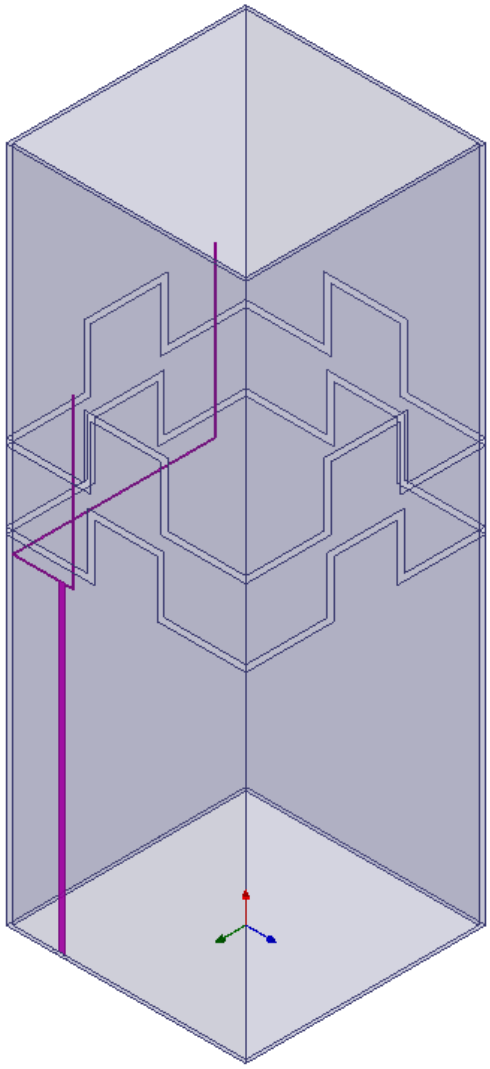

Fig. 2.1: Dual band slot antenna fed by T-junction microstrip line.

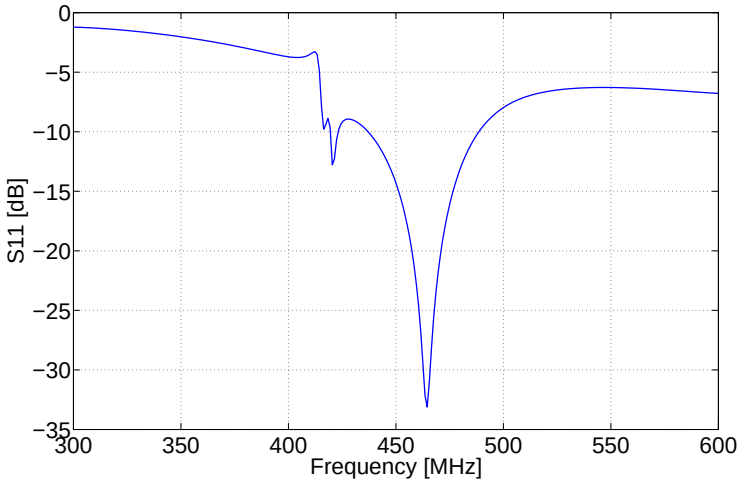

Fig. 2.2: Reflection coefficient of dual band slot antenna.

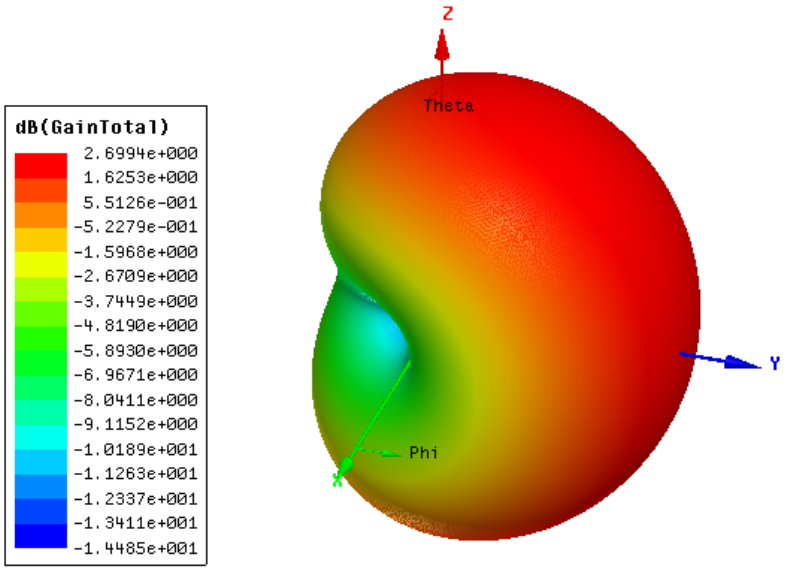

Fig. 2.3: 3-D gain plot at 445 MHz.

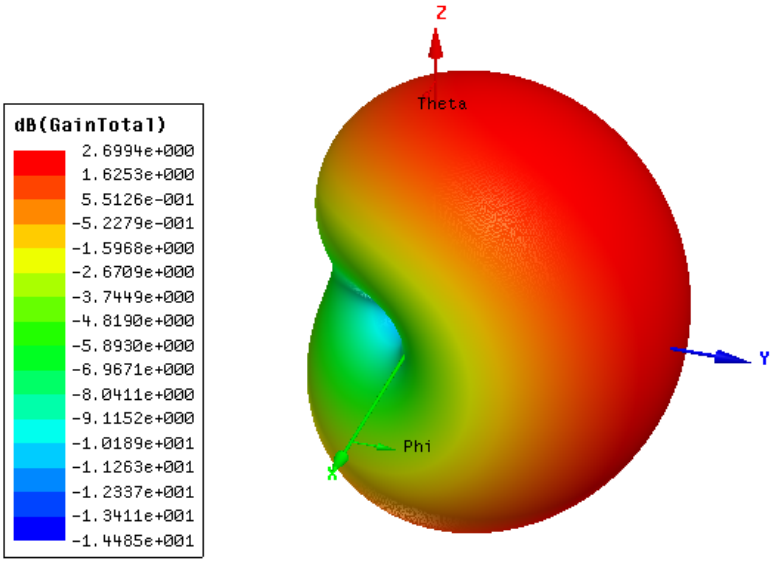

Fig. 2.4: 3-D gain plot at 450 MHz.

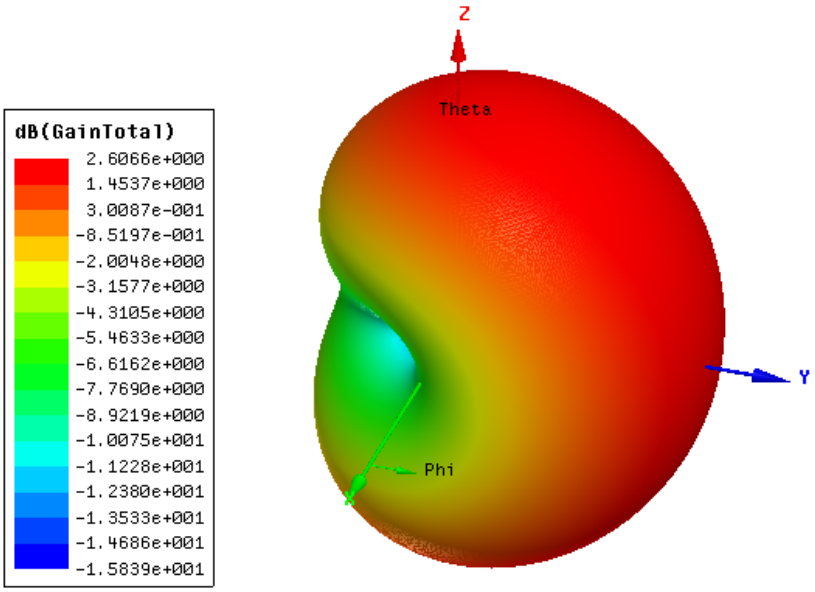

Fig. 2.5: 3-D gain plot at 455 MHz.

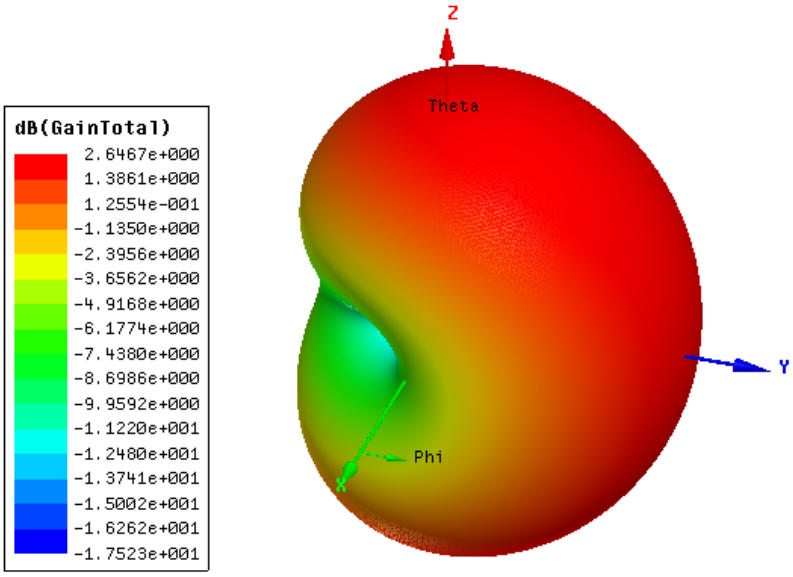

Fig. 2.6: 3-D gain plot at 460 MHz.

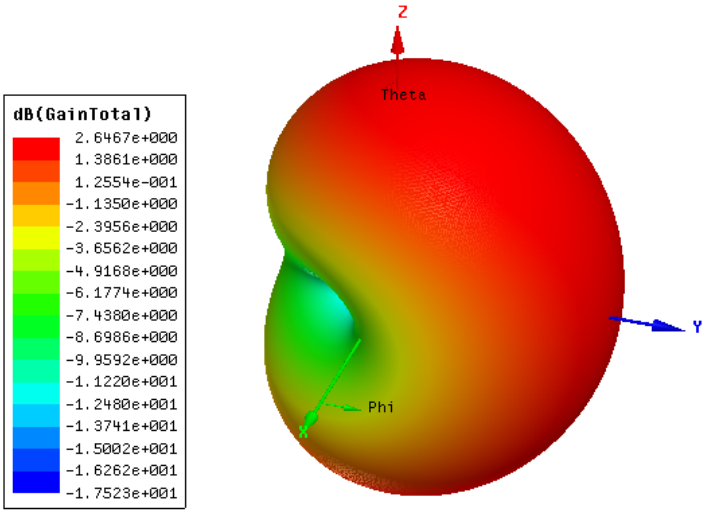

Fig. 2.7: 3-D gain plot at 465 MHz.

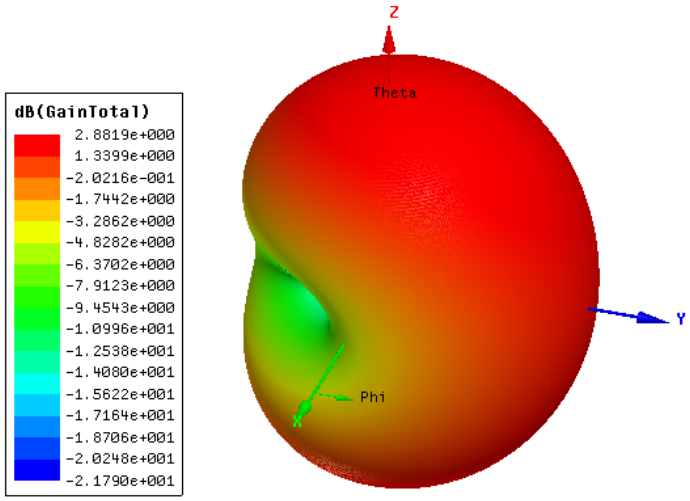

Fig. 2.8: 3-D gain plot at 470 MHz.

2.4 UHF Cavity-backed Slot Antennas for CP

Cavity-backed circularly polarized slot antennas were previously studied by Mahmoud and Chandak [13, 15]. Cross slot antenna was designed and was operating in the frequency range of 2.4 GHz-2.6 GHz, fed by a straight strip-line. But this design uses only one piece of solar panel (i.e. one side of a CubeSat), and was for much higher frequency. It should be noted that the need for the cavity for all these designs, including this thesis project, is to shield the feedline from electronics that will be housed inside 3U CubeSat.

2.4.1 Effect of Cavity Depth on the Performance of Slot Antenna for 3U CubeSat

Since we needed to put a shield or metallic wall as the innermost layer for our CubeSat design so we proceeded on to check its effect in our design. Simulation model for this purpose is shown in figure 2.9. Thickness of first or outer substrate (Rogers 4003C, $\epsilon_r = 3.55$) was 1.542 mm and thickness of the second or inner substrate (Rogers 5880, $\epsilon_r = 2.2$) was 24 mm. Hence the total depth of cavity is 25.542 mm. There is single slot etched at a height of 150 mm from bottom of 3U CubeSat.

We performed a comparative study to check the effects of cavity depth. Depth of the

cavity was varied from 5 mm to 25.524 mm. In figure 2.10, solid red curve shows the reflection coefficient curve, when the depth of cavity was 5 mm and blue colored curve shows the result when the depth of cavity was 25.524 mm. There was an increase in -10 dB impedance bandwidth as the depth of cavity was increased from 5 mm to 25 mm, while the resonance frequency kept on decreasing with the increase in cavity depth. This result was in agreement with what has been stated in [20]. Depth of the cavity influences the bandwidth of slot antenna. We cannot make the cavity as deep as 25.542 mm in our fabricated prototype since it will leave very limited space inside the 3U CubeSat for placement of electronic equipment. Hence we decided to keep the depth of cavity between 6 mm to 10 mm.

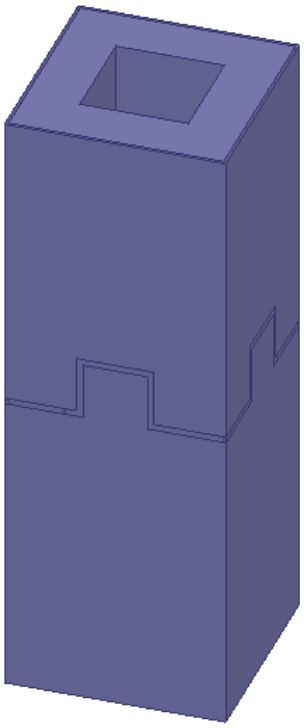

Fig. 2.9: Simulation model for studying the effect of cavity depth.

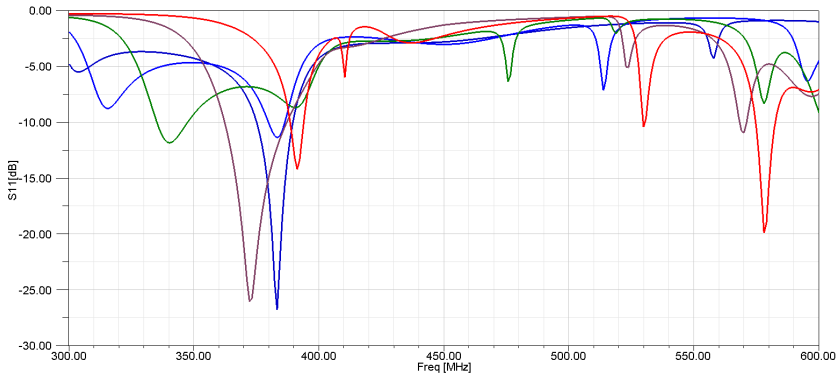

Fig. 2.10: Reflection coefficient for different depths of cavity.

2.4.2 Addition of Top and Bottom Shields

Our 3U CubeSat structure needed to be shielded from top and bottom as it was not practical to send a CubeSat into space with top and bottom surfaces uncovered. So we ran a simulation to check any possible side effects of placing top and bottom metallic covers (figure 2.11). This structure had two substrates. Outer substrate wass Rogers 4003 ($\epsilon_r = 3.55$ and standard thickness = 1.524 mm) and the inner substrate is Rogers 5880 ($\epsilon_r = 2.2$ and standard thickness = 3.175 mm) so the total thickness = 4.699 mm.

Reflection coefficient and gain plots are shown in figure 2.12 and figure 2.13. Minimum reflection coefficient was -27 dB at 464 MHz. -10 dB impedance bandwidth was approximately 10 MHz and -15 dB impedance bandwidth is approximately 4 MHz. Gain had maximas in the z-direction, hence it was concluded that placement of metal covers did not harm our design and we could include them in our final design.

2.4.3 Solution of Isolation Issue Between Two Slot Antennas

One of our design goals was to achieve isolation between slot antennas for uplink and downlink transmission. To probe this issue, we tried two different schemes for feeding slot antennas and ran a comparison between them. In the figure 2.14 and 2.15 below, we showed the phases of ports that were used to excite the slots. In figure 2.14, if we go CCW from side 1 of the 3U CubeSat then the sequence of excitation magnitudes along with their phases is

1V∠0° (side 1),1V∠0° (side 2),1V∠90°(side 3),1V∠90° (side 4), respectively. We term this model as simulation model-I. There is another way, we can assign the phases to the feed ports for this model and that is our simulation model-II and is shown in figure 2.15. We put the results of both models for comparison to see which one could provide better results. It should also be noted that we inverted the upper slot. This was done to add modularity and ease in the process of fabrication for this project. Reflection coefficient curves for simulation model-I and simulation model-II have been shown from figure 2.16 to figure 2.19. Though there was a difference between the lengths of slots, but both the upper and lower slots were resonant at the same frequency (452 MHz) for both simulation models, which is not desirable.This was due to strong coupling of the surface currents that were circulating on the surface of 3U CubeSat.

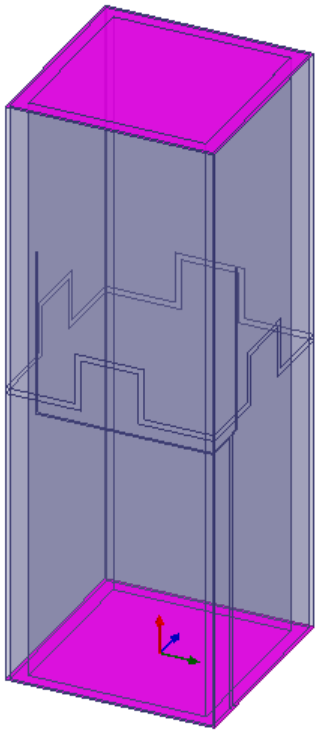

Fig. 2.11: Structure for simulation with top and bottom shields.

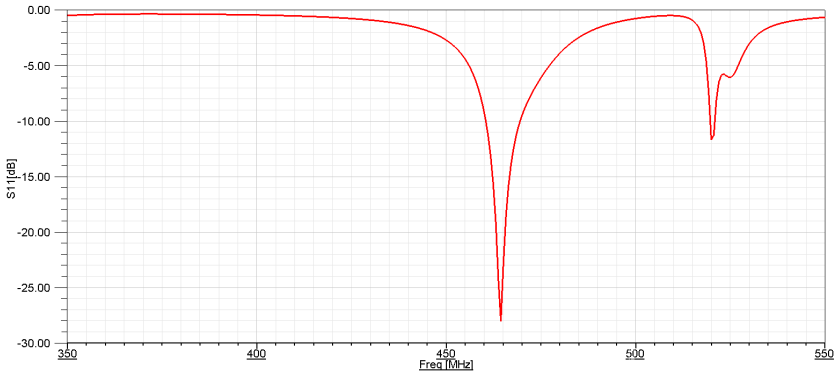

Fig. 2.12: Reflection coefficient with top and bottom shields.

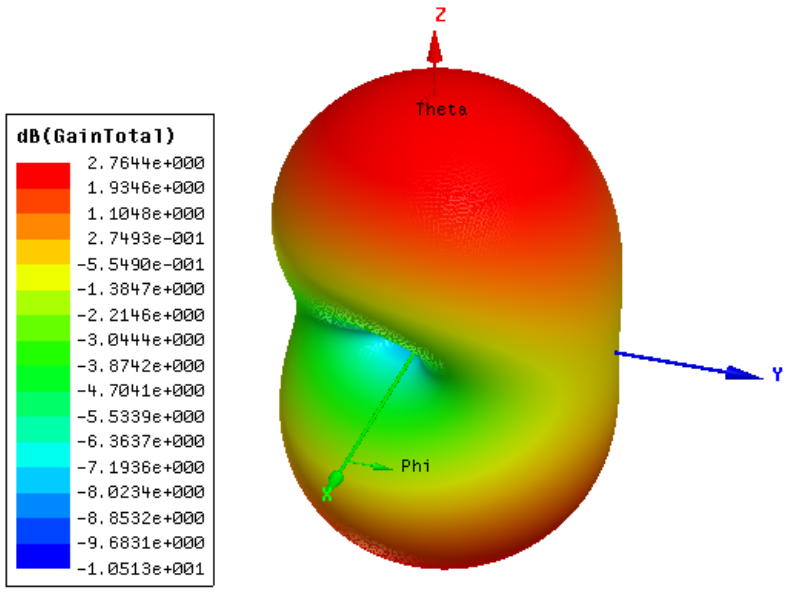

Fig. 2.13: 3-D gain plot with top and bottom shields.

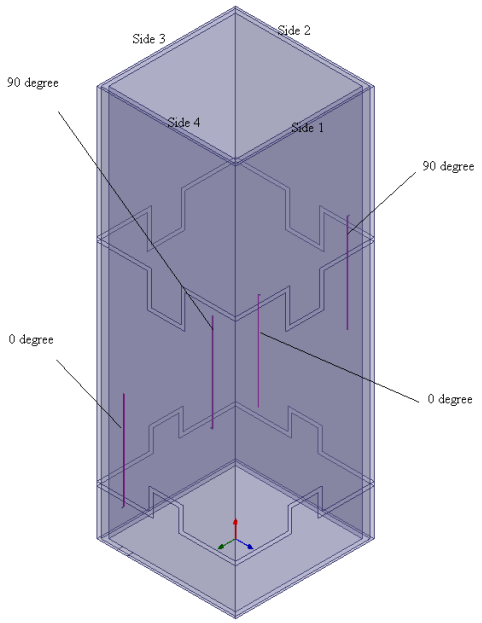

Fig. 2.14: Simulation model-I.

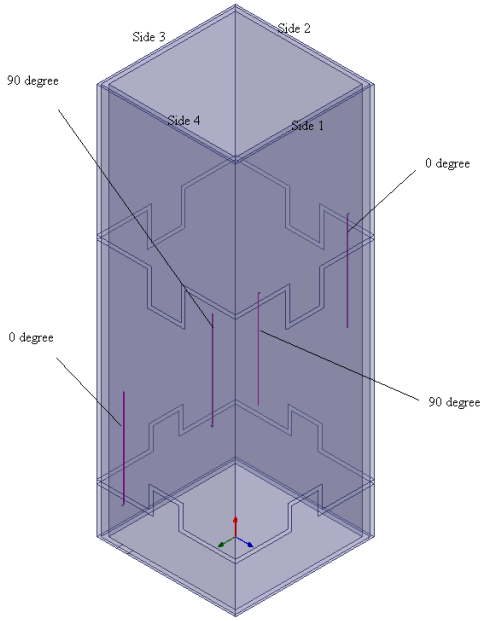

Fig. 2.15: Simulation model-II.

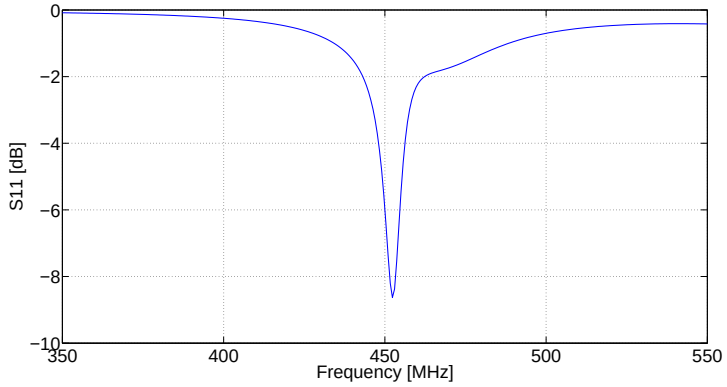

Fig. 2.16: Reflection coefficient of bottom slot for simulation model-I.

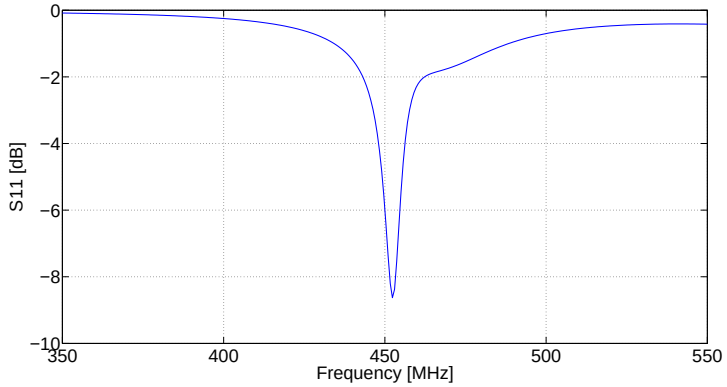

Fig. 2.17: Reflection coefficient for bottom slot for simulation model-II.

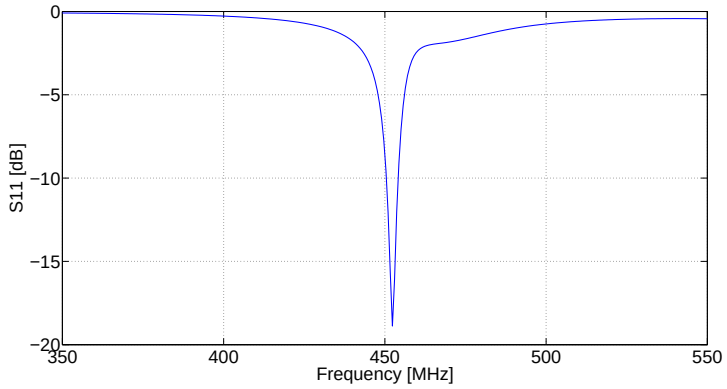

Fig. 2.18: Reflection coefficient of top slot for simulation model-I.

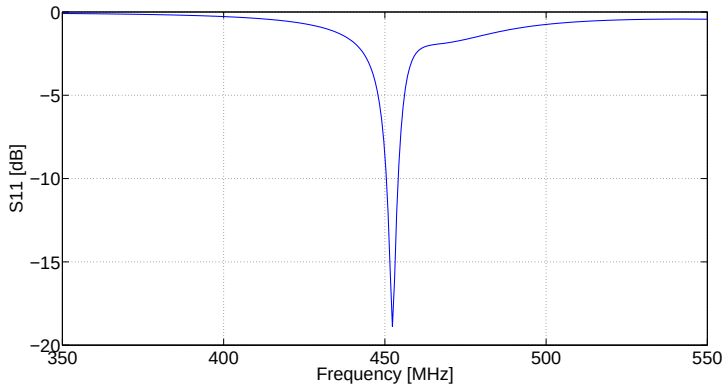

Fig. 2.19: Reflection coefficient of top slot for simulation model-II.

To combat with this problem, we cut a slot, 3 mm wide, at a height of 148.5 mm from the base of 3U cubeSat and inserted a metal sheet that 'cuts through' surface of 3U CubeSat right in the middle (at the height of 150 mm). The model is shown in figure 2.20. The dimensions of the metal sheet are 200 mm by 200 mm. The distance of the lower slot from the bottom is 30 mm and the distance of upper slot from the bottom is 270 mm. Upper and lower slot are same in shape but they differ from each other in terms of length. Lower slot has been designed to resonate at 450 MHz while the upper slot is designed to resonate at 465 MHz. Length of lower slot is 624 mm and length of upper slot is 532 mm. As shown in figures 2.21 and 2.22, lower slot is resonant at frequency of 451 MHz and upper slot is resonant at the frequency of 462 MHz. The slot that has been cut in the middle surface restricts the current for both slots to flow in their independent ground planes which implies that, using this technique, we can control and tune the resonant frequencies of two slots by varying their lengths and they will not 'interfere' with each other. Plot of isolation between the four ports has been shown in figure 2.23 and can it can be seen that isolation $<$ - 30 dB for all the ports.

2.5 Semi-final Design of Dual Band CPd Slot Antennas

Overcoming the problem of isolation we changed the thickness of inner substrate for attaining good impedance bandwidth. Total thickness of two substrates was changed from

3.048 mm to 6.35 mm. The metal plate was inserted in the structure such that it just 'fits' in the middle of CubeSat and was not protruding out from the CubeSat surface. The model is shown in figure 2.24. The results from simulation are shown from figure 2.25 to figure 2.30. Minimum reflection coefficient for bottom slot is is -23 dB at 454 MHz. -10 dB impedance bandwidth is 4 MHz only. It will increase if we increase the width of inner substrate further. Minimum reflection coefficient for upper slot is -28 dB at 484 MHz. -10 dB impedance bandwidth is 3 MHz for upper slot. AR is excellent and stays well below 3 dB for all the high-gain points for both the upper as well as lower slots.

2.6 Final Practical Design

Since our design will be fabricated in modular fashion so decided to run the simulations for one half of the CubeSat and compared it with the design when both of the halves will be put together. We used T-junction feedline method for these simulations because that would be the practical method to generate CP in our design. We ran two type of simulations and compared the results.

1. Half CubeSat model with T-shaped feed
2. Full CubeSat model with T-shaped feed

Plots for the reflection coefficient have been shown in figure 2.31 and figure 2.32. These reflection coefficient curves have been shown for lower slots only. For the T-shaped feedline, -10 dB bandwidth is 14 MHz while for the case of stripline feeds, -10 dB bandwidth is 5 MHz. For both cases, AR bandwidth is lesser than 1 MHz for T-shaped feedline as shown in figure 2.33 and figure 2.34. This bandwidth can be increased using phase shifter component. We found one of such component after surveying the market and technical details of this component can be read at Mini Circuits website [21].

2.7 Future Work

In the future, a more efficient way to achieve circular polarization for 3U CubeSat can be used. One of the methods that may be employed is to use QCN-7+ Ultra-Small

Power Splitter. Specifications of this component can be seen at Mini Circuits website [21]. Bandwidth enhancement techniques can be used for both uplink and downlink channels. One of the method to increase the bandwidth is to modify the feedline and to make it tapered or to add stubs in it. Though this research has been performed for slot antennas to operate in 450 MHz - 500 MHz band but the Cube Satellites at other frequencies can also be built using these techniques and solutions as discussed in this thesis.

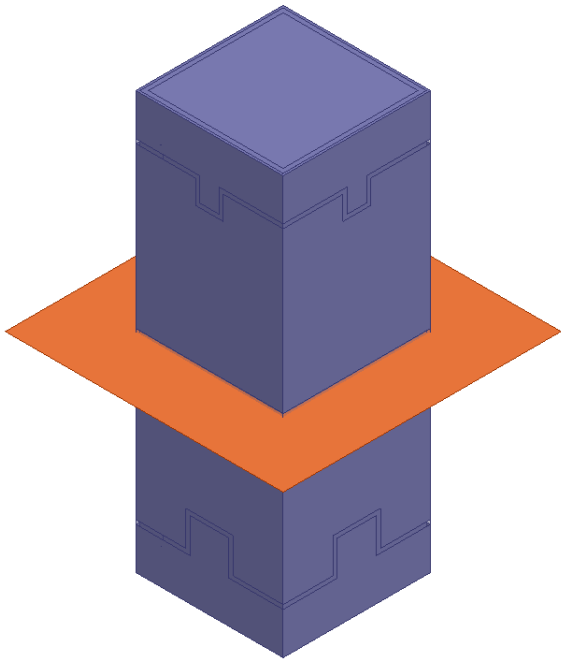

Fig. 2.20: Simulation model with metal divider in the middle of 3U CubeSat.

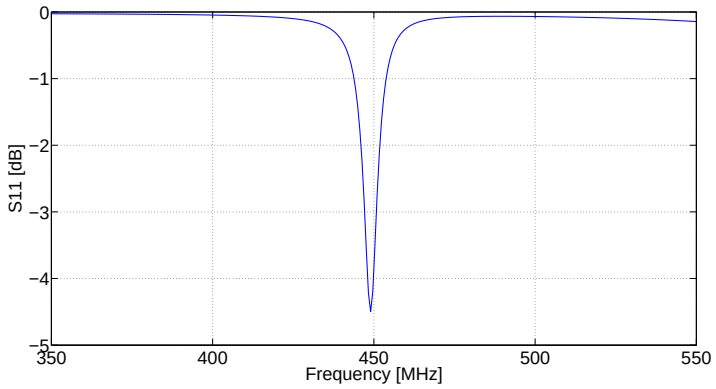

Fig. 2.21: Reflection coefficient for bottom slot.

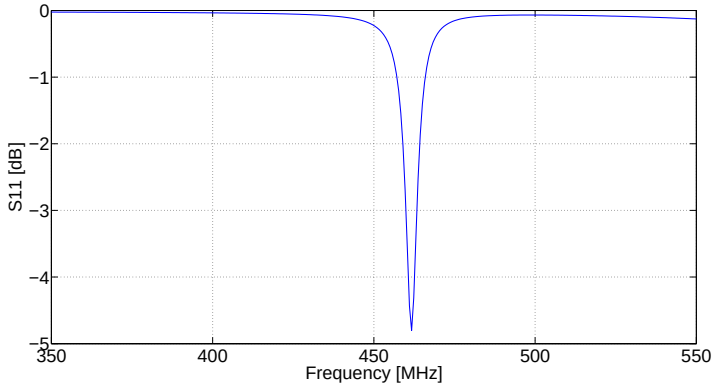

Fig. 2.22: Reflection coefficient for top slot.

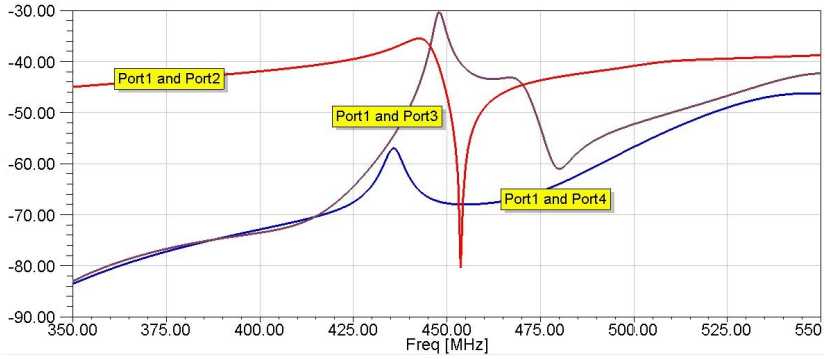

Fig. 2.23: Isolation between the feedlines.

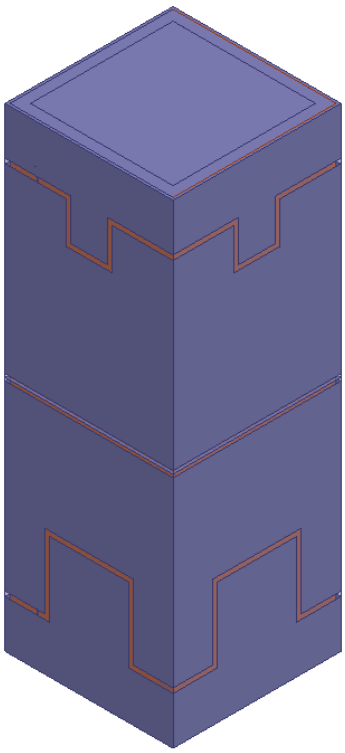

Fig. 2.24: Structure that has been simulated.

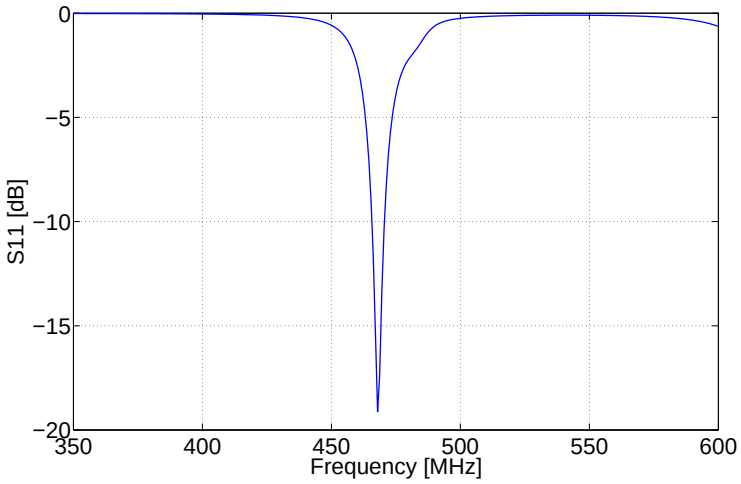

Fig. 2.25: Reflection coefficient of bottom slot.

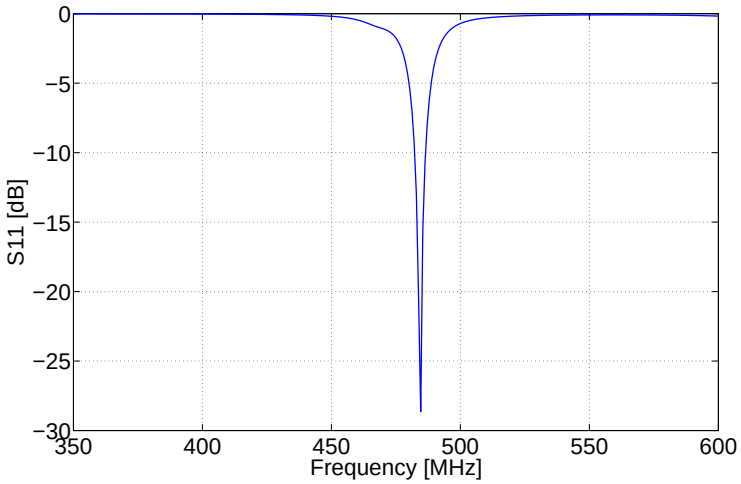

Fig. 2.26: Reflection coefficient of top slot.

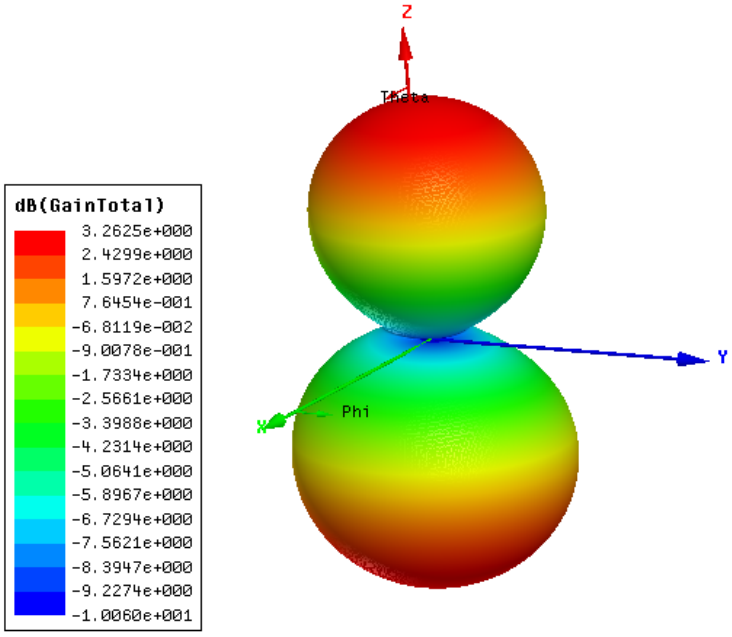

Fig. 2.27: 3-D gain plot for bottom slot at 467 MHz.

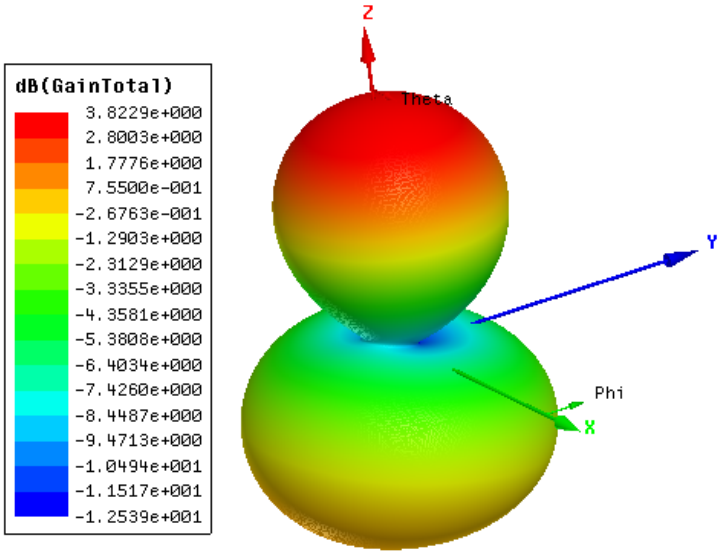

Fig. 2.28: 3-D gain plot for top slot at 484 MHz.

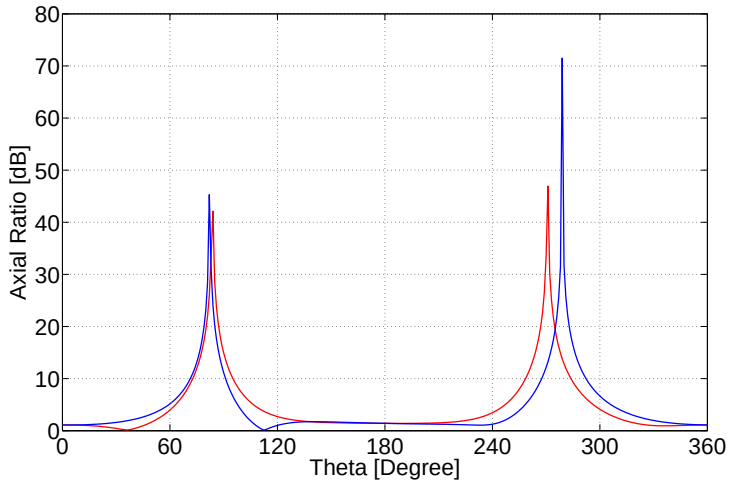

Fig. 2.29: AR plot for lower slot at 467 MHz.

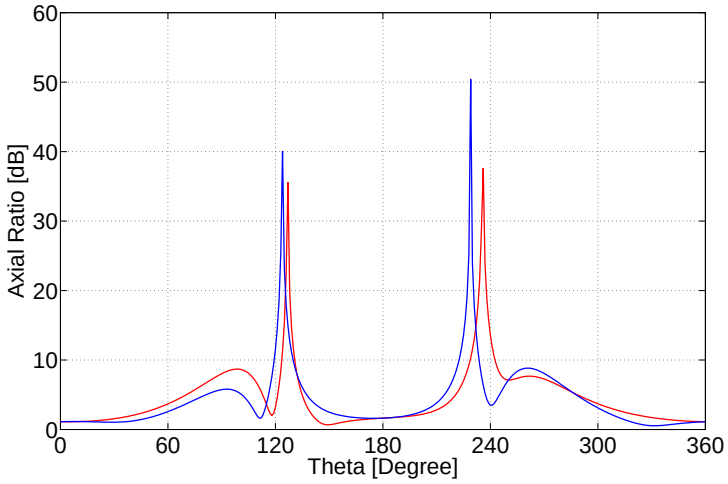

Fig. 2.30: AR plot for upper slot at 484 MHz.

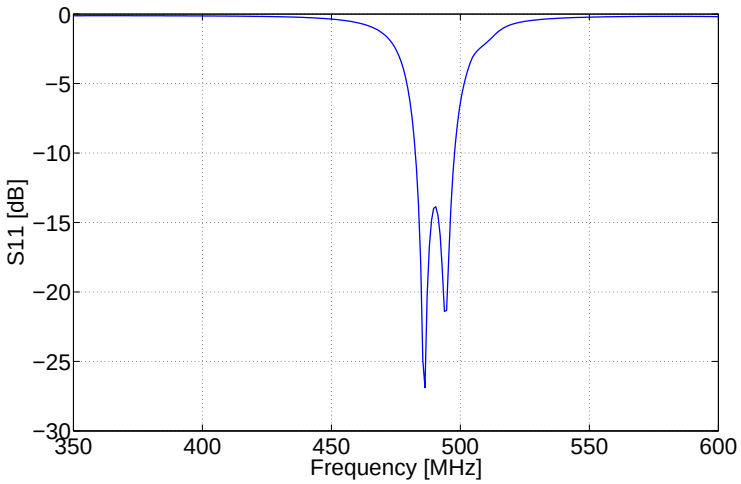

Fig. 2.31: Reflection coefficient for 1.5U CubeSat model with T-type feed.

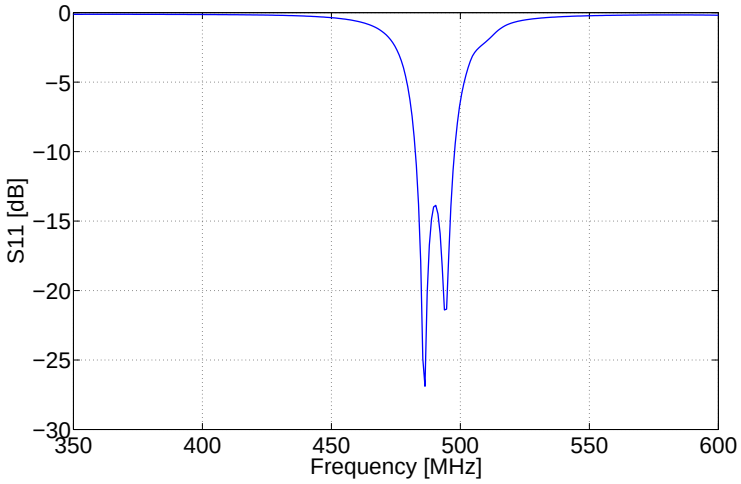

Fig. 2.32: Reflection coefficient for 3U CubeSat model with T-type feed.

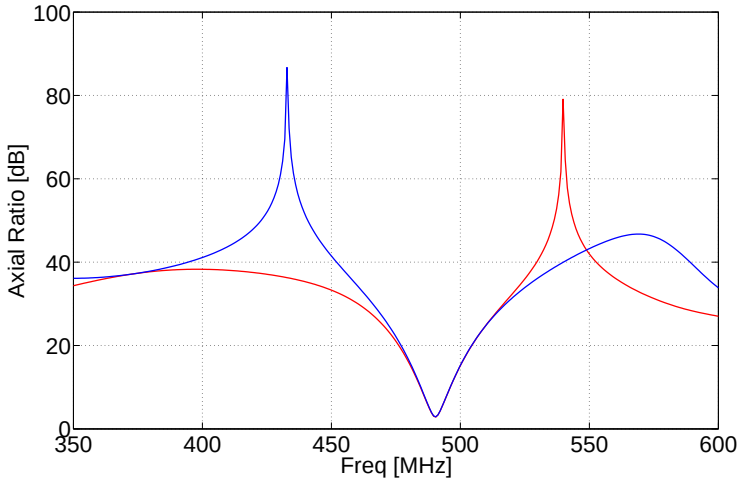

Fig. 2.33: AR bandwidth with T-type feed (1.5U CubeSat).

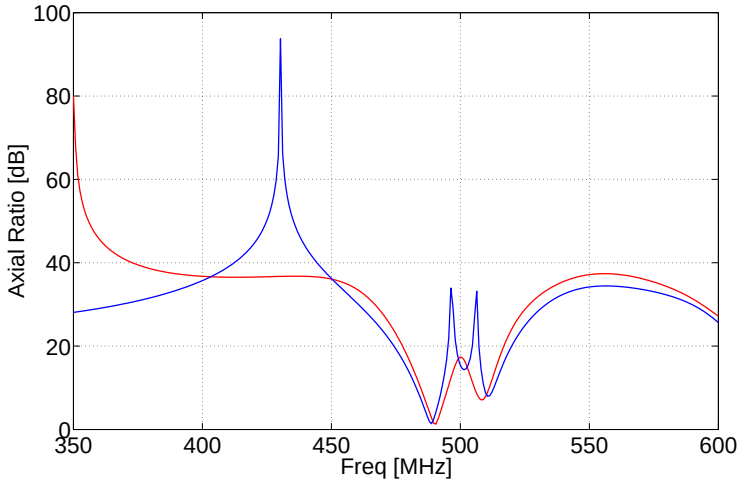

Fig. 2.34: AR bandwidth with T-type feed (3U CubeSat).

References

[1] H. Booker, "Slot aerials and their relation to complementary wire aerials (babinet's principle)," *Electrical Engineers - Part IIIA: Radiolocation, Journal of the Institution of*, vol. 93, no. 4, pp. 620–626, 1946.

[2] D. Farr, C. Weston, T. Nielson, C. Frazier, E. Stromberg, J. Miller, A. Swenson, B. Carrick, W. Nelson, V. Vangeison, T. Evans, W. Cox, B. Byers, J. Hidalgo, C. Perkins, C. Fish, and C. Swenson, "Auroral spatial structures probe," in *Radio Science Meeting (USNC-URSI NRSM), 2014 United States National Committee of URSI National*, Jan. 2014.

[3] M. Mainmaiti, "Study of inkjet printing as an ultra-low-cost antenna prototyping method and its application to conformal wraparound antennas for sounding rocket sub-payload," Master's thesis, Utah State University, Logan, UT, 2013.

[4] W. Imbriale and J. Yuen, *Spaceborne antennas for planetary exploration.* Wiley, 2006.

[5] Rogers Corporation. [Online]. Available: https://www.rogerscorp.com/documents/609/acm/RT-duroid-6002-laminate-data-sheet.pdf

[6] D. M. Pozar, *Microwave engineering; 4th ed.* Hoboken, NJ: Wiley Global Education, 2011.

[7] R. Garg, *Microstrip antenna design handbook.* Norwood, MA: Artech House, 2001.

[8] R. Sefa, F. Tefiku, and A. Maraj, "Analysis of arrays of printed strip dipole antennas," in *Software, Telecommunications and Computer Networks (SoftCOM), 2011 19th International Conference on*, Sep. 2011.

[9] A. K. Agrawal and W. Powell, "A printed circuit cylindrical array antenna," *Antennas and Propagation Society International Symposium, 1986*, vol. 24, pp. 549–552, Jun. 1986.

[10] E. Levine, "Double-sided printed arrays with large bandwidth," *IEE Proceedings H (Microwaves, Antennas and Propagation)*, vol. 135, pp. 54–59(5), Feb. 1988. [Online]. Available: http://digital-library.theiet.org/content/journals/10.1049/ip-h-2.1988.0010

[11] N. Uzunoglu, N. Alexopoulos, and J. Fikioris, "Radiation properties of microstrip dipoles," *IEEE Transactions on Antennas and Propagation*, vol. 27, no. 6, pp. 853–858, Nov. 1979.

[12] P. Sharma and K. Gupta, "Analysis and optimized design of single feed circularly polarized microstrip antennas," *IEEE Transactions on Antennas and Propagation*, vol. 31, no. 6, pp. 949–955, Nov. 1983.

[13] M. N. Mahmoud, "Integrated solar panel antennas for cube satellites," Master's thesis, Utah State University, Logan, UT, 2010.

[14] M. Jamali, "A study on conformal antenna solutions for cube satellites," Master's thesis, Utah State University, Logan, UT, 2012.

[15] M. Chandak, "Design and characterization of circularly polarized cavity-backed slot antennas in an in-house constructed anechoic chamber," Master's thesis, Utah State University, Logan, UT, 2012.

[16] S. Nakao, R. Joseph, and T. Fukusako, "A circularly polarized l-shaped and rectangular slot antenna with an l-shaped probe for wideband characteristics," in *Microwave Conference Proceedings (APMC), 2010 Asia-Pacific*, Dec. 2010.

[17] J. Jamali, R. A. Sadeghzadeh, and M. Naser-Moghadasi, "A novel design of small square slot antenna with circular polarization characteristics for x-band applications," *Electromagnetics*, vol. 33, no. 3, pp. 249–255, 2013. [Online]. Available: http://dx.doi.org/10.1080/02726343.2013.769408

[18] T.-Y. Han, "Broadband circularly polarized square-slot antenna," *Journal of Electromagnetic Waves and Applications*, vol. 22, no. 4, pp. 549–554, 2008. [Online]. Available: http://dx.doi.org/10.1163/156939308784150236

[19] K.-L. Wong, C.-C. Huang, and W.-S. Chen, "Printed ring slot antenna for circular polarization," *IEEE Transactions on Antennas and Propagation*, vol. 50, no. 1, pp. 75–77, Jan. 2002.

[20] A. Rudge, *The handbook of antenna design.* London, UK: P. Peregrinus, 1982.

[21] Mini Circuits. (2015). [Online]. Available: http://www.minicircuits.com/pdfs/QCN-7.pdf

Appendices

Appendix A

ASSP Project

A.1 Effect of Temperature on the Substrate and Antenna Properties

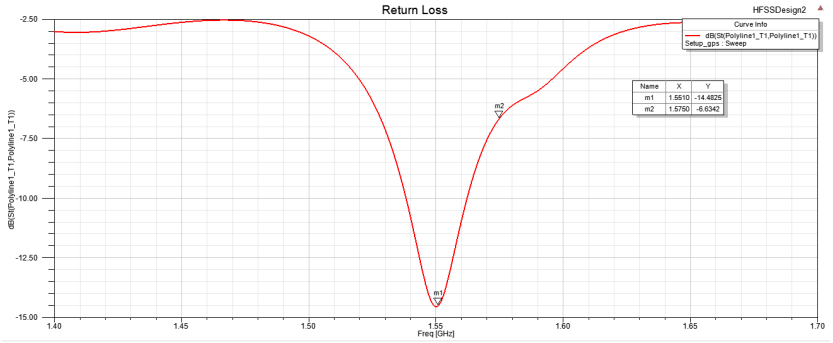

Fig. A.1: Reflection coefficient of GPS antenna when $\epsilon_r = 5.2$.

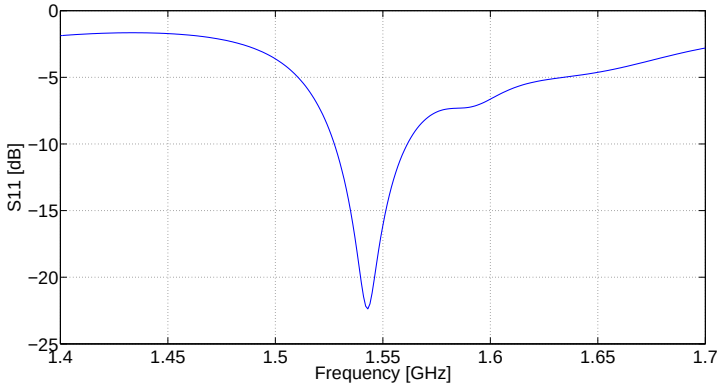

Fig. A.2: Reflection coefficient of GPS antenna when $\epsilon_r = 5.72$.

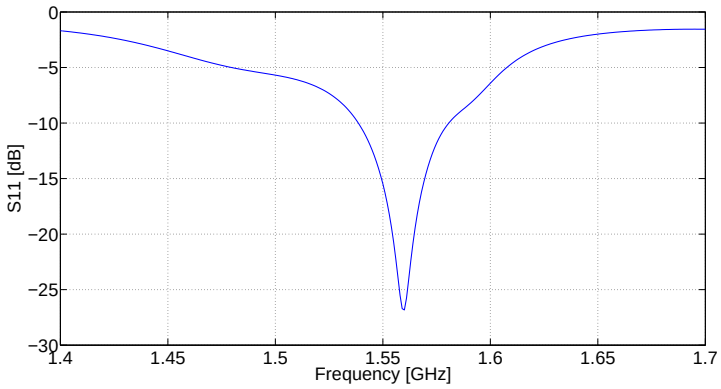

Fig. A.3: Reflection coefficient of GPS antenna when $\epsilon_r = 4.68$.

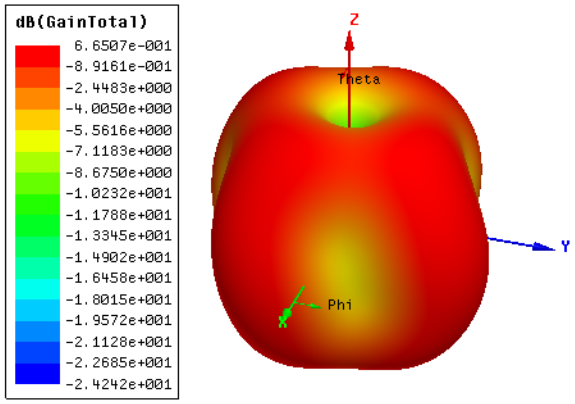

Fig. A.4: 3-D gain plot when $\epsilon_r = 5.2$ and frequency = 1.575 GHz.

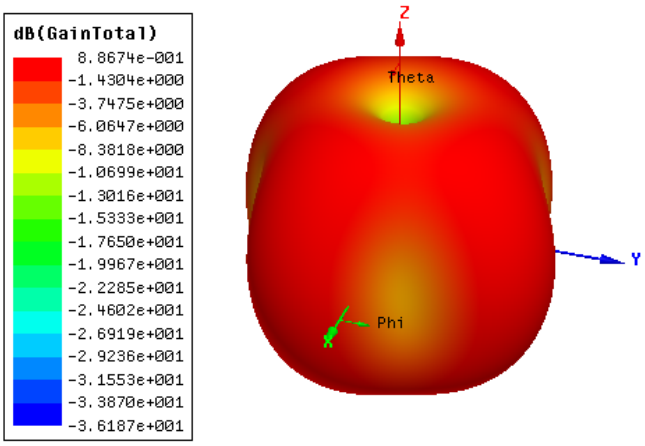

Fig. A.5: 3-D gain plot when $\epsilon_r = 5.2$ and frequency = 1.527 GHz.

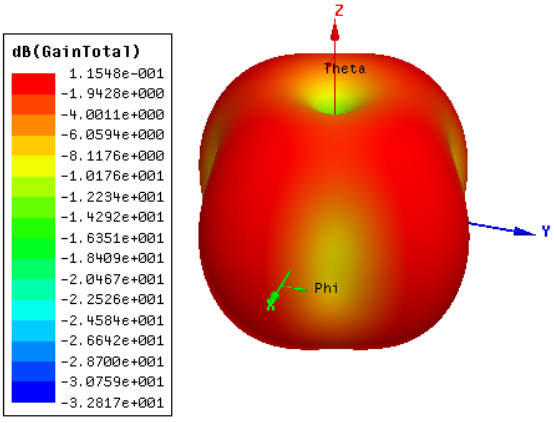

Fig. A.6: 3-D gain plot when $\epsilon_r = 5.2$ and frequency = 1.622 GHz.

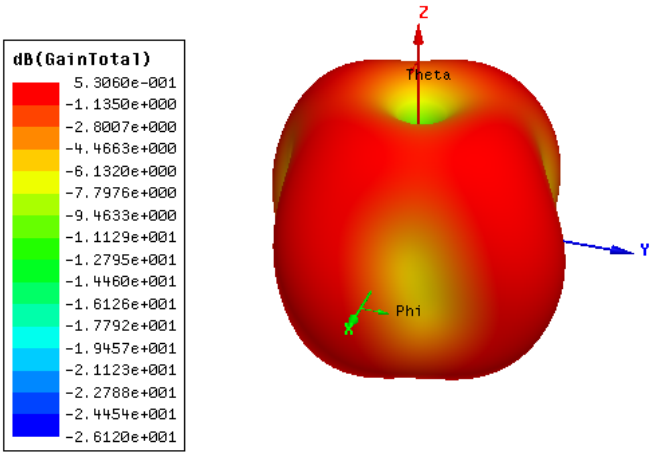

Fig. A.7: 3-D gain plot when $\epsilon_r = 5.72$ and frequency = 1.575 GHz.

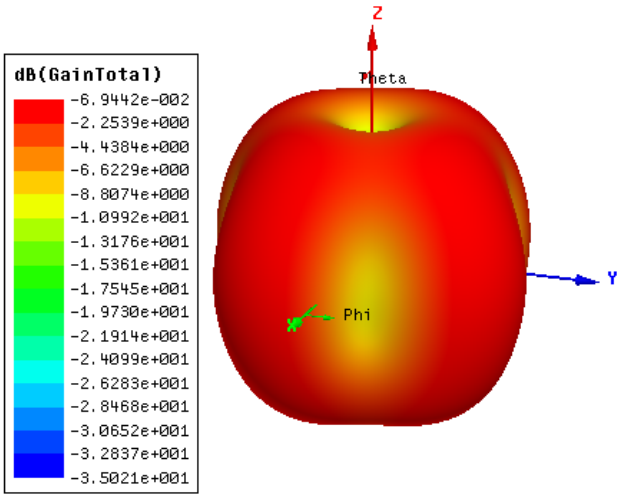

Fig. A.8: 3-D gain plot when $\epsilon_r = 5.72$ and frequency = 1.622 GHz.

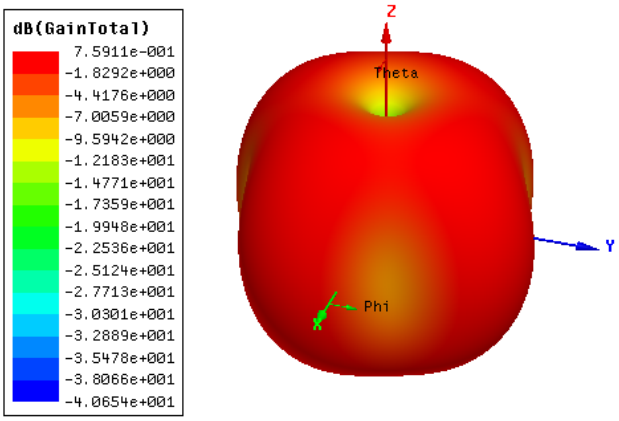

Fig. A.9: 3-D gain plot when $\epsilon_r = 5.72$ and frequency = 1.527 GHz.

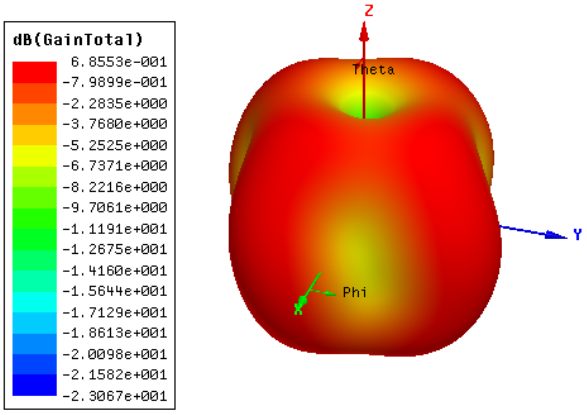

Fig. A.10: 3-D gain plot when $\epsilon_r = 4.68$ and frequency = 1.575 GHz.

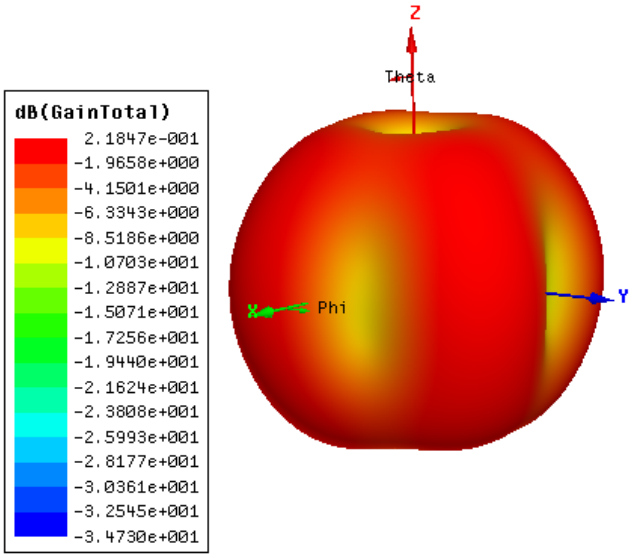

Fig. A.11: 3-D gain plot when $\epsilon_r = 4.68$ and frequency = 1.622 GHz.

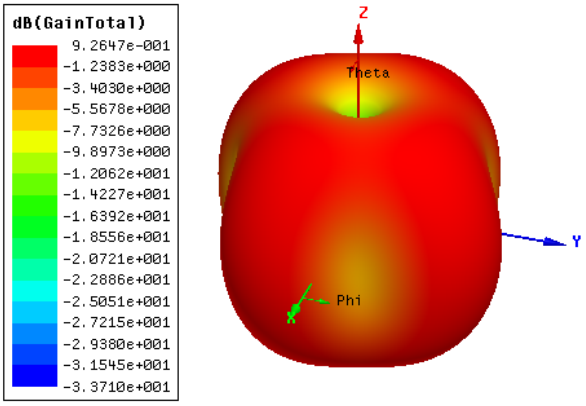

Fig. A.12: 3-D gain plot when $\epsilon_r = 4.68$ and frequency = 1.527 GHz.

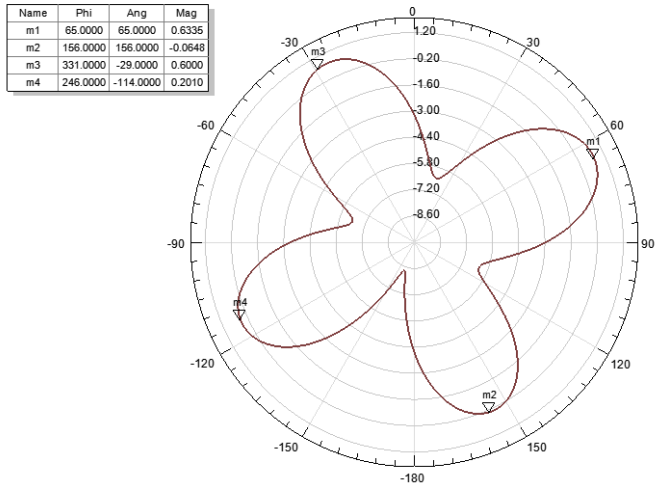

Fig. A.13: 2-D gain plot when $\epsilon_r = 5.2$ and frequency = 1.575 GHz.

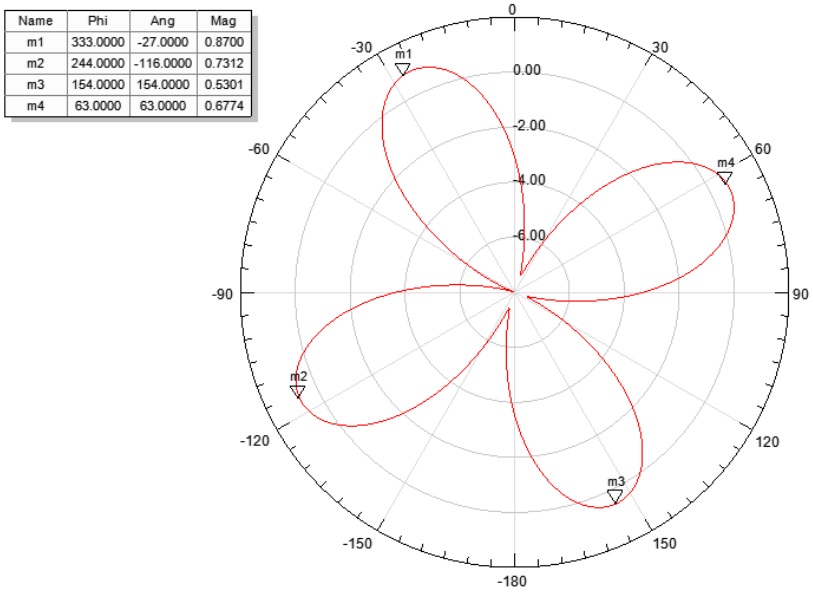

Fig. A.14: 2-D gain plot when $\epsilon_r = 5.2$ and frequency = 1.527 GHz.

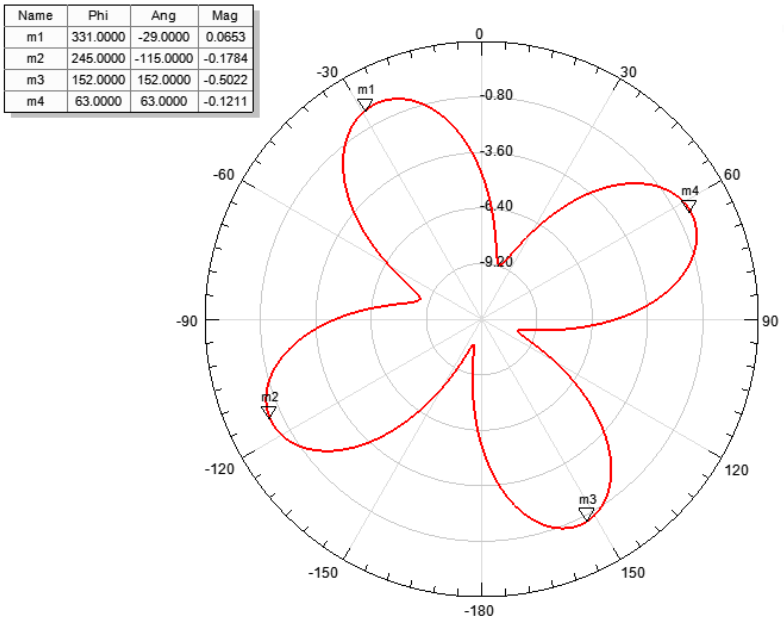

Fig. A.15: 2-D gain plot when $\epsilon_r = 5.2$ and frequency = 1.622 GHz.

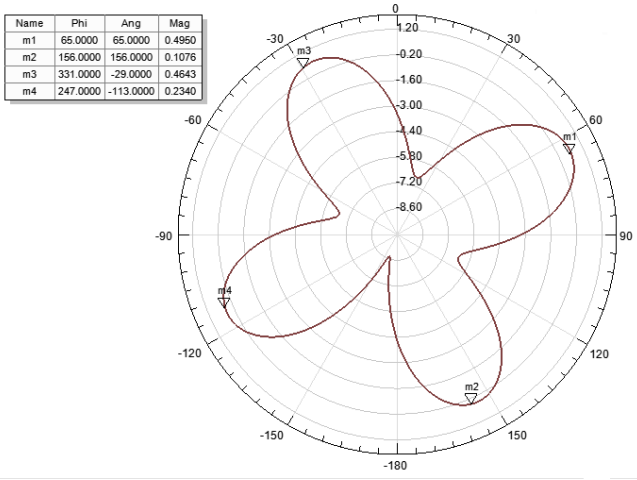

Fig. A.16: 2-D gain plot when $\epsilon_r = 5.72$ and frequency = 1.575 GHz.

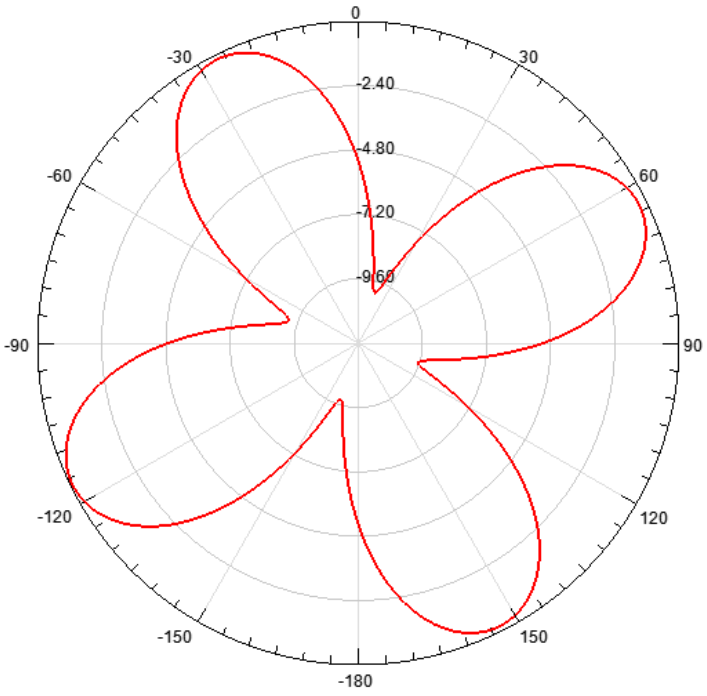

Fig. A.17: 2-D gain plot when $\epsilon_r = 5.72$ and frequency = 1.622 GHz.

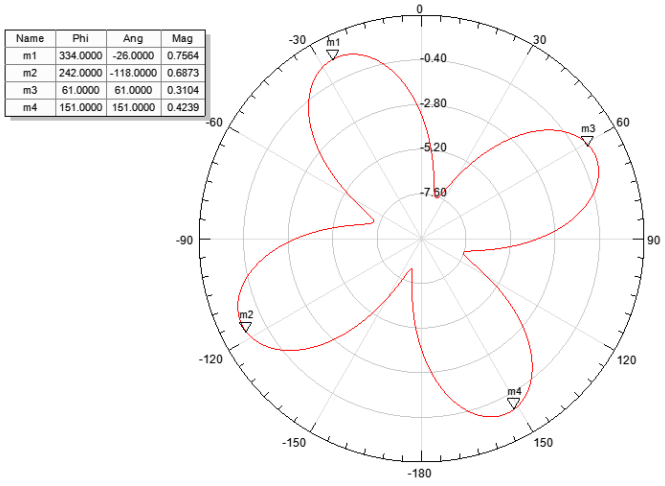

Fig. A.18: 2-D gain plot when $\epsilon_r = 5.72$ and frequency = 1.527 GHz.

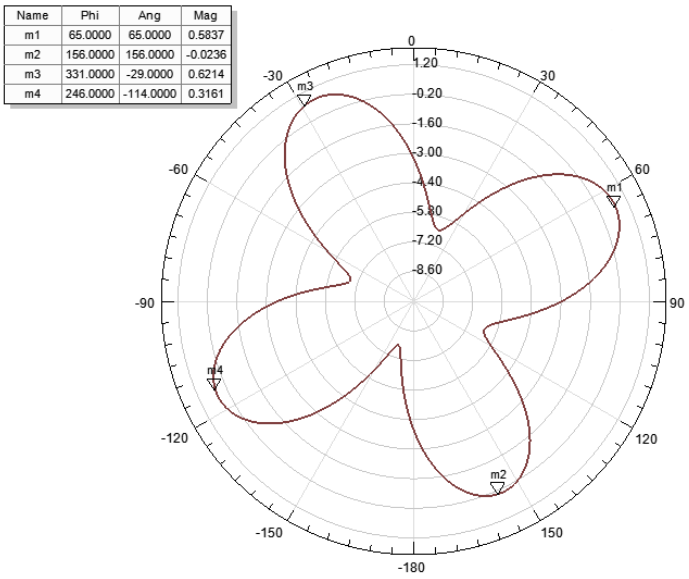

Fig. A.19: 2-D gain plot when $\epsilon_r = 4.68$ and frequency = 1.575 GHz.

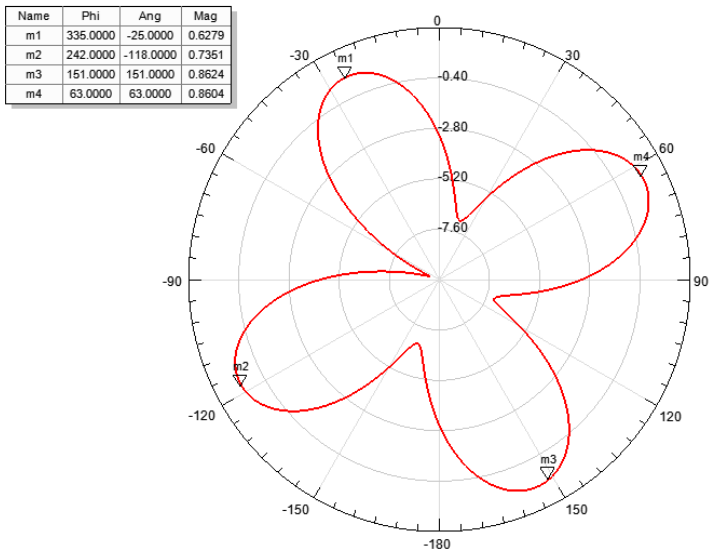

Fig. A.20: 2-D gain plot when $\epsilon_r = 4.68$ and frequency = 1.527 GHz.

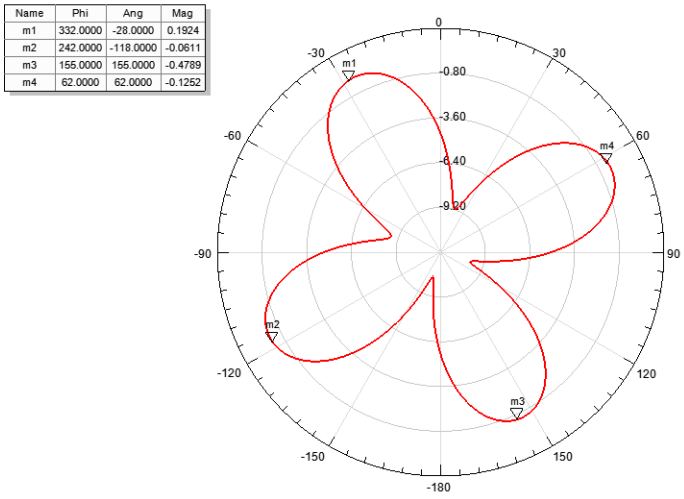

Fig. A.21: 2-D gain plot when $\epsilon_r = 4.68$ and frequency = 1.622 GHz.

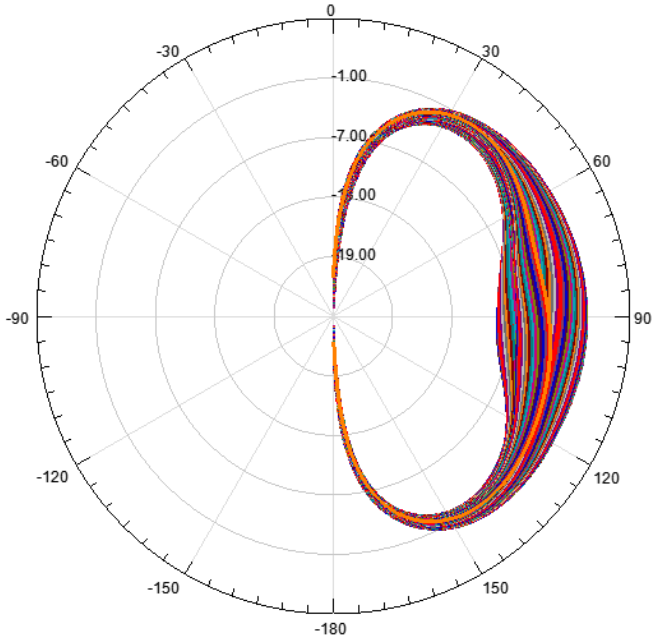

Fig. A.22: 2-D gain plot(vertical cuts) when $\epsilon_r = 5.2$ and frequency = 1.575 GHz.

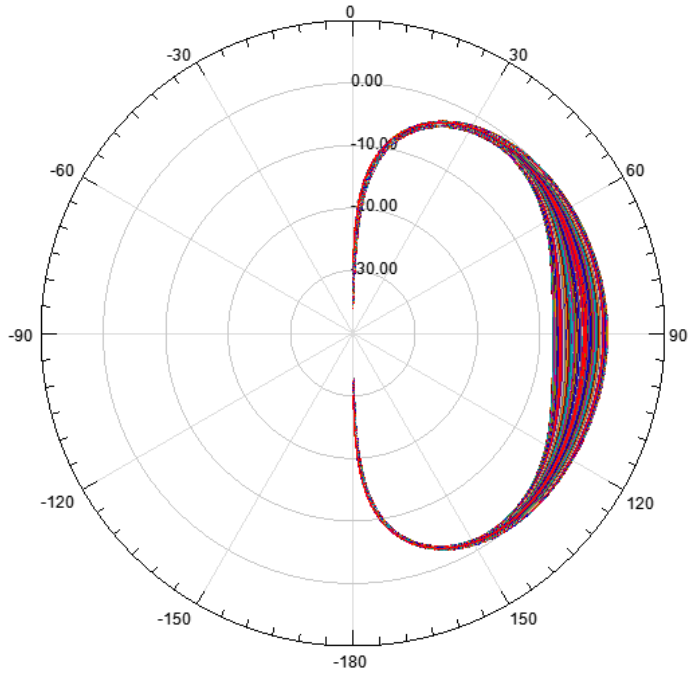

Fig. A.23: 2-D gain plot (vertical cuts) when $\epsilon_r = 5.2$ and frequency = 1.527 GHz.

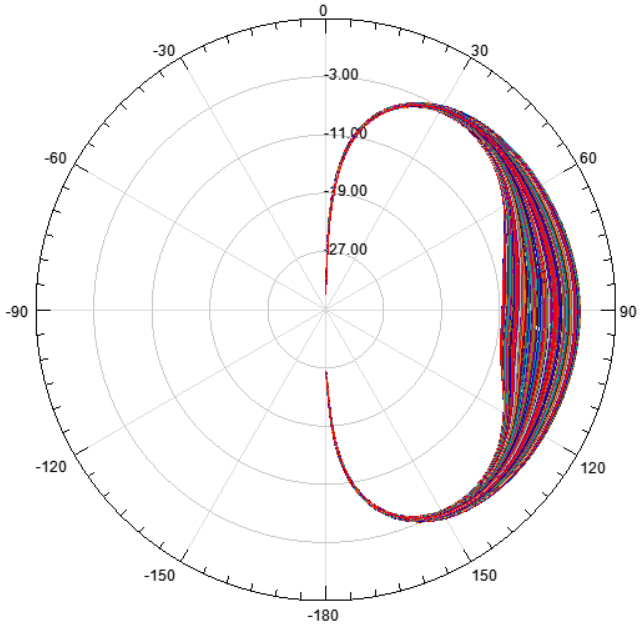

Fig. A.24: 2-D gain plot (vertical cuts) when $\epsilon_r = 5.2$ and frequency = 1.622 GHz.

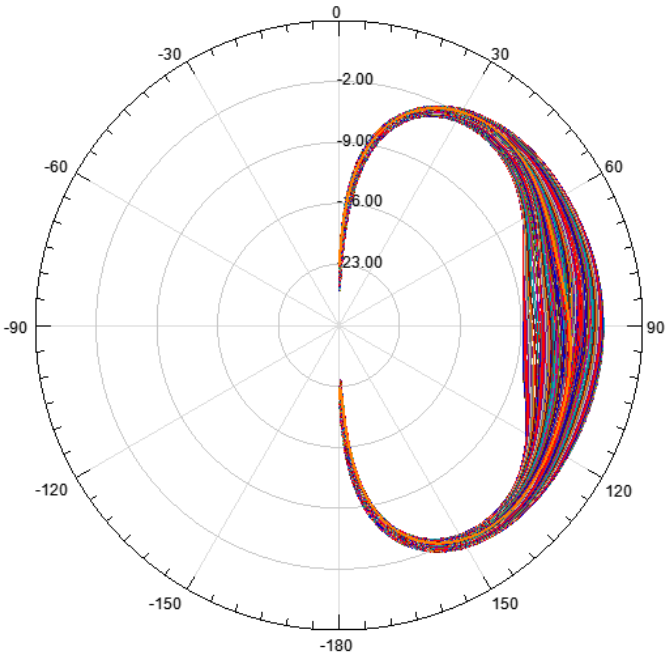

Fig. A.25: 2-D gain plot (vertical cuts) when $\epsilon_r = 5.72$ and frequency = 1.575 GHz.

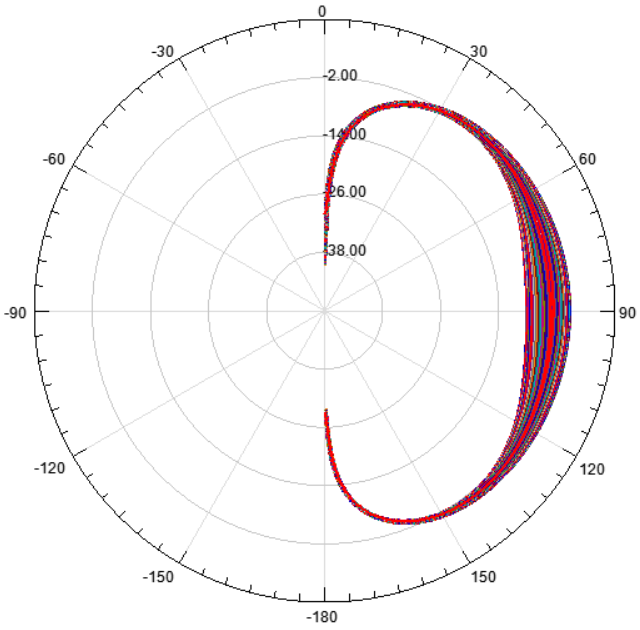

Fig. A.26: 2-D gain plot (vertical cuts) when $\epsilon_r = 5.72$ and frequency = 1.527 GHz.

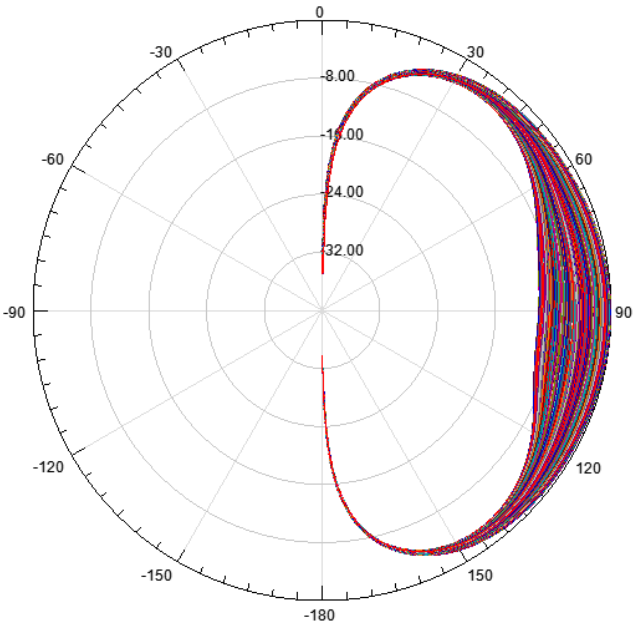

Fig. A.27: 2-D gain plot (vertical cuts) when $\epsilon_r = 5.72$ and frequency = 1.622 GHz.

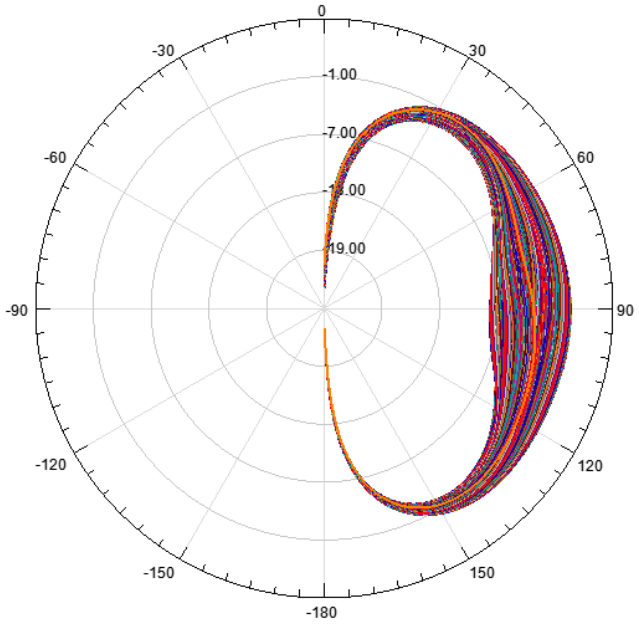

Fig. A.28: 2-D gain plot (vertical cuts) when $\epsilon_r = 4.68$ and frequency = 1.575 GHz.

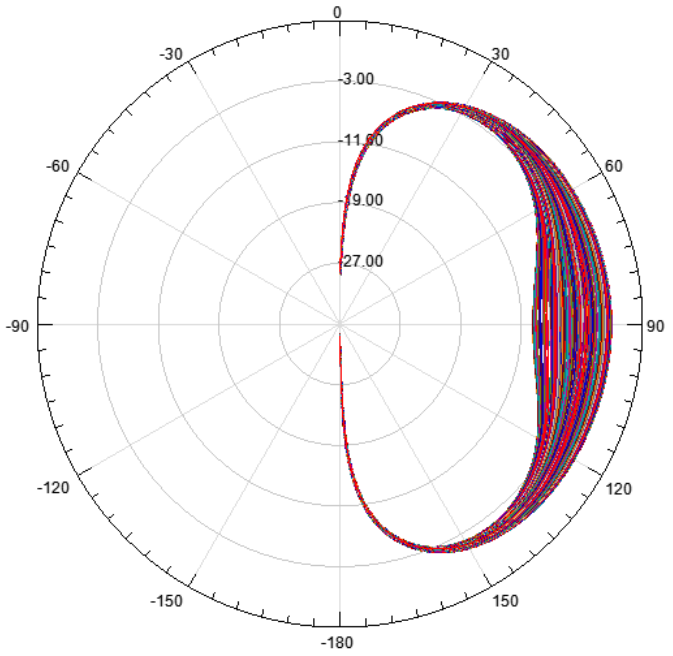

Fig. A.29: 2-D gain plot (vertical cuts) when $\epsilon_r = 4.68$ and frequency = 1.527 GHz.

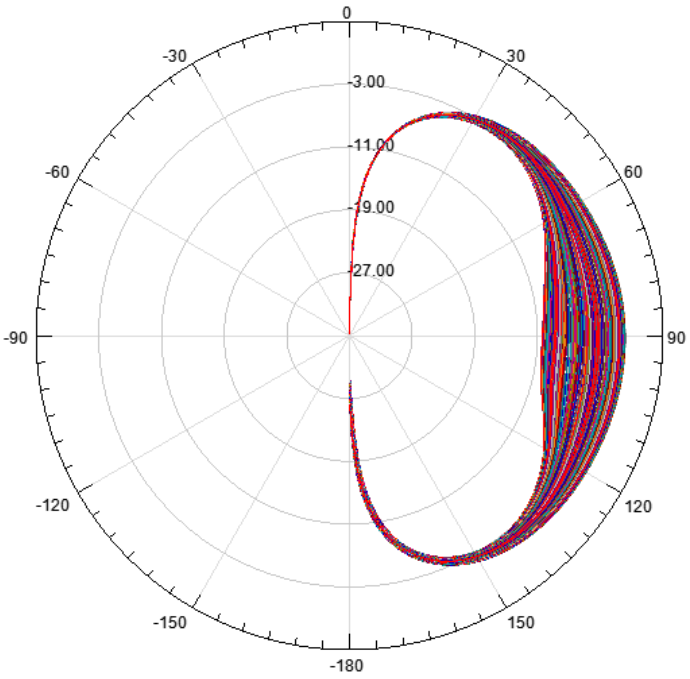

Fig. A.30: 2-D gain plot (vertical cuts) when $\epsilon_r = 4.68$ and frequency = 1.622 GHz.

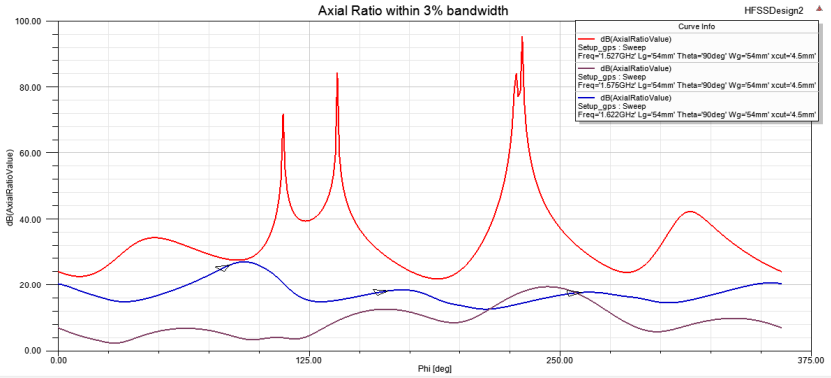

Fig. A.31: Axial ratio when $\epsilon_r = 5.2$ and frequency = 1.575 GHz.

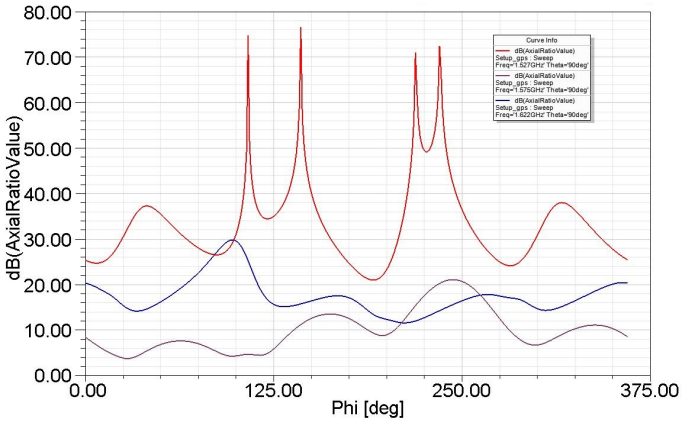

Fig. A.32: Axial ratio when $\epsilon_r = 5.72$ and frequency = 1.575 GHz.

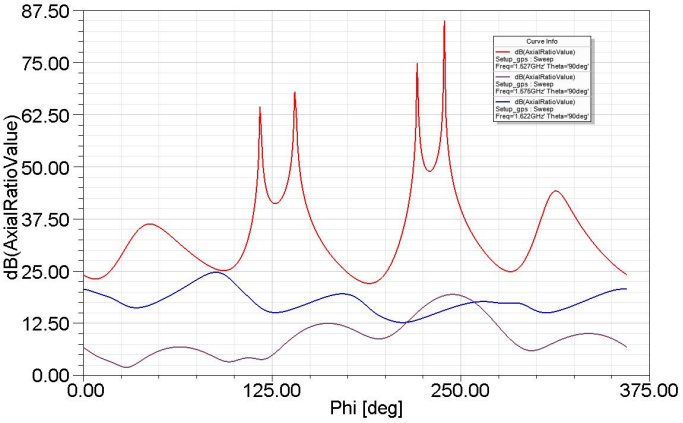

Fig. A.33: Axial ratio when $\epsilon_r = 4.68$ and frequency = 1.575 GHz.

A.2 Cylindrical S-band Array Antennas with Suspended Middle Metal Layer and Grounded Middle Metal Layer

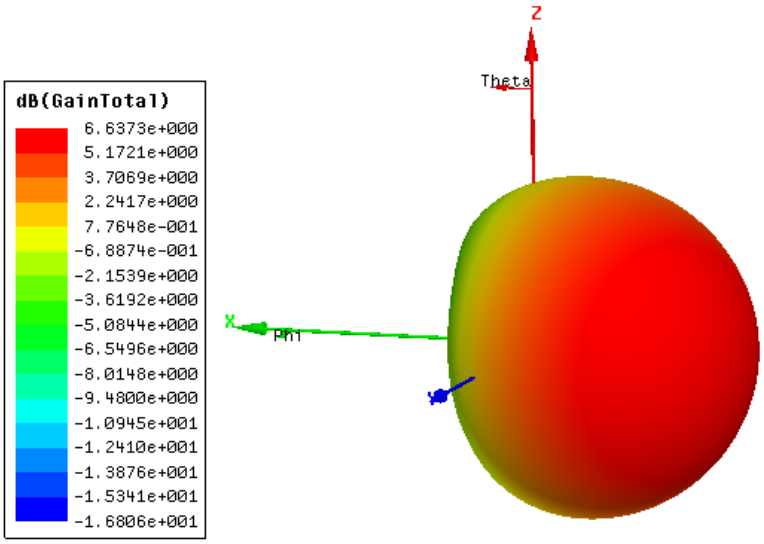

Fig. A.34: 3-D gain plot for perfect ground.

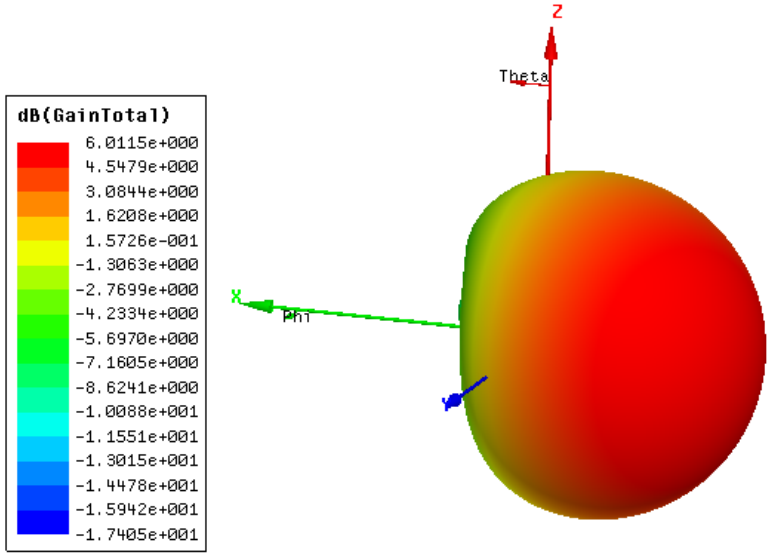

Fig. A.35: 3-D gain plot for suspended ground.

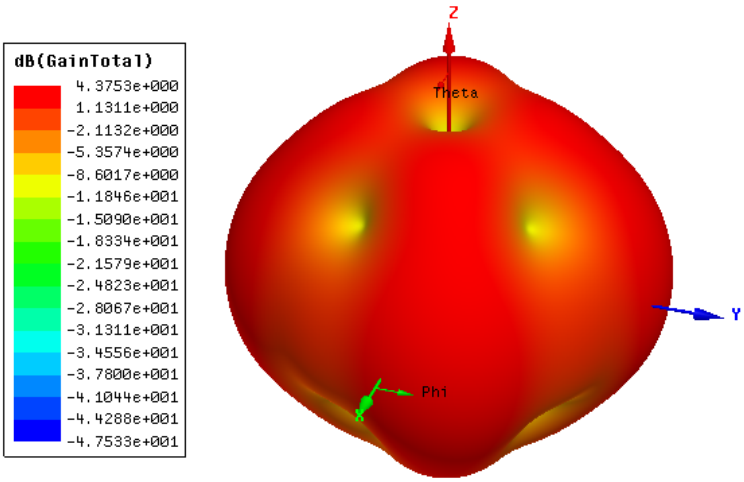

Fig. A.36: 3-D gain plot for perfect ground.

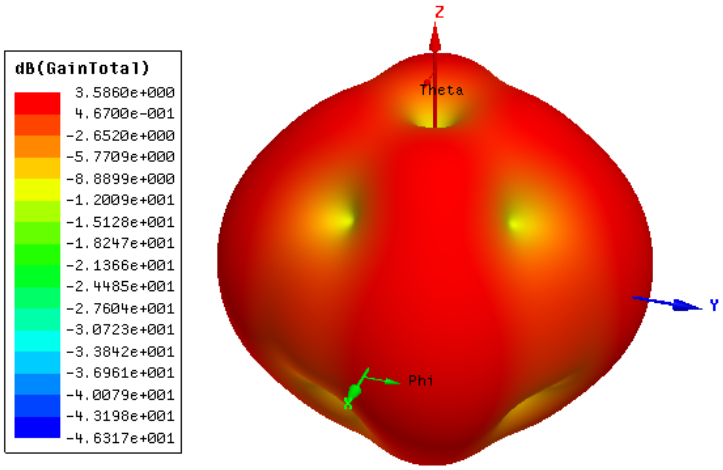

Fig. A.37: 3-D gain plot for suspended ground.

A.3 Four T-shaped Strip Dipoles Excited along with Four S-band Antennas and Four GPS-band Antennas

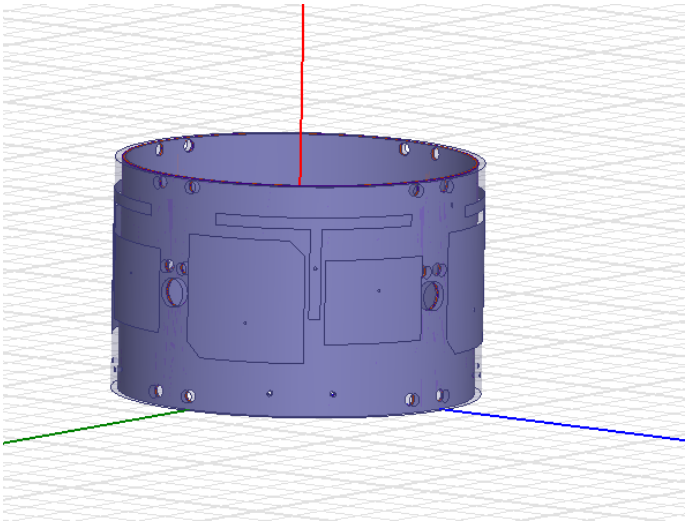

Fig. A.38: Four strip dipoles excited along with four S-band antennas and four GPS-band antennas.

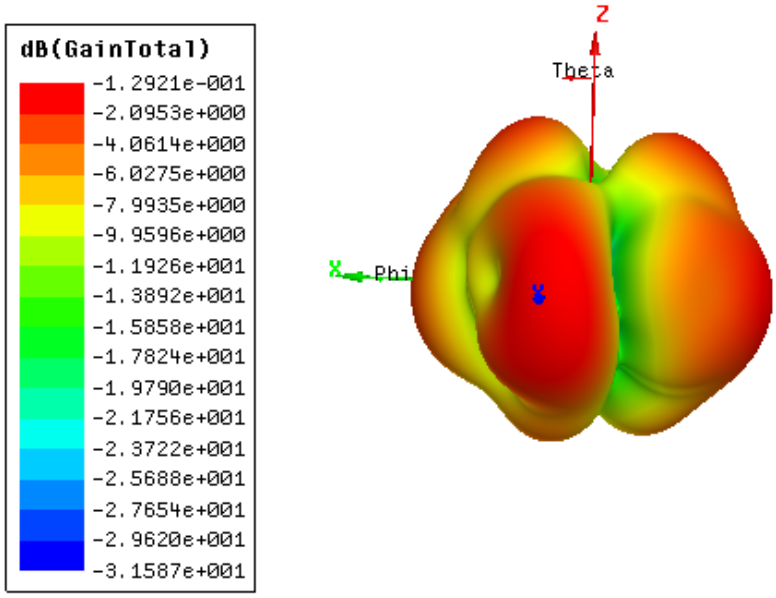

Fig. A.39: 3-D gain plot.

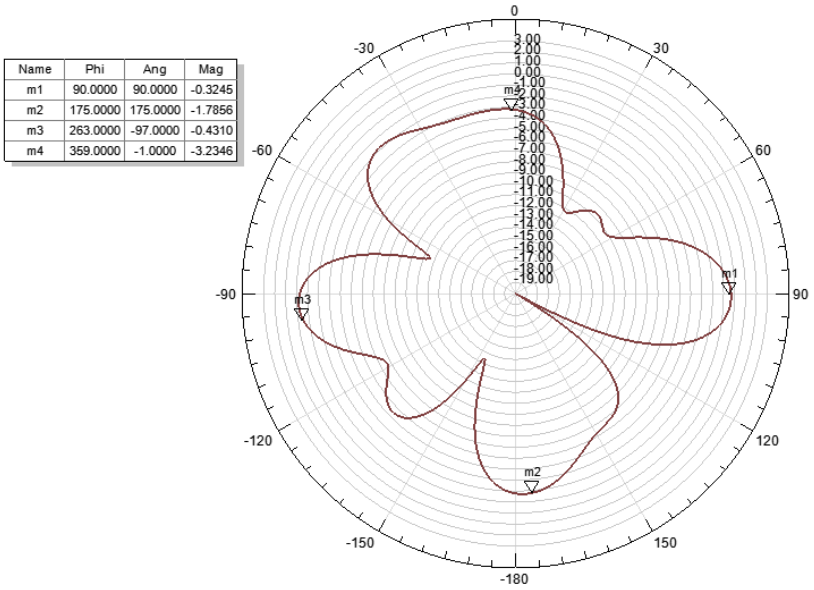

Fig. A.40: 2-D gain plot for theta = 90 degree.

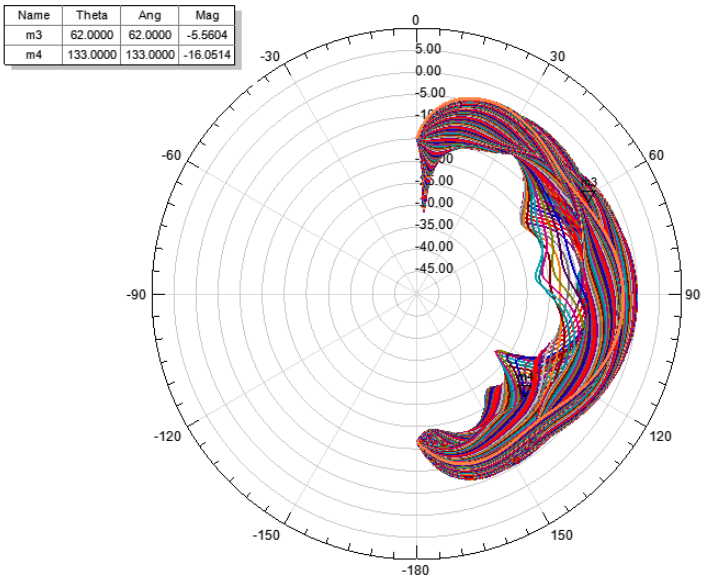

Fig. A.41: 2-D gain plots for all phi (0 degree to 360 degree).

A.4 12 Strip Dipoles Excited along with Four S-band Antennas and Four GPS-band Antennas

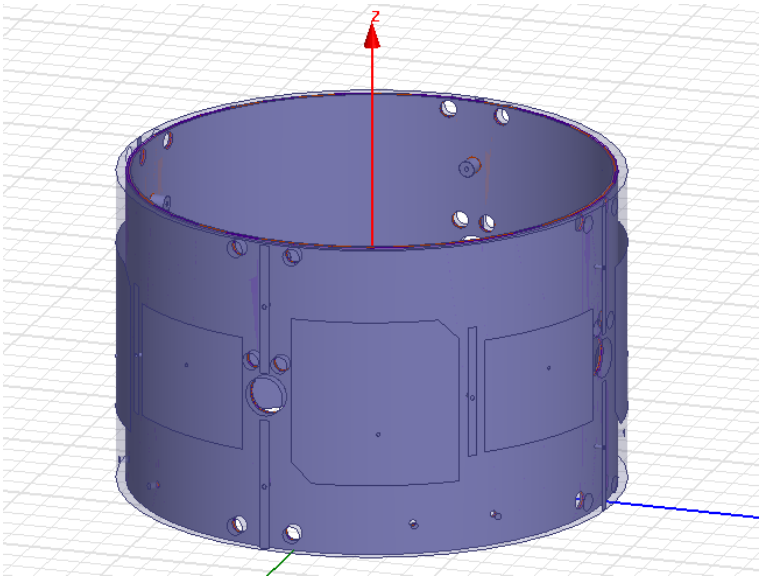

Fig. A.42: Four S-band antennas simulated along with 12 additional microstrip dipole antennas.

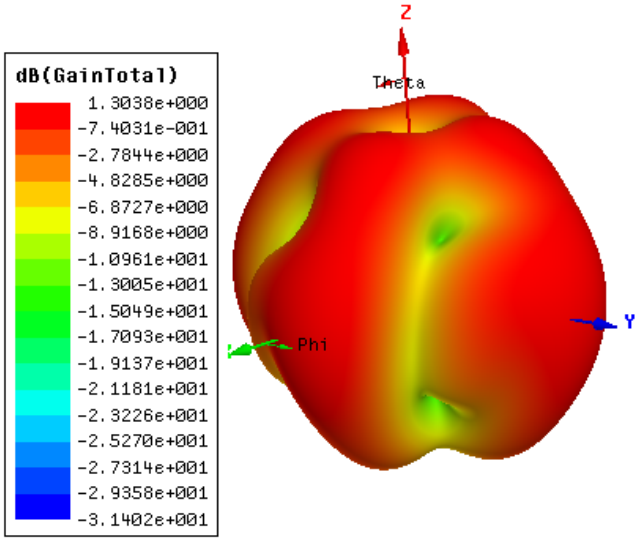

Fig. A.43: 3-D gain plot of four S-band antennas with 12 additional microstrip dipoles.

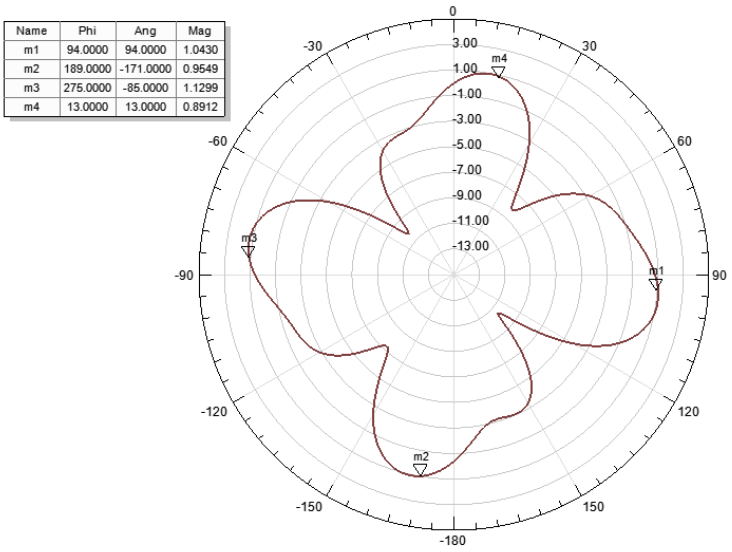

Fig. A.44: 2-D gain plot for theta = 90 degree of four S-band antennas with 12 additional microstrip dipoles.

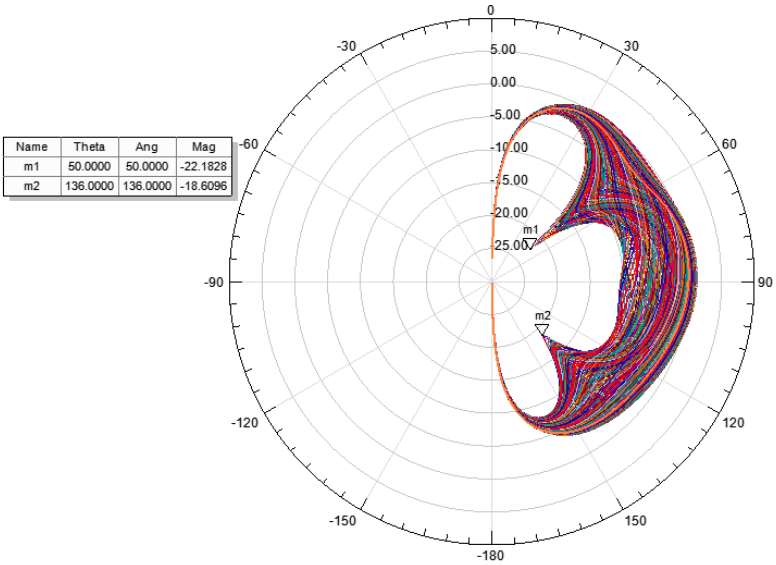

Fig. A.45: Vertical cuts for phi (0 degree to 360 degree) of four S-band antennas with 12 additional microstrip dipoles.